Quantitative MRI characterization of brain tissues in stroke patients.

Auteur : Bonghi, Sabrina
Promoteur(s) : Phillips, Christophe
Faculté : Faculté des Sciences appliquées
Diplôme : Master en ingénieur civil biomédical, à finalité spécialisée
Année académique : 2020-2021
URI/URL : http://hdl.handle.net/2268.2/13221

UNIVERSITY OF LIÈGE
SCHOOL OF ENGINEERING AND COMPUTER SCIENCE

Quantitative MRI characterization of brain tissues in stroke patients

Author:
Sabrina BONGHI

Supervisors:
Pr. Christophe PHILLIPS - GIGA-CRC in vivo imaging

Collaboration with University College London:
Pr. Martina CALLAGHAN - Wellcome Centre for Human Neuroimaging
Pr. Jenny CRINION - UCL Queen Square Institute of Neurology

Master's thesis carried out to obtain the degree of Master of Science in Biomedical Engineering

Academic year: 2020-2021

UNIVERSITY OF LIÈGE

Abstract

Faculty of Applied Sciences

Master in Biomedical Engineering

Quantitative MRI characterization of brain tissues in stroke patients

Sabrina BONGHI

Supervisor: Pr. Christophe PHILLIPS

Academic year: 2020-2021

Strokes are the second leading cause of death worldwide, the second leading cause of dementia and the leading cause of non-traumatic acquired motor disability in adults. Therefore, a pressing need exists to improve the revalidation treatment after strokes. The aim of the rehabilitation research is to discover and understand the relationship between brain, behaviour, and recovery after a stroke in order to use brain reorganization following a stroke to predict functional outcomes. This master thesis focuses on strokes inducing lesions in the left hemisphere which are causing aphasia and specifically anomia. The research investigates the brain plasticity and tissue microstructure properties changes in these patients through transversal studies. MRI data were acquired for both patients and controls using a specific "multi-parametric mapping" protocol, providing quantitative maps of tissue MR properties.

The first transversal study compares the brains of stroke victims against control reference subjects, from a morphological and microstructural point of view. The aim of the microstructural comparison is to find out whether lesions in the left hemisphere induce changes in the right hemisphere, which appears normal on conventional MRI. The second research compares the microstructures of patients' brains in relation to their performance. A third, more methodologically oriented research aims to determine the importance of the chosen data treatment pipeline by comparing the results obtained with two different pipelines on the control subjects.

The study of brain microstructures is carried out via a voxel-based quantification (VBQ) analysis. The data is first segmented and warped in the MNI standard space using the "Unified Segmentation" (US) method for control subjects and its extension for lesioned brains, the "Unified Segmentation with Lesion" (USwL) approach for patients. The data is then smoothed using a tissue weighted smoothing approach, for GM and WM separately.

Statistical tests showed GM atrophy for patients in some regions of the right hemisphere (brain stem, right thalamus proper, right supplementary motor cortex and right lingual gyrus). Futhermore, there is a significant decrease in MT values for patients versus controls in a voxel located in the WM of the right hemisphere; this could reflect a variation in the amount of myelin between patients and healthy subjects.

No voxel showed a difference within the patient group in terms of their performance.

Comparing the results of two different pipelines on the control data revealed a large number of voxels with statistically significant differences. This highlights the importance of the data processing performed.

Acknowledgements

This master thesis, which is the result of 5 years' study at the University of Liège, has been the longest project I have ever done. I would like to sincerely thank all the people who, from far or near, contributed to its realization but also people who supported me during these 5 years.

First, I would like to sincerely thanks Pr. Christophe Phillips, my academic supervisor. Through his courses, I discovered and appreciated medical imaging and medical statistics. He allowed me to do my master thesis in this field. I thank him for giving me his trust and his time. His precious advice allowed me to do this work in the best possible way.

Then, I would like to thank Martina Callaghan and Jenny Crinion who proposed the topic of this thesis with the material support and gave me the opportunity to collaborate with the University of London.

I would also like to thank Nora Vandeleene, PhD student at the University of Liège at the CRC in vivo imaging for her support and sharing of knowledge throughout my master thesis.

Finally, I would like to thank my relatives who have always supported me in the choice and realization of my studies.

Contents

List of Figures

List of Tables

List of Abbreviations

ALI	**A**utomatic **L**esion **I**dentification
BNT	**B**oston **N**aming **T**est
BOLD	**B**lood **O**xygen **L**evel-**D**ependent
CAT	**C**omprehensive **A**phasia **T**est
Co-SS	**Co**mprehension of **S**poken **S**entences
Co-SW	**Co**mprehension of **S**poken **W**ords
Co-WS	**Co**mprehension of **W**ritten **S**entences
Co-WW	**Co**mprehension of **W**ritten **W**ords
CSF	**C**erebro**s**pinal **f**luid
CT	**C**omputed **T**omography
GLM	**G**eneral **L**inear **M**odel
GM	**G**rey **M**atter
hMRI	**h**istology using **MRI**
fMRI	**f**unctional **M**agnetic **R**esonance **I**maging
FWHM	**F**ull-**W**idth-at-**H**alf-**M**aximum
Min-P	Word **Min**imal **P**airs
Mo-w	Repetition of **Mo**nosyllabic **W**ords
MRI	**M**agnetic **R**esonance **I**maging
MPM	**M**ulti-**P**arametric **M**apping
MT	**M**agnetisation **t**ransfer
Nam-A	**Nam**ing **A**ctions
Nam-O	**Nam**ing **O**bjects
NW	Repetition of **N**on-**W**ords
PALPA	**P**sycholinguistic **A**ssessment of **L**anguage **P**rocessing in **A**phasia
PD	**P**roton **D**ensity
qMRI	**q**uantitative **M**agnetic **R**esonance **I**maging
RF	**R**adio **f**requence
SPM	**S**tatistical **P**arametric **M**apping
TPM	**T**issue **P**robability **M**ap
TE	**e**cho **t**imes
US	**U**nified **S**egmentation
USwL	**U**nified **S**egmentation **w**ith **L**esion
VBM	**V**oxel-**b**ased **m**orphometry
VBQ	**V**oxel-**b**ased **q**uantification
WM	**W**hite **M**atter

List of Symbols

M_z	magnetization in the longitudinal plane	Am^{-1}
M_{xy}	magnetization in the transverse plane	Am^{-1}
R_1	longitudinal relaxation rate	s^{-1}
R_2^*	effective transverse relaxation rate	s^{-1}
T_1	longitudinal relaxation	s
T_2	transverse relaxation	s
T_2^*	effective transverse relaxation	s

Chapter 1

Introduction

The topic of this master's thesis was defined in collaboration with the University College London. In this work, quantitative images obtained via MRI in stroke patients are used to characterize post-stroke brain tissues.

1.1 Motivation

Strokes are the second leading cause of death worldwide [2]. Furthermore, it is the second leading cause of dementia and the leading cause of non-traumatic acquired motor disability in adults. After a stroke, 60% of patients recover their independence and 40% of patients retain significant after-effects [2]. These irreversible consequences of a stroke can lead to depression [2, 17]. Furthermore, 20% of patients die within a year [2]. Stroke is therefore a serious affliction that should not be ignored.

The aim of rehabilitation research is to discover and understand the parallel between brain, behaviour, and recovery after a stroke in order to use brain changes following a stroke to predict functional outcomes [36] and improve the revalidation treatment to diminish the seriousness and the number of people suffering from disabilities. Given the percentages of disabled and dependent people, a pressing need exists to improve the rehabilitation after a stroke. A better understanding of our brain is crucial to achieve this goal.

This work is based on data from patients who have suffered from stroke but more particularly patients with anomia after a stroke in the left hemisphere. The behaviour of patients with aphasia [1], and specifically anomia [2], changes enormously over time. Such a change in behaviour necessarily results from cerebral plasticity and / or a change in the property of cerebral tissues. This prompts neurologists to collect data from these patients in order to study and understand this behavioural change.

A study from Oxford University has already been conducted using fMRI data from eighteen right-handed, native English speakers who suffer from aphasia as a result of a single left-hemisphere stroke [6]. Two different experiments were realized. Each experiment was performed at two different moments: before an anomia treatment program (T1) and after 6-week of the anomia treatment (T2) [6].

In the first experiment, data was also acquired 3 months after treatment. The first experiment consisted in asking the patient to name tasks represented on pictures without any cues at three different times: before (T1), directly after (T2), and 3 months after (T3)

[1] Aphasia is a language disorder (speech, listening or reading disorder) that can occur as a result of a stroke.

[2] Anomia is a part of aphasia that reflects the difficulty remembering the names of people and objects.

anomia treatment. In the second experiment, subjects are helped with an auditory cue to name the task in the scanner. This second experiment is performed twice, at T1 and T2 [6]. Both experiments demonstrated the effect of a naming aid thanks to the blood oxygen level-dependant (BOLD) signal. This signal that can be observed on fMRI shows the activity in the brain. When there is a phonetic cue, the brain needed less activity to perform the task. The results of the study showed that the treatment improved speech production and that the performance following the treatment was still valid 3 months after this latter was stopped. The study also evaluates the accuracy and reaction time according to the phonemic cueing. As expected, accuracy was higher for word cues and lower for no cues. Accuracy and reaction time improved over time and were further improved in treated items than in untreated items. By observing the activity, this study detected the parts of the brain involved in speech recovery i.e. neural mechanisms underlying anomia treatment and following anomia treatment [6].

The results of this study are very interesting for developing new treatments and improving speech production for these patients [6]. However, no treatment outcome was correlated with variables such as age, time since stroke, duration of treatment or lesion volume. Neglecting these aspects could distort the results. Furthermore, the data set used did not allow this result to be quantified. Indeed, the study shows where changes in the brain take place by observing its activity but does not quantify these changes. Quantitative images represent tissue by assigning a value to each voxel. This assigned value reflects the physical properties of the voxel. This master thesis attempts to overcome the limitations of conventional images by using qMR images to quantify macrostructural and microstructural measure of GM and WM through an *in vivo* voxel-based quantitative (VBQ) analysis. Multi-parameter mapping (MPM) is used here. It is a raw data acquisition protocol, with which the qMRIs are constructed. The validation and the feasibility of the MPM approach in chronic aphasia post-stroke populations were already studied [15]. Indeed, London study results reveal GM and WM differences between patients with aphasia and control subjects through a MPM approach [15]. This study was performed using SPM 12. This thesis continues this work. As the MPM approach is valid and feasible on patients with aphasia following a stroke, it can be used to determine structural brain plasticity and the changes in tissue microstructure properties in these patients.

In this master thesis, the idea is not to evaluate one type of treatment and observe the consequences but rather to characterize the change in different brain tissues in aphasic patients following a stroke compared to healthy people. Since this work would allow us to observe the microstructural changes in the brain, the outcome will be connected to behavioural changes. A better understanding of behavioural changes would allow the development of better post-stroke treatments for aphasic patients.

1.1.1 Aim of the thesis

The goal of this master thesis is to investigate whether the qMRI data are sensitive to structural brain plasticity and tissue microstructure properties changes. The study of this brain plasticity and microstructure will help to improve validation treatment.

Concretely, this document attempts to answer the following two questions:

1. Are there any morphological or microstructural differences in the right hemisphere between patients and controls?

2. Are there microstructural differences between patients according to their performance?

The analysis of damaged data is difficult, which encourages universities to collaborate (see 1.2). This master thesis aims to bring together the methods developed by two universities, the University College London and the University of Liege. These two universities share their segmentation method. The delineation of lesions is very important. Lesion segmentation is the first step in the neuroimaging process to find links between brain structure, function and behaviour after a stroke. This accurate segmentation of post-stroke lesions is important to further characterize healthy looking tissue. It is a critical step in assessing the relationship between behavioural changes and microstructural changes in brain tissue [12, 36]. A good segmentation method is therefore desirable.

1.2 Collaborating researchers

Data has been collected by the University College London and they was then provided by Jenny Crinion, the Professor of Cognitive Neuroscience in University College London.

Acquiring data for such a study takes a tremendous amount of time. It is therefore crucial once the data has been collected to use the best possible method in order to obtain an optimal result. Collaboration between researchers improves both efficiency and profitability. When the communication channels are open, it is easier to find the desired information or to find advice from other researchers in order to use the data collected optimally to obtain the most accurate result possible. Basing new research on studies previously carried out saves time and therefore increases the speed of medical progress. University College London and University of Liège collaborate in order to share their discoveries and thus help science to progress more quickly.

The manual detection of abnormal brain tissue by a trained professional is laborious, time-consuming and depends on the person who segments the data [12]. It is therefore necessary to use automated methods to detect brain damage. A combination of methods involving collaboration between different universities using different methods to segment seems to be a good idea to find the optimal automatic segmentation.

Two different methods to delineate lesions will be merged in this study.

- The first one is the method developed by the Institute of Neurology in University College London. It is an automated lesion identification (ALI) method based on the detection of outlier voxels.
- The second one was developed by the Cyclotron Research Centre of the University of Liège which is called Unified Segmentation with Lesion (USwL)

1.3 Outline of this thesis

Firstly, medical knowledge about stroke and the imaging means to detect it will be presented. Then, MRI analysis techniques will be discussed.

Similar work on other pathologies will be briefly introduced in order to show examples of the results of the method used in this master thesis. These previous works show the usefulness of the use of parametric maps to detect and quantify microstructural changes in the brain.

The next chapter will list the materials available to carry out this work i.e. all data used as well as a description of the method used previously to obtain the a priori lesion masks, which were available prior to the thesis.

The second half of the work will explain the method used on the data to achieve the objective. The data pipeline, both on patients and controls data consists into 4 main parts: segmentation, normalization, smoothing and mask creation.

- Segmentation: Estimation of the probability maps of each brain tissue
- Normalization: Warping all images in a common space
- Smoothing: Blurring of the data to reduce variability between images and noise
- Mask creation: Assignment of one tissue class per voxel

Different statistical tests are then performed and explained. These different tests attempt to discover if there are any morphological or microstructural differences in the right hemisphere between patients and controls and/or if there are microstructural differences between patients according to their performance. Furthermore, two different pipelines are used on control subjects and a F-test is realized to know if there are any differences between the results of these two pipelines.

Finally, this master thesis shows the results obtained from these statistical tests before ending with a short discussion and conclusion.

Chapter 2

Background

This chapter covers the necessary background about the medical condition considered here, MR imaging, and previous works.

2.1 Medical Background

The focus on this work is on stroke, and more specifically stroke induced aphasia with anomia.

2.1.1 Stroke

From a medical point of view, neurologists already know what a stroke is and how it happens. A stroke is the sudden death of brain cells caused by a heart or vascular problem [1]. There are two types of stroke [17, 35, 49, 52]:

- Ischaemic stroke: The blood is not delivered to its destination, the brain. Either blood is blocked by a clot formed in an artery inside the brain (thrombotic stroke) or blood is not delivered to the brain because of a blood clot in an artery outside the brain (embolic stroke). This type of stroke represents about 80% to 90% of cases.
- Haemorrhagic stroke: Stroke is caused by a ruptured blood vessel causing blood to escape into the brain.

Some factors can increase the risk of stroke. They are basically the same as those for coronary heart disease and other vascular diseases [17]. There are lifestyle-related factors: current smoking, alimentation (fruits and vegetables), physical activity and alcohol intake. History of hypertension, diabetes, heart problems, psychosocial stress and depression can also increase the risk of a cerebrovascular accident [13]. Despite these known causes, in 30% of cases, no cause could be detected [5].

The impairment due to a stroke shows a wide diversity of symptoms [48]. Disability varies according to the location of the damaged cells, the premorbid condition and the neurological recovery of the patient [48]. Impairments after a stroke can be spatial neglect, visual neglect, language problems, paralysis and/or sensory loss. Most people are right-handed and thus have the language areas in the left hemisphere, while visual and spatial perceptions are located in the right hemisphere. Sensory and motor areas are found in both hemispheres. After a stroke affecting a motor or sensory area in the brain, motor and/or sensory loss will be seen in the part of the body opposite the lesion. This is due to the fact that the right (left) hemisphere controls initiating motor activity and receives sensory information from the opposite site of the body, i.e. the left (right) side [48].

2.1.2 Aphasia

Stroke can lead to aphasia. Aphasia is a language disorder ranging from difficulty of finding words to a complete loss of the ability to express oneself [42]. Aphasia is usually caused by lesions in perisylvian regions in the left hemisphere [15]. This region is located around the sylvian fissure, circled in red in FIGURE 2.1. Indeed, 97% of people have language control primarily in the left hemisphere [48]. However, studies show that the right hemisphere is also involved in language recovery [6, 15, 16]. For instance, a patient touched by aphasia caused by a left middle cerebral artery ischaemic stroke developed a sudden worsening of speech production following another stroke in the right hemisphere [16]. That leads to the following hypothesis: there is the plasticity of the right hemisphere to improve the recovery of the capacities following a stroke affecting the left hemisphere.

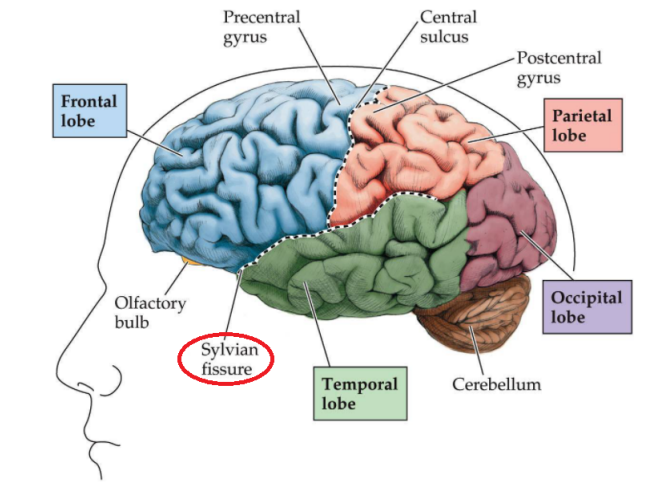

FIGURE 2.1: Brain lateral view [37].

Anomia

Anomia is the most relevant symptom of aphasia [51]. Anomia is characterized by difficulty naming objects when speaking and writing. Nevertheless, the ability to speak is not affected [42] and the understanding is intact [48].

2.2 Technical Background

This section contains all the techniques (machines, data acquisition, analysis methods, conventions) that are necessary for the understanding of this work.

2.2.1 Stroke diagnosis

When a person is a suspected victim of a stroke, it should be taken care of as quickly as possible. Indeed, early recognition is a key. Stroke is a medical emergency. Time is of the essence. The brain is an energy-intensive organ. If its energy intakes are not sufficient, it will suffer and lose a large number of its neurons very quickly. Treating a patient quickly with the right treatment decreases the disabling consequences that the stroke can create [30]. There are signs that alert. For example, a non-symmetrical smile, a weaker arm less sensitive to pain than the other one, a loss of coordination, impaired speech, and a visual change are not insignificant signs in the suspicion of a stroke. At the slightest sign, people have to act quickly and reach for emergency care. Brain imaging should be performed as soon as possible to confirm or not the suspicion of stroke.

There are two different imaging tests that allow to observe the inside of the head, including soft tissue, bones, brain and blood vessels. These are CT scan and MRI. These imaging techniques are used to diagnose stroke [49].

CT scan

CT scan uses X-ray to take pictures through the brain. The patient is lying horizontally on the table, which is moving very slowly in order to acquire images of small slice of the brain and an X-ray machine rotates around his head. With the help of a computer, it is possible to obtain the image of any slice of the brain [49]. CT scan is less expensive and less noisy but MRI gives better images for small area in the brain [31] and so it is generally used in confirming a stroke.

MRI

MRI uses the magnetic properties of the proton to provide images of the inside of the body. MRI provides a more sensitive stroke diagnosis than CT [40]. MRI can detect small brain abnormalities that do not appear on a CT scan image [49]. For its non-invasiveness and its more detailed images, MRI is the recommended imaging technique for detecting strokes when possible. Since MRI uses a very strong magnet, metal on or inside the patient may be dangerous. Therefore, it is forbidden to scan someone with metal parts that are not compatible with MRI. For example, patient suspected of having a stroke with a cardiac defibrillator will go in the CT scan and not in the MRI. MRI is a more complicated examination with ferromagnetic contraindications and problems with claustrophobia. It is because of these contraindications that CT scan is sometimes used to the detriment of the accuracy of the examination.

In this work, images obtained by an MRI are analysed. It seems thus judicious to go deeper into this technique. The following section gives more details on the acquisition of images by MRI.

2.2.2 MRI physical principle

MRI is a non-invasive imaging technique that can look inside the brain [50]. The body is made up largely of water molecules. MRI observes biological tissues inside the body through the magnetic properties of one of their major constituents, the hydrogen nucleus. The machine is constantly subjected to a powerful static magnetic field B_0. Because the spin quantum number of an hydrogen nucleus is $\frac{1}{2}$, hydrogen nuclei have 2 possible states: up and down. The protons therefore align themselves parallel to this B_0 field in the two possible, up and down, orientations. There are more up spin with a lower energy than down spin generating a net longitudinal magnetization aligned with B_0. Moreover, all the spins precess at the Larmor frequency w_0, such that $w_0 = \gamma B_0$ where γ is the gyromagnetic ratio of the nuclei. Precessing at the same frequency but not the same phase, they are randomly oriented in any direction along the plane perpendicular to B_0. The resultant of all spins is therefore zero in the transverse plane, which induces a zero transverse magnetization. At this moment, only longitudinal magnetization is therefore present. Radio frequencies (RF) are then added to disturb the B_0 field. When $w_{RF} = w_0$, some up spins change their energy level to go to the next level and become down, which decreases the intensity of the longitudinal magnetization. RF pulse represents the oscillating magnetic field B_1 and induces a transverse magnetization because with this RF disturbance, the spins keep on precessing but they are also rephased together. When there is no more RF disturbance, transverse and longitudinal relaxations take place. The transverse relaxation, corresponding to the dephasing of the spins, is ten times faster than the longitudinal relaxation which corresponds to the energy jump of the spins [24]. When B_1 ceases, the protons return to their equilibrium state and the time it takes to reach the initial configuration depends on what surrounds the protons

[24, 29]. It is therefore possible to differentiate the different tissues constituting the brain using an MRI thanks to the combination of high-powered magnets and RF pulses.

This change in magnetization when B_1 ceases, corresponds to the relaxation phenomenon. There are two variables that characterize this macroscopic effect: T_1 and T_2 [24, 29].

T_1 relaxation time measures the time it takes for protons to return to their ground state in the direction of B_0. The Equation 2.1 represents this longitudinal relaxation. At a time equal to T_1, 63% of the initial longitudinal magnetization is recovered following the application of RF pulse (see 2.2) [27]. In this work, the longitudinal relaxation rate R_1 which is equal to $\frac{1}{T_1}$ will be used to characterize longitudinal relaxation.

$$M_z = M_0(1 - e^{\frac{-t}{T_1}}) \tag{2.1}$$

where,

- M_z is the longitudinal magnetization at time t
- M_0 is the longitudinal magnetization at the equilibrium state

When t=T_1, we have:

$$M_z = M_0(1 - e^{-1}) = 0.63M_0 \tag{2.2}$$

T_2 relaxation time measures the decrease of magnetization in the transverse plane (M_{xy}) when RF excitation ceases. This decrease is the consequence of the progressive dephasing of spinning dipoles [19]. The Equation 2.3 represents this T_2 relaxation. At a time equal to T_2, 37% of the maximum transverse magnetization remains (see 2.4). In this work, R_2^* will be used to characterize the transverse relaxation rate which is equal to $\frac{1}{T_2^*}$. The star means that the inhomogeneities in B_0 within each voxel is taken into account in addition to the spin-spin interaction characterized by T_2 to prompt the progressive dephasing of spins.

$$M_{xy} = M_0 e^{\frac{-t}{T_2}} \tag{2.3}$$

where,

- M_{xy} is the transverse magnetization at time t
- M_0 is the longitudinal magnetization at the equilibrium state

When t=T_2, we have:

$$Mxy = M_0 e^{-1} = 0.37M_0 \tag{2.4}$$

Since T_1 and T_2 values are properties of tissue, we can detect different tissues by the contrasts that result from the image. A T_1-weighted image will emphasize the contrast of two tissues with different T_1 values, whereas the contrast of a T_2-weighted image will represent the T_2 variation between the tissues. There are also other contrast techniques that can be used such as PD-weighted image which highlights the difference in proton density between the tissues or even the MT-weighted image which refer to the interaction between free proton in water and the protons bound at a macromolecule of tissue [21]. Each tissue has its own macromolecular composition. Therefore, the degree of interaction between molecules is tissue specific. This provides a contrast between tissues [21]. The choice of weighted image acquisition will depend on what we want to see.

2.2.3 Conventional MRI vs Quantitative MRI

Conventional MRI

Conventional images give qualitative representation of brain tissues with different contrasts. A conventional image of a damaged brain will give the delineation of the lesion with very little supplementary data. Indeed, conventional MRI provides information that can be seen directly through the naked eyes of a radiologist. It is therefore mainly morphological information.

Quantitative MRI

Acquiring quantitative data requires more steps compared to conventional MRI [45]. Despite this longer acquisition time, there is a great interest in the field of neurosciences for quantitative MRI because it provides additional information compared to conventional images. Indeed, unlike conventional MR images, quantitative maps attributes a value on each voxel which reflects the physical properties quantitatively and not only relatively as in conventional MRI. It enables to study *in vivo* microscopic parameters in brain tissues [10]. In quantitative images, one not only has a contrast as a result, one also has values which are quantified in standardized units. Quantification allows a physical interpretation and standardization increases the comparability across participants and scanners [8, 14]. With quantitative images, one has information on the nature of the signal which is linked to a biological change.

In addition to being sensitive, quantitative MRI is also specific to brain microstructures (myelin, iron and water concentrations, etc.) [10]. Furthermore, quantitative images, unlike conventional images, account for factors such as the sequence type and its parameters, the scanner used and so on. This facilitates comparison between images and allows to process and compare more data together. The quantitative images allow the control of all the uninteresting factors to make an estimate of the desired parameter.

Quantitative MRI has many advantages. However, some clinical research does not benefit from it probably because of the lack of available protocol and processing software [10]. In addition, qMRI requires longer acquisition time and processing is more complicated.

2.2.4 VBM vs VBQ

Voxel-based morphometry (VBM) and voxel-based quantification (VBQ) are both image analysis methods. Both are applicable *in vivo* to the whole brain based on medical imaging. Their voxel-by-voxel statistical analysis makes it possible to directly identify changes within the brain. Unlike VBM, VBQ can only be applied on quantitative images.

VBM is a neuroimaging method which determines changes in local concentrations inside brain tissue through voxel-wise comparison of local tissue concentrations between two or more groups of participants, or with respect to a regressor, for example age. The VBM technique consists, first of all, in segmenting and normalizing the images in order to ignore large-scale differences. Once normalization has been achieved, modulation is performed to adjust the amount of material per voxel to maintain the total volume of tissue. Indeed, modulation consists of scaling the amount of tissues in the voxels to preserve the total volume of the different tissues. For example, the GM of a subject with atrophied GM will be spread out in the normalized brain image. The modulation will indicate that there is less than 100% of GM in the voxel in order to maintain the total volume. Then, tissue segments as GM and WM segments are smoothed to have a better overlap between images. Finally, a statistical analysis is performed on all voxels

to detect significant differences. VBM thus compares the volume of tissue, for example the volume of GM [3, 41].

VBQ goes further than VBM. Indeed, to carry out a VBQ analysis, it is necessary to have a segmented image in order to know where the different classes of tissues are located. In quantitative images, each tissue has a range of voxel values that represents it. In order not to distort the values of the voxels by mixing the classes during the smoothing, this must be done by tissue class (see 4.1.3). In the same idea of conservation of voxel values, there is no modulation during a VBQ analysis and a mask creation for each tissue class is performed after the smoothing so that a voxel belongs to only one class of tissue. Since the values express a (semi-)quantitative physical property, VBQ provides information about changes in tissue properties. In contrast to morphological analysis, processing on quantitative images provides neuroimaging biomarkers for myelination and iron content and therefore informs about the properties of the tissues. It is thus possible to obtain information on the macrostructural and microstructural properties of these tissues.

2.2.5 MPM protocol

MPM is a protocol which generates quantitative maps. This protocol has been validated for use in multi-centre imaging studies. Indeed, MPM provides quantitative parameters that are not site or time point dependent, which is an advantage. Furthermore, MPMs have a high resolution and allow reliable observation of brain microstructures [14].

These maps generate neuroimaging biomarkers for myelination and iron content for example and make it possible to carry out an *in vivo* study to analyse the macro- and microstructures of brain tissue [15].

Creation

Quantitative maps creation is shown in two different ways in FIGURE 2.2. The upper part actually displays the data (left) and output (right), while the lower part shows the underlying model.

MPM quantitative maps are created from three series of multi-echo spoiled gradient echo images. The three series are defined by a different weighting: there are T_1-, PD- and MT-weighting. These scans are acquired with a relevant selection of the repetition time (TR), the flip angle and the off-resonance MT pulse [10]. In order to minimize acquisition time, TR is as small as possible but must be large enough to contain the excitation pulse and sufficient echo. The resulting weighted images correspond to the extrapolation of the signals to an echo time of 0 ms. This extrapolation increases the signal-to-noise ratio (SNR). For R_1, PD and MT, the echo time series is not even observed. Only the fit in TE=0 is useful because it has a better SNR. The same flip angle for all echoes of the same parameter is used, chosen to obtain appropriately contrasted images. The flip angle is smaller for the PD echo series than for the T_1 echo series and this is the case for this study. Indeed, for this specific study, the MTw and PDw had a repetition time of 23.7 ms and flip angle of 6 degrees whereas these parameters for T1w were 18.7 ms and 20 degrees. MTw was achieved through the application of a Gaussian-shaped RF pulse 2 kHz off resonance with 4 ms duration and a nominal flip angle of 220 degrees.

R_1 and PD can be found from only two acquisitions that have a different flip angle. To estimate the rate of decay R_2^*, least square optimization combining PD, T_1 and MT signals was performed. ESTATICS is the acronym for "estimating the apparent transverse time

from images with different contrasts". The combination of the 3 contrasts PD, MT and R_1 at different echo times allows to decrease the noise and to have a better robustness. The result is an R_2^* map with high resolution and good contrast between the different brain tissues [10, 18].

B_1 corresponds to the magnetic component of the RF pulse i.e. the excitation pulse. There are two kinds of B_1 map. B_1+ reflects the amount of RF which is transmitted to the sample to excite spin and create the signal whereas B_1- reflects the signal that the coils receive [29]. The RF pulse is not transmitted and detected homogeneously throughout the brain. This transmission and this reception are done thanks to the coils around the head, which have spatially varying sensitivity profiles. Sensitivity is higher near the coils. Therefore, the SNR will be higher in the shallow parts of the brain. Correction of B_1 field inhomogeneity is also included in the protocol for accurate estimation of qMRI parameters. In FIGURE 2.2, correction B_1+ corresponds to f_t and correction B_1- is represented by f_r.

The output of the MPM protocol is the estimation of high-quality multi-parameter qMRI maps (R_1, R_2^*, PD, MT saturation).

For this master thesis, quantitative maps of 4 parameters are available. Each parameter provides different physical information. This master thesis is not about the neurological interpretation of the results, but it is useful to have an idea of what each parameter can give as information. Each of the parameters R1, R2*, MT and PD provides additional knowledge:

- The R_1 signal depends on the proton density but also on the fat and lipid content. It informs about the amount of myelin. Myelin is represented by a short T_1 [28].
- R_2^* refers mainly to the amount of iron in the tissue. The age can be estimated using this parameter. This is a study that had already been done with MPM protocol (see 2.3.1). With age, haemoglobin will build up in some areas of the brain. The more haemoglobin there is, the more iron there is. The more iron there is , the faster the phase shift and therefore the larger R_2^*.
- PD parameter detects water levels. The PD parameter can highlight certain lesions such as those caused by oedema, for example.
- The MT signal highlights macromolecules. Therefore, myelin represents a large portion of the MT signal.

Available data to create qMRI

All the images needed to create the quantitative maps have been previously acquired. These data (called "raw data") are images not used in the processing of this work but useful for constructing the quantitative maps on which this work is based. For each subject, raw data consists into:

- 6 echo's of MT-weighted data (magnitude and phase)
- 8 echo's of PD-weighted data (magnitude and phase)
- 6 echo's of T1-weighted data (magnitude and phase)
- B1 mapping
- B0 mapping
- 3 localizer slices

These main images were acquired with a 1 mm isotropic resolution using a field of view of 256 mm head-foot, 240 mm anterior-posterior and 176 mm right-left. Gradient echoes were acquired with alternating readout gradient polarity at six equidistant echo times (TE) ranging between 2.2 and 14.7 ms for T1w and MTw acquisitions and at eight TE ranging between 2.2 and 19.7 ms for PDw.

2.2.6 MNI brain

MNI space is a common brain space defined by the Montreal Neurological Institute. This standard space was built by using a large series of MRI scans on healthy brains [23]. The aim of this standardization is to define a brain that is as representative as possible of the population. The use of this template improves communication between researchers. Indeed, if all researchers use the same brain template, the coordinates will be the same and it will be easier to compare the results. The MNI template has been used in the work with this objective in mind. The images used in this work have therefore all been warped to be in standard MNI space.

2.3 Previous work

This section gives examples of studies that have already been carried out, using quantitative MRIs built with MPM (which are created with the `hMRI toolbox`). These have taken advantage of qMRI over conventional MRI to obtain results using statistical analysis. Three studies are highlighted here:

- Age-related differences in brain microstructure [11]
- Multiparameter quantitative histological MRI values in high-grade gliomas to prevent recurrence [8]
- Alterations in normal-appearing gray and white matter of patients with multiple sclerosis [7]

2.3.1 Age-related differences in brain microstructure

Neurodegenerative diseases increase with age. However, what alters normal ageing processes to cause neurodegeneration is still unclear [11].

The use of quantitative maps created with the MPM protocol has enabled age-dependent differences in healthy brain microstructures to be highlighted in order to quantify the normal changes in brain microstructures during aging.

A VBM analysis and a VBQ analysis were performed. Statistical analyses were then used to highlight differences in the brain, taking into account age, gender, total intracranial volume and scanner used [11].

This study led to several results. First, the VBM analysis showed the regions where GM atrophy occurs. Reductions were primarily discovered in frontal regions. The paper also reports normal changes with age in R_1, R_2^*, PD, and MT signals depending on location in the brain. The effective transverse relaxation rate increases in some areas of the brain where the iron level increased (basal ganglia, red nucleus, extensive cortical regions) and decreases in others where the iron level is reduced (along the superior occipitofrontal fascicle and optic radiation). The MT saturation decreases with demyelination and so signal decrease is identified within WM. The longitudinal relaxation rate also decreases with demyelination. The results were located along the optic radiation and in the genu

of the corpus callosum with age. The effective proton density decreases in some areas of the brain (putamen, pallidum, caudate nucleus, red nucleus) and increases in other parts (optic radiation, superior regions of WM) [11]. FIGURE 2.3 reflects the whole brain pattern of aging obtained with this study.

Furthermore, the F-test result shows a negligible dependence on the scanner used [11].

The results help to build a quantitative baseline. From this base, it is easier to differentiate between healthy ageing and pathological neurodegeneration [11].

2.3.2 Multiparameter quantitative histological MRI values in high-grade gliomas to prevent recurrence

Quantitative MRI has also been exploited to detect the risk of recurrence after surgery for a brain cancer that is high-grade gliomas. It is very complicated to detect the damaged part of the brain with conventional MRI because brain parenchyma microscopically impaired by high-grade gliomas is difficult to identify with this technique [8]. The aim of this neuro-oncology study is to find the relationship between microscopic parameters in the area surrounding the surgical cavity and the existence of high-grade gliomas recurrence [8].

This study shows that quantitative MR parameters differ within the initial perioperative area between the region where high-grade gliomas will subsequently reappear and the area where it will not [8]. In the region where it recurs, the MT_{sat} and R1 have smaller values. Furthermore, R_2^* is also lower in this region. Note that another paper [9] studied glioblastoma effects on quantitative MRI of contralateral normal-looking WM and noticed that R_2^* was smaller in the peritumoral brain zone compared to the contralateral hemisphere [9]. This suggests looking also at the values of the voxels that are located in the healthy part of the brain.

To conclude, this study on high-grade gliomas shows that recurrence can be detected by observing the voxel values before it is clinically and radiologically evident on conventional MRI.

2.3.3 Alterations in normal-appearing gray and white matter of patients with multiple sclerosis

Multiple sclerosis (MS) is an autoimmune disease that affects the central nervous system. There are two main types of multiple sclerosis. The first is relapsing-remitting MS characterized by the onset of disorders within a few days happening in isolated attacks and which may or may not regress completely within a few weeks. The second is progressive MS which progresses steadily over time. Quantitative MRI and MPM protocol were used to analyse the change in brain microstructure because conventional MRI does not detect changes in normal appearing brain tissue [7].

This study involves two groups. The first involves 36 MS patients and the second 36 age-matched healthy controls. This study compares these two groups.

After data processing (segmentation, normalization, smoothing), a statistical analysis on voxel values of quantitative parametric maps highlights that patients with multiple sclerosis have a lower value in MT, R_2^* and R_1 within normal-looking cortical GM and normal-appearing WM. However, in normal appearing deeps GM, MT value is smaller but R_2^* and R_1 values do not significantly differ. Furthermore, cognitive score was related

to MT within lesions, which was not suspected at all beforehand. This study also showed the link between atrophy and changes in quantitative parameters [7].

2.3.4 Conclusion

These previous studies highlight the interest of using qMRIs. The analysis of these quantitative maps allows the extraction of microstructural information, which is not possible with conventional images.

In this work, the same idea as these previous studies has been considered. Quantitative MRIs are used for the same reasons as in these studies. The aim is to extract more information that cannot be seen with the naked eye or by volume change. This additional quantitative information could highlight brain plasticity and changes in the microstructure of brain tissue that could be located in the healthy-looking part of the brain. With quantitative maps, the detection of abnormal variation in brain tissue could be faster and thus give earlier warning of a disease that already exists or is about to appear. Quantitative maps could therefore be useful to prevent a possible relapse of a cured patient, for example.

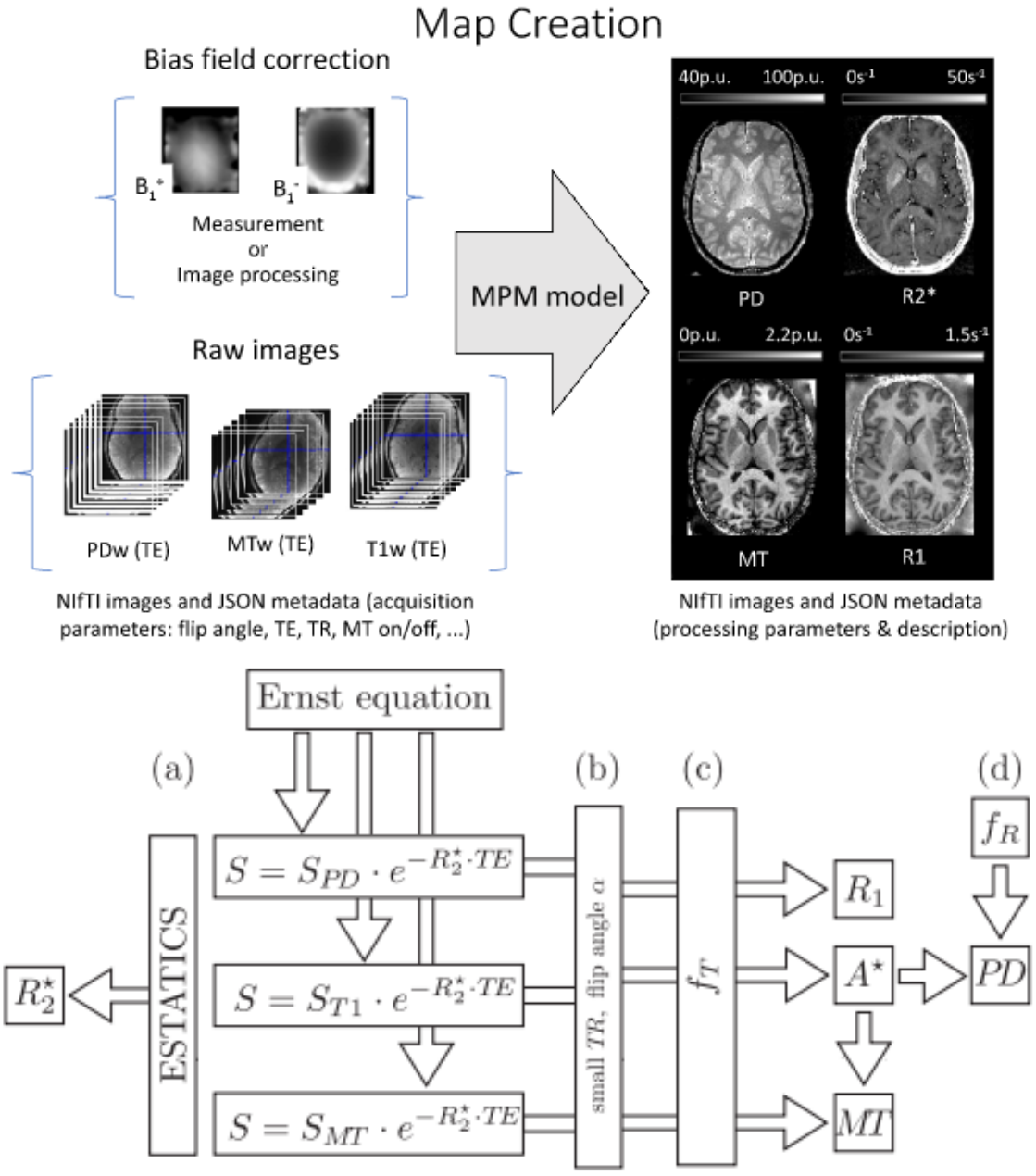

FIGURE 2.2: MPM creation [10].

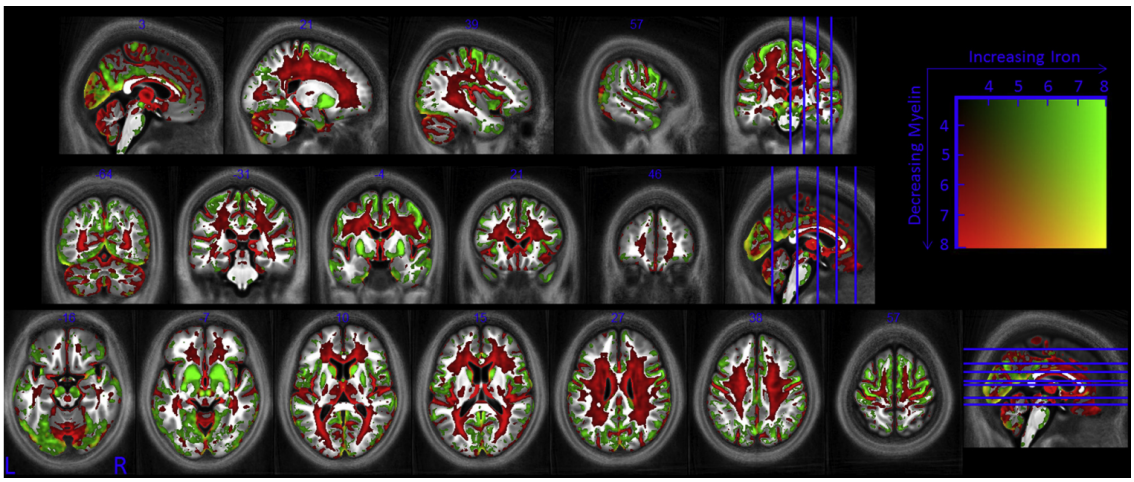

FIGURE 2.3: Whole brain pattern of aging. Demyelination is reflected by a decrease in the MT and R_1 signal. An increase in the R_2^* signal means an increase in the iron level. This figure shows the results of a t-test with an uncorrected p of 0.001. [11]

Chapter 3

Materials

This chapter refers to the material resources used for this master thesis. First, it explains the data used in this work. Secondly, it explains the method used previously by the University College London to find an a priori mask of the damaged areas in the brain.

3.1 Data

The data used has been acquired at the National Hospital for Neurology and Neurosurgery-University College London. Participants were scanned in a 3T whole body MR system (Magnetom TIM Trio, Siemens Healthcare, Erlangen, Germany) using the standard 32 channel transmitter-receiver headcoil. The data used in this master thesis are listed in this section. This thesis focuses on using the 4 parametric maps obtained via the MPM approach and to analyse them.

3.1.1 Patients

Data has been collected from 29 patients. All patients are English native speakers who had a left hemisphere stroke for at least 5 months before the scanning session. In addition, they present premorbid right handedness and have a normal or corrected to normal vision and hearing.

In addition to raw data, there were, for each patient, 4 quantitative maps as well as the lesion mask obtained with the ALI method.

- **Quantitative maps:** The quantitative maps A, MT, R_1 and R_2^* were previously acquired. Note that the quantitative map A is directly related to the proton density but is different from the quantitative map PD. The FIGURE 3.1 shows the qMRIs of Patient 35.
- **Lesion masks:** All images obtained by the ALI method (see 3.2) were provided. Among these images, there are the tissue probability maps of GM, WM, lesions and CSF, the deformation indices to go from subject space to MNI space and vice versa and the lesion mask obtained.

All subject-specific information are listed in the TABLE A.2 in the Appendix. This information, such as age, gender, time after stroke and scores obtained in the linguistic assessment, is necessary for the statistical analysis. The different linguistic tests performed in this study are detailed in section 5.1.

Two patients, P32 and P34, were removed from the study because the information on these patients was not complete. Patient P14 was also removed from the study because the mask obtained with the ALI method was completely wrong (outside the brain). Poor

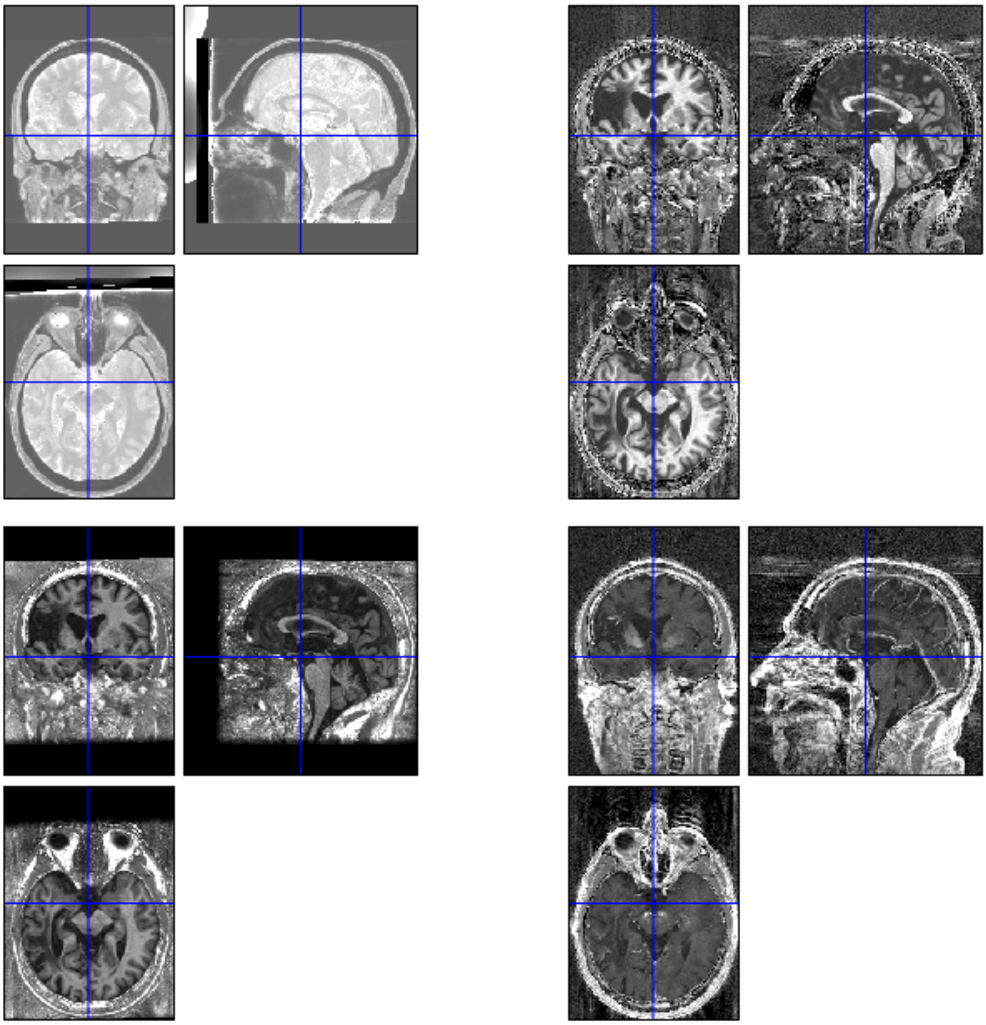

FIGURE 3.1: Quantitative maps of patient 35. From left to right and top to bottom: A, MT, R_1 and R_2^* maps.

normalization with the ALI method for this subject could explain this unlikely result. Furthermore, the A map of patient 16 contains outliers for GM and WM and will therefore not be used in the statistical analyses.

3.1.2 Control subjects

Similar to the patient data, raw data and qMRI from 17 healthy individuals were available. An example of qMRIs is represented in FIGURE 3.2. This FIGURE shows the qMRIs corresponding to control number 23. The selection of healthy subjects was based on the age of the patients in order to feature age-matched controls.

It was relevant that the controls were of a similar age to that of the patients. Indeed, there are changes in the brain with age such as: significant demyelination (principally in the WM), GM volume reduction, decrease and increase in iron concentration in specific regions [11]. If an elderly control is compared with a young patient, the microstructural

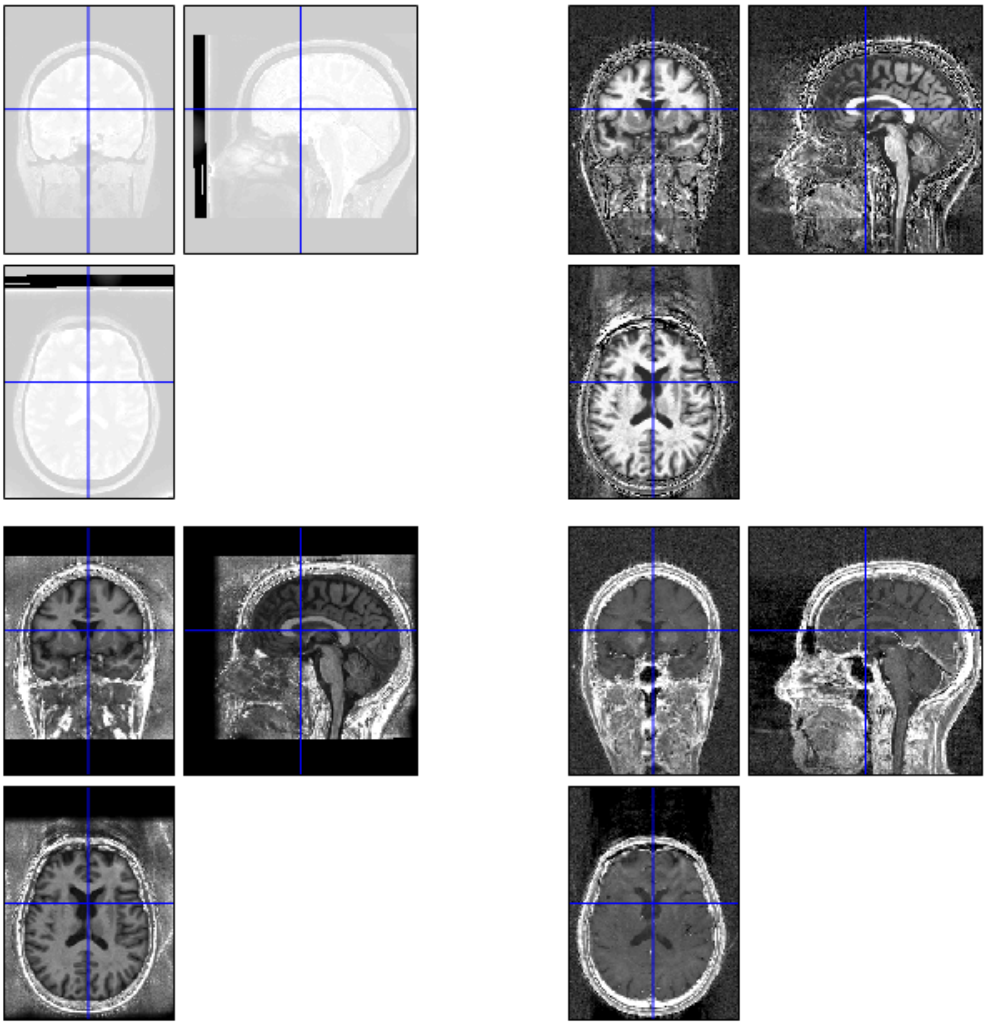

FIGURE 3.2: Quantitative maps of healthy control subject 23. From left to right and top to bottom: A, MT, R_1 and R_2^* maps.

changes in the brain tissue may reflect this age difference and thus not only the differences due to stroke as desired [12].

3.2 Automatic Lesion Identification

As explained in Chapter 1, this work is a continuation of a study carried out within University College London. Lesional masks have already been detected using the Automatic Lesion Identification (ALI) method. FIGURE 3.3 shows two examples of masks obtained by ALI method, one for patient 3 and one for patient 35. This section explains the different steps to obtain these masks.

The segmentation method implemented in SPM 12 is designed for non-injured brains. Therefore, another method must be found when analysing a lesioned brain. The first step in analysing such a brain is to detect where the lesion is located. A method based on

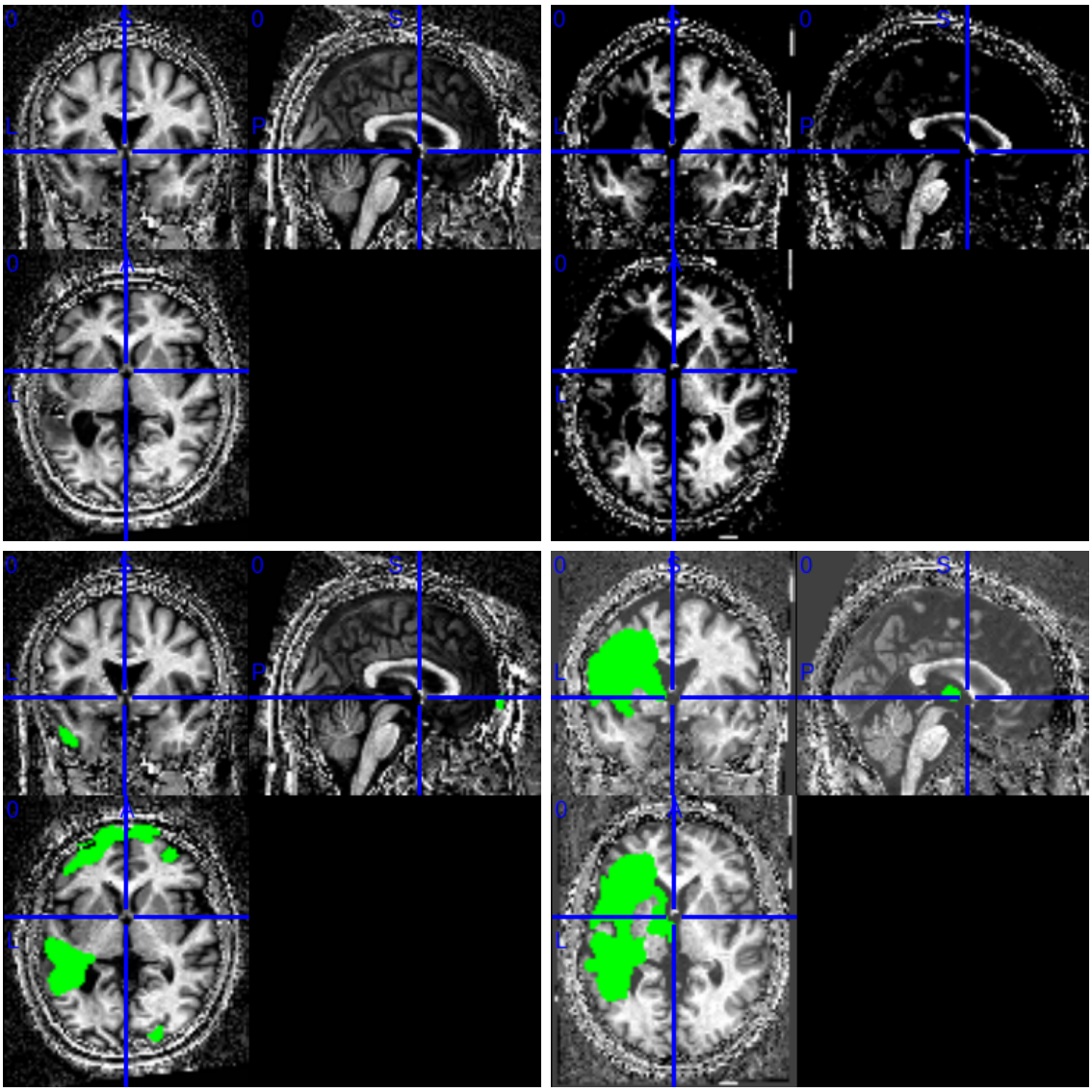

FIGURE 3.3: ALI mask in green superimposed on warped MT qMRI. Left: Patient 3; Right: Patient 35.

quantitative voxel values has been previously used to detect an a priori mask of lesions. This method is "Automatic Lesion Identification" (ALI).

In this ALI method, lesion voxels are supposed to be those with particular GM or WM values, which deviate from the usual tissue value found in controls. Therefore, this method considers lesions as outliers in GM and WM tissues [12]. Due to financial and time constraints in clinical studies using MRI, it is not uncommon for only one anatomical image to be acquired to perform these studies. Typically, it is the T_1-weighted image that is acquired. The advantage of the ALI method is that only one reference anatomical image is required to use the method [12]. Furthermore, this method is valid for any brain lesion, regardless of size and location [12].

The ALI method consists in 4 main steps [12]

1. Segmentation and normalization of the reference anatomical image.
2. Smoothing of normalized GM and WM segments.

3. Outlier detection
4. Outlier voxels assignation to the lesion class

The FIGURE 3.4 schematizes and illustrates the different steps of ALI method.

3.2.1 Segmentation and normalization

First, the segmentation is performed on the reference anatomical image by using a modified segmentation procedure of the unified segmentation-normalization implemented in SPM software in Matlab [12]. Indeed, using the unified segmentation-normalization, the damaged voxels are misclassified, identified as healthy tissue even if their values differ. A modified procedure is thus necessary. The solution is to add a class to the algorithm. Thus, there would be a lesion class in addition to the GM, WM and CSF classes. A voxel belongs to this lesion class if its value deviates from the values expected in the other tissue classes. It turns out that lesions are more evident in WM than in GM. Therefore, it was decided to ignore the GM when calculating the spatial prior of the lesion class. The prior of this class is defined as [12]:

$$P_{extra} = \frac{P_{WM} + P_{CSF}}{2}, \tag{3.1}$$

where P_{WM} is the standard priors of WM and P_{CSF} the one corresponding to the CSF.

Following this segmentation with the addition of the lesion class, some abnormal voxels are still misclassified. To overcome this issue, the segmentation method can be applied iteratively by considering the estimated extra class acting as prior to the next generation in order to gradually decrease the number of misclassified voxels.

3.2.2 Smoothing

Smoothing reduces noise and variability between different segmented images, making it easier to compare them. It should be noted that only lesions within GM or WM are detected using the ALI method. Therefore, smoothing is performed only on GM and WM. A Gaussian kernel of 8 mm FWHM is applied [12]. If the method is applied to identify tiny lesions, it is better to use low smoothing.

3.2.3 Outliers detection

Each voxel belonging to a lesioned segment in the GM is compared to the corresponding voxel in a healthy brain. When the voxel in the lesioned brain has a very low probability of belonging to GM, it is part of the fuzzy set F_{GM}. The same method is applied to the WM to find the fuzzy set F_{WM} [12].

3.2.4 Grouping GM and WM lesions

Once the two fuzzy clustering of outliers F_{GM} and F_{WM} are determined, they must be combined to obtain the fuzzy set F_{les}. Indeed, F_{GM} and F_{WM} represent voxels that have a very low probability of belonging to GM and WM respectively. There is therefore a high probability that they are part of F_{les}. The fuzzy set of lesion class is determined by the union of F_{GM} and F_{WM} :

$$F_{LES} = F_{GM} \cup F_{WM} = max(F_{GM}, F_{WM}) \tag{3.2}$$

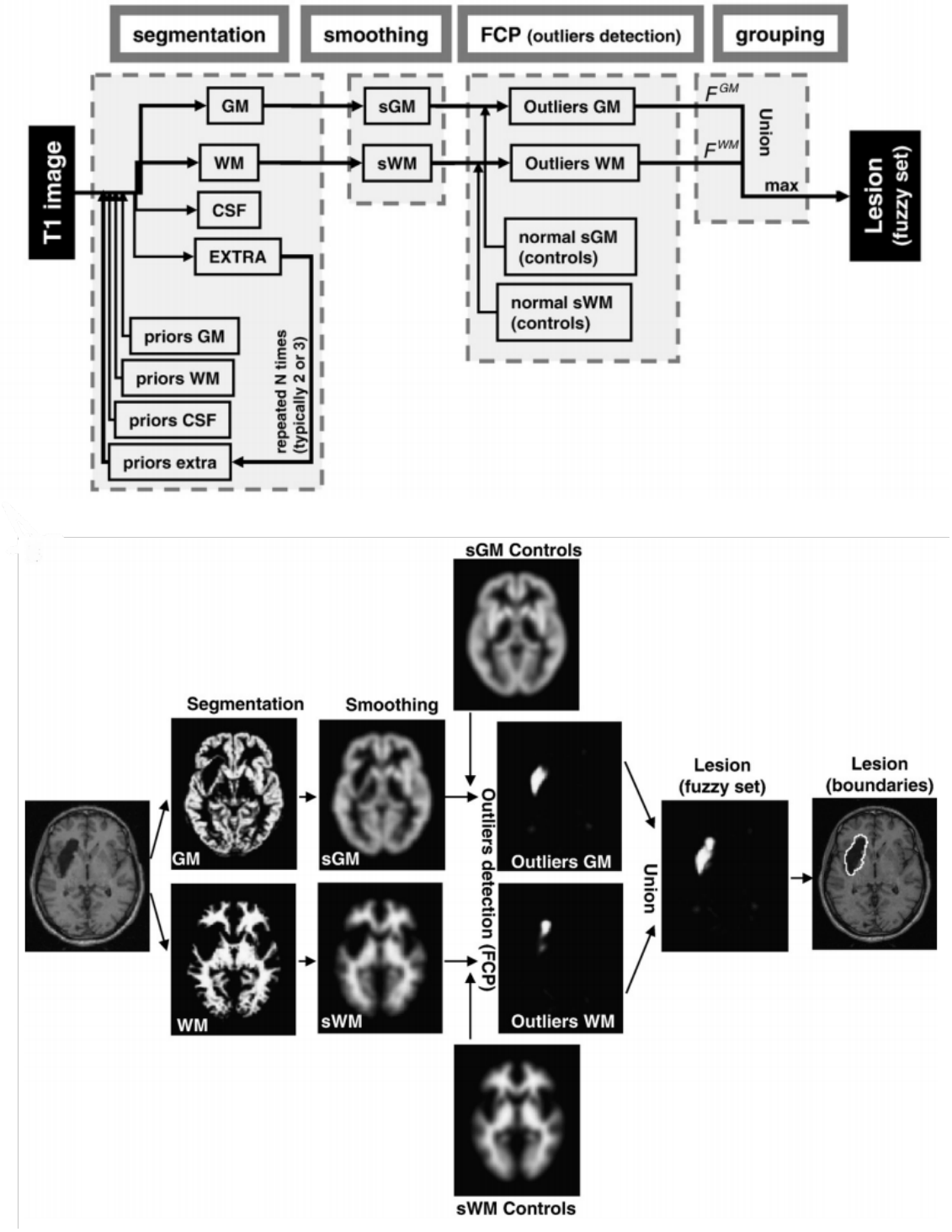

FIGURE 3.4: Schematic view of the different steps and illustration, from segmentation to grouping, of the automatic lesion identification method [12].

Chapter 4

Methods

This chapter describes the different processing steps carried out on patients and control data in order to achieve the aim of the work. As a reminder, the idea is, using qMRIs, to detect structural brain plasticity and tissue microstructure properties changes in aphasic stroke patients with anomia diagnosis. All processing is done with SPM12 and some home-made scripts.

The first part of this chapter describes the pipeline used to process both the patients and control data. The processing on the control data was adjusted to be as close as possible to the one applied to the patients in order to compare the quantitative values of the brain tissues between the two groups.

The second part explains an alternative pipeline applied to the control subjects which differs from the one used on patients. This section highlights the importance of using the same pipelines on both groups of data that one wishes to compare in order to avoid introducing bias in the results.

4.1 Similar pipeline for patients and control subjects

4.1.1 Spatial pre-processing

The patient data, in contrast to the data from healthy subjects, contains lesioned tissue. Therefore, a modified version of the segmentation method used on healthy subjects must be used to introduce the lesion class. The segmentation of lesioned brains requires an additional step compared to healthy brains. Indeed, in order to perform the segmentation on patients using the USwL method, it is necessary to have an idea of the location of the lesion and therefore to have an a priori mask. Thereby, an a priori lesion mask must be defined before starting the segmentation of the lesioned brain.

Masks cleaning

It is necessary to have approximate lesion masks to use the Unified Segmentation with Lesion (USwL) approach. The ALI approach previously performed on the data provided a lesion mask. A visual check of the masks given by the ALI method was performed. After this visual inspection, the masks were cleaned. Some masks obtained with the ALI method contained small portions in inappropriate places, where the brain appeared to be healthy. For most patients, keeping the largest lesion found by ALI when the MT image was the input image of ALI method seemed to be a good solution. Nevertheless, for the others the processing to obtain some masks had to be adapted. TABLE 4.1 shows all the masks that have undergone different pre-processing.

Subject	Mask description	Mask cleaning
01	The mask extends into the right hemisphere covering the ventricles.	The lesioned part of the right hemisphere was removed by setting the voxels to 0.
11	The mask extends slightly into the right hemisphere and three small volumes are badly segmented as lesion	The lesioned part of the right hemisphere was removed by setting the voxels to 0 and only the biggest volume is kept for the lesion
14	Normalization with ALI seems to have failed, the mask is outside the brain	This patient is not included in this work.
18	The mask extends into the right hemisphere covering the ventricles.	The lesioned part of the right hemisphere was removed by setting the voxels to 0 and only the biggest volume is kept for the lesion
21	The mask extends slightly into the right hemisphere.	The lesioned part of the right hemisphere was removed by setting the voxels to 0 and only the biggest volume is kept for the lesion.
24	The mask extends slightly into the right hemisphere for no reason.	The lesioned part of the right hemisphere was removed by setting the voxels to 0.
25	The mask extends slightly into the right hemisphere covering a part of ventricule.	The lesioned part of the right hemisphere was removed by setting the voxels to 0 and only the bigger volume is keeped for the lesion.
34	The lesion mask contains 4 separated parts. The two larger ones are indeed lesions while the two smaller ones are segmentation errors and are not lesions	The two largest lesions are kept with a threshold of 1200 mm^3 on the volume

TABLE 4.1: Tips for cleaning uncommon masks.

Masks in the subject space

The USwL approach needs a predefined lesion mask in the subject space. However, the masks in the dataset received from London is normalized in MNI space. Therefore, the cleaned masks must be uned to obtain masks in subject space. Knowing the deformations from MNI space to subject space (this information was included in the data), the inverse normalization was easily done using NORMALIZE WRITE module in the SPM Batch. Since this is a deformation of a binary image because it is a mask, a nearest-neighbours interpolation has been performed.

Co-register

In order to run the USwL method with images of the same size that have identical coordinates, the mask images were aligned with the qMRI images. This correction has been achieved using COREGISTER-RESLICE module in the SPM Batch.

4.1.2 VBM

The VBM analysis provides information on the volumes of each tissue by observing the concentrations of voxels in the standard MNI space. There is a density modulation by the volume change induced by the elastic ing of the image. If the tissue had to be stretched during the fitting to be in the MNI space, its proportion in the corresponding voxel will have decreased in order to preserve the total volume of the tissue. Conversely, a compressed tissue will have a higher concentration. [3, 41] VBM is a data processing and statistical analysis approach which uses template priors and a segmentation method to extract some information in the image [12] and specifically the morphological changes [39], relying on estimated maps of local tissue volume/density. In this work, the VBM analysis for the stroke patient data is performed using `USwLesion` toolbox and the data from the control subjects is performed using the segmentation process implemented in `hMRI toolbox`.

Segmentation and normalization on patient data

Once the lesion masks were cleaned, in the subject space and aligned with the qMRI images, the USwL approach could be performed. The `toolbox USwL` has been developed by the University of Liege and is compatible with `SPM12` on Matlab. The method used is the same as in the usual US approach available in `SPM12` which normalizes brain images into a standard reference space and gives posterior probability maps of the brain tissue for healthy tissue [20]. In USwL, the algorithm is adapted to handle brain lesions. In this case, compared to US approach, a tissue class, the lesion class, is added. Indeed, in USwL approach, the standard tissue probability map (TPM) used for healthy brain is extended by adding a subject-specific lesion probability map. This extension is derived by estimating a preliminary spatial deformation from subject to the MNI space and carefully updating the TPM with a new tissue class, the lesion class, showing which healthy tissue class can be affected by the lesion [22].

The FIGURE 4.1 shows the USwL method. First, this method takes as input the standard healthy TPM. The TABLE 4.2 indicates which class correspond at which tissue.

Class numbers	1	2	3	4	5	6
Tissues	GM	WM	CSF	skull	soft tissues	air

TABLE 4.2: Different classes considered in the TPM of the healthy brain.

In addition of standard healthy TPM, there are the patient's anatomical reference MRI (in our case, the T1-weighted image), the patient's approximate lesion mask (in our case, the mask obtained with ALI method) and the patient's multiple anatomical MRIs (in our case, the A, R1 and MT qMRIs).

First step: The first step of USwL consists in masking out the patient's anatomical reference image with the approximate mask and segmenting the masked out resulting image, which only shows healthy tissues.

Second step: The estimated deformation is then applied to the approximate mask to bring this one into the same space as the TPMs.

Third step: "TPM updating" is performed, adding a seventh class, the lesion class, to take lesions into account along with affected healthy tissue [22], e.g. GM and WM for an anomia stroke patient. The lesion class is inserted in third position between WM and CSF. This first segmentation, which adds the class of lesions, is based only on the anatomical reference image, the T1-weighted image.

Fourth step: A second segmentation based on the new subject-specific TPM is performed. This second segmentation takes into account additional information from the quantitative images A, R1 and MT. Therefore, since the segmentation is based on more than one image, this second segmentation is a multichannel segmentation.

Fifth step: All the patient's images and posterior probability tissue maps (for GM, WM and CSF) are warped into the MNI common space. After the normalization, a modulation (i.e. scaling the warped images by the Jacobian determinants [46]) is applied to the warped probability maps in order to preserve the quantity representing the total volume of each tissue.

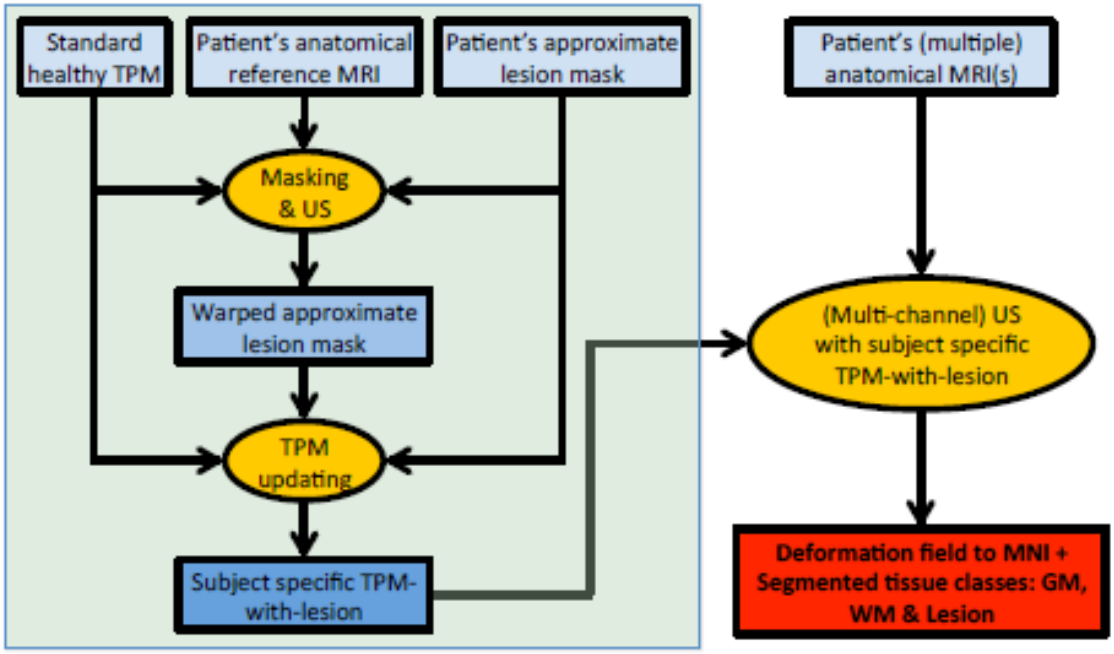

FIGURE 4.1: Unified segmentation with lesions [22].

The use of multiple patient's anatomical MRIs has already been successful in a previous study on multiple sclerosis [7] and the use of the multi-channel approach with different qMRIs was also successful in that study. The multi-variate approach with well-contrasted patient's anatomical MRIs can be useful. Indeed, lesion voxel values may be similar in one tissue class for one qMRI but quite different in another. In our case, since we are using A, MT and R_1 qMRIs as anatomical MRIs, there are 3 values that are different in nature per voxel. The more anatomical MRIs there are at the input and therefore the more variables there are in the multi-variate model, the more hope there is that the

lesion has a different value on at least one of the dimensions. It is for this reason that the multi-variate approach has been used here. This allowed to use the advantage of having several anatomical images at our disposal but note that R_2^* map is not used to perform USwL. The R_2^* map was not included to add a variable in the USwL multi-variate approach because the image is noisy and not well contrasted.

Knowing that WM and GM can be directly affected by this type of lesion [15], the USwL implementation is launched with the constraint that the WM and GM are potentially affected by the lesion and therefore may need to be updated. Furthermore, a bias correction is applied with a light regularization (0.001) and a 60 mm cutoff. MRI images are usually biased by a smooth artefact that modulates the intensity of the image, which can hamper automated image processing. In addition, an intra-cranial volume (ICV) mask is applied on the images. The qMR image showing high intensity noise outside the brain, it is relevant to suppress everything outside the brain because only the tissue inside the brain is of interest for this work.

In summary, after the application of USwL method, images are segmented (i.e. probability maps of each brain tissue are estimated) and normalized (i.e. registered into a common space). FIGURE 4.2 shows the results of segmentation and normalization on two patients. By observing the segmented images, it can be concluded that the USwL processing has worked correctly.

Segmentation and normalization on control subjects

For the 17 control subjects, the same process as applied to the patients is used. However, here there is obviously no lesion class and since the tissue distribution in a healthy subject is already more or less known, the segmentation process in controls is much easier compared to patients. The US method, implemented in hMRI toolbox, which does not include the lesion class can be used. The segmentation and normalization process is therefore simplified, with one less class for the controls. In fact, the segmentation and normalization process for the control subjects is equivalent to the second part of the USwL process. FIGURE 4.3 illustrates the segmentation and normalization process of the control subjects. It is important to carry out similar processing on patients and healthy subjects in order to be able to compare the results obtained in the two groups.

One of the spatial processing modules of the hMRI toolbox is called SEGMENTATION and takes care of both segmentation and normalization of the data. In order to ensure that the segmentation parameters are equivalent in patients and controls, a multi-channel segmentation is performed with the 3 parametric maps A, MT, R1. In addition, as in the patient processing, an intensity bias correction is applied to multiple anatomical MRIs, i.e. on A, MT and R_1 qMRIs. This bias correction has a light regularization (0.001) and 60 mm cutoff for the bias FWHM in order to apply exactly the same correction as on the patient data. Then the normalization is performed with a nonlinear spatial registration by warping the images to align them in the MNI space.

FIGURE 4.4 shows the results obtained on subject control 01 and control 23 after segmentation and normalization. The segmentation of the 3 tissue classes looks all fine. These images show that the images in the subject space have been warped in a common standard space and that the normalization has been carried out without incident.

4.1.3 VBQ

Warped qMRIs

The VBQ analysis is applied to the warped qMRIs. However, at this stage, these maps are not yet created for patient data. To compensate for this, a normalization of the qMRIs is carried out on patient qMRI. The USwL method outputs the deformation from subject space to MNI space. This deformation is then applied to the patients' qMRIs to obtain the warped qMRIs in the MNI space. For the control subjects, the warped qMRI were already created at this step because they are created directly with the SEGMENTATION module of the hMRI toolbox.

One way of finding out whether the normalization went well is to create the 4 average maps of the 4 warped qMRI types (A, MT, R_1 and R_2^*). FIGURE 4.5 shows the different averages of the patients warped qMRIs whereas FIGURE 4.6 is the one related to the control subjects. By observing the different contrasts between the tissues in each image, it can be concluded that the normalization went smoothly. Mean qMRI images of both patients and controls maps have also been created. These mean images of all subjects can be used as representative anatomical maps of the data being processed. A visual way to observe the results is to superimpose the significant voxels, found during the statistical analysis, on these anatomical maps when the two groups are compared.

Tissue specific smoothing

Although the images have been warped to be in the common MNI space, there are residual misalignments between the subjects as well as some potential noise in the images. Smoothing allows to reduce noise and the remaining inter-subject anatomical variability [10, 12]. Smoothing must be used carefully with an adequate method to preserve the quantitative character of the qMRIs. Indeed, the problem with quantitative maps is that a certain value is attributed to GM and another to WM. If one blurs the image, one mixes the signal from different tissues, WM with GM for example. This would introduce a partial volume effect. The solution to overcome this problem is to perform a tissue class specific smoothing, taking into account the amount of tissues in each voxel when not mixed, thus the quantitative values can still be interpreted. In tissue specific smoothing, the signal is not modulated. Here, the aim is to preserve the concentration and not the volume. Therefore, in tissue specific smoothing, unlike in VBM analysis, there is no modulation so that the different tissue classes are not mixed [10, 43]. This approach to smooth within a specific tissue when a VBQ analysis is performed was introduced in a previous study to detect changes in normal ageing [4].

For both patients and control subjects, this tissue specific smoothing has been realized thanks to the `hMRI toolbox`. The paper [10] describes this tool which allows to create MPM maps. There is in this toolbox a process hMRI maps module of which one of the spatial processing operations is tissue-weighted smoothing. Using this part of the hMRI toolbox, tissue specific smoothing for GM and WM, was applied to the warped qMRIs. A Gaussian smoothing of 6 mm seems to be a good compromise to minimize the variations between subjects while keeping sufficient spatial resolution.

This combination of weighted and smoothing is carried out in the following way [4, 10, 43]:

$$\text{signal}_{TWS} = \frac{g * w_j s(\phi_j)}{g * w_j} m_{TPM} m_j \tag{4.1}$$

where,

- signal_{TWS} is the signal in the resulting tissue-weighted smoothed image
- g* indicates the convolution with a Gaussian smoothing kernel
- w_j is the tissue weights for the participant j in the MNI space
- $s(\phi_j)$ represents participant-specific quantitative map warped to group space by deformation ϕ_j
- m_{TPM} is the TPM-specific mask identifying voxels with probability > 5%. Only voxels with a minimum amount of available tissue are considered.
- m_j is the participant-specific mask defined as $g * w_j > 5\%$. Voxel with a value smaller than 5% are set to zero.

The smoothed tissue class of the participant j is thus represented by $g * w_j$ which is in the denominator in Equation 4.1. Thus the resulting signal takes into account the entire class of tissue.

Mask creation

This smoothing allows to facilitate comparison between individuals. Indeed, spatial smoothing minimizes inter-subject anatomical variability during the creation of the GM mask and the WM mask.

Note that after smoothing, a voxel can belong to several tissue classes. Therefore, creating a tissue specific binary mask is useful to ensure that a given voxel belongs to only one class. The mask creation is the next step after the smoothing. To create masks, the MASK CREATION module of `hMRI toolbox` is used. This step, which follows smoothing, makes it possible to associate each voxel with a single class of interest, GM and WM, or none. The idea is to look at the whole population. At this stage, for each patient we have the smoothing of modulated warped tissue segments for the GM tissue and the WM tissue. However, one considers that the patient brain is composed of GM, WM but also CSF and lesions. Therefore, the data corresponding to the CSF and lesions must also be entered as input. Since the algorithm for creating the masks only takes smoothed images as input, the images representing the CSF and lesion probability maps in MNI space were simply smoothed with the SMOOTHING module implemented in SPM. For these two classes of tissues, tissue specific smoothing was not used as the smoothed parametric maps of these tissues are not required to perform the voxel-wise mapping analysis.

The algorithm creating the masks takes all these smoothed tissue maps and gives a percentage of belonging to each tissue class for each voxel. Then the tissue with the highest average probability map for a certain voxel is assigned to that voxel. However, in addition to having the highest probability to belong to a tissue, the average probability of the voxel must exceed 20% for the voxel to be included in the mask. This makes it possible to have a delimitation, that the GM does not extend outside the brain, for example. These two conditions to belong to the mask ensure that only one class is associated at a specific voxel and that non-brain tissues are excluded.

The creation of the tissue masks is carried out in the same way in the control subjects, except that there is no lesion class.

4.2 Alternative pipeline for control data

The `hMRI toolbox` contains a pre-defined spatial processing pipeline wrapping up all the steps to perform the spatial processing. Once started, this processing performs segmentation, normalization, tissue-weighted smoothing and mask creation in one go with the process and the parameters previously encoded.

In order to get a first idea and to use a previously implemented tool, one started to play with the control data by applying this pipeline. However, this latter is a bit different from the one used on the patient data. Indeed, it performs the segmentation based on a single anatomical image (uni-channel US). The MT map was used as anatomical image. Furthermore, no bias correction is applied on the anatomical image given as input to the program. Nevertheless, as can be seen in FIGURE 4.7, it seems to segment the different tissues and warp into MNI space just as well.

The processing of the controlled data using this pipeline has allowed to get a taste of the results we could obtain. By using two different pipelines, one can observe whether the processing on the data has an influence on the voxel values and thus whether the result is influenced by the processing (see section 6.3).

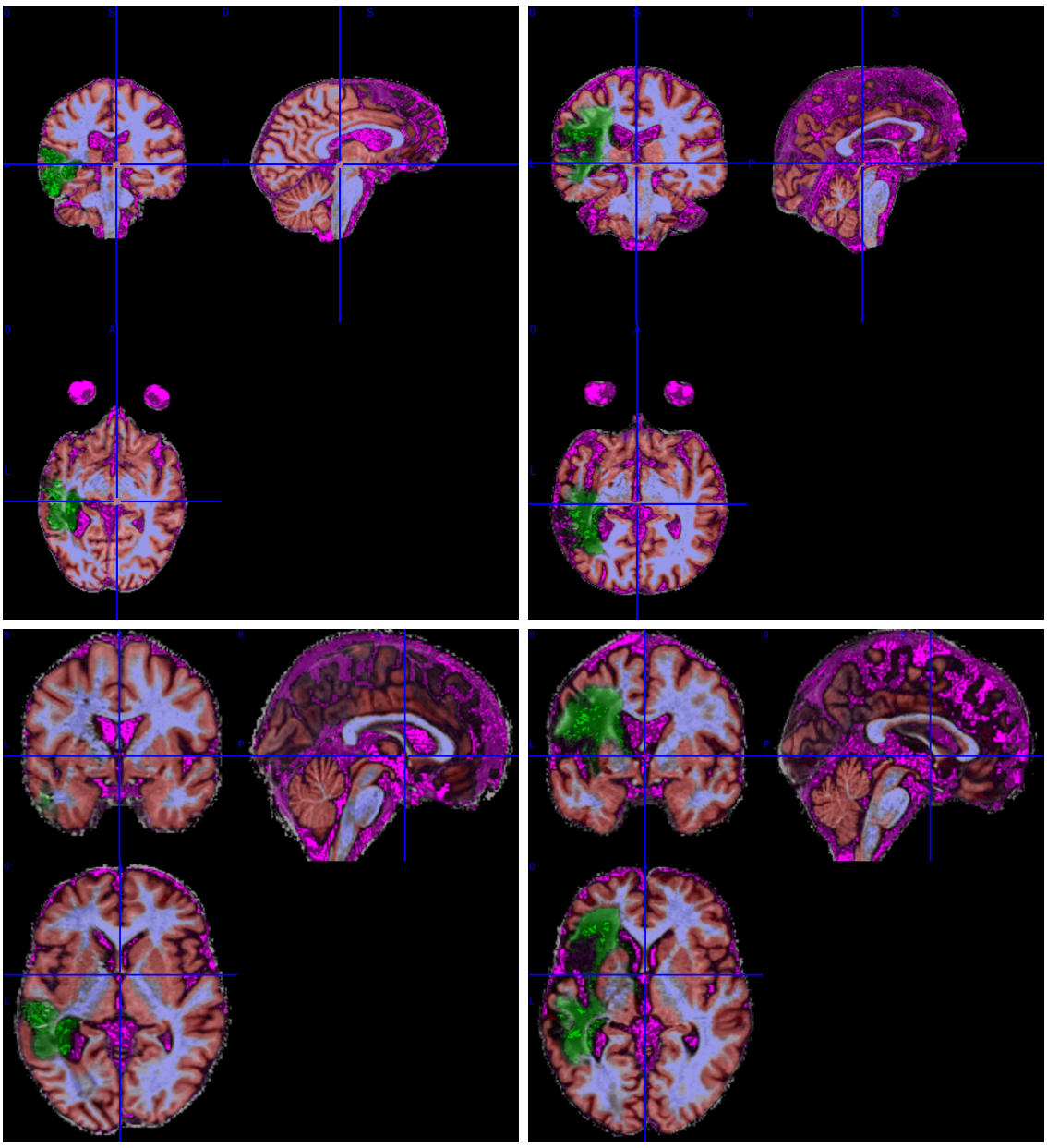

FIGURE 4.2: Superposition of the 4 main classes of tissues: GM (red), WM (light blue), CSF (purple) and lesion (green). Left: Patient 3; Right: Patient 35; Top: subject space; Bottom: MNI space.

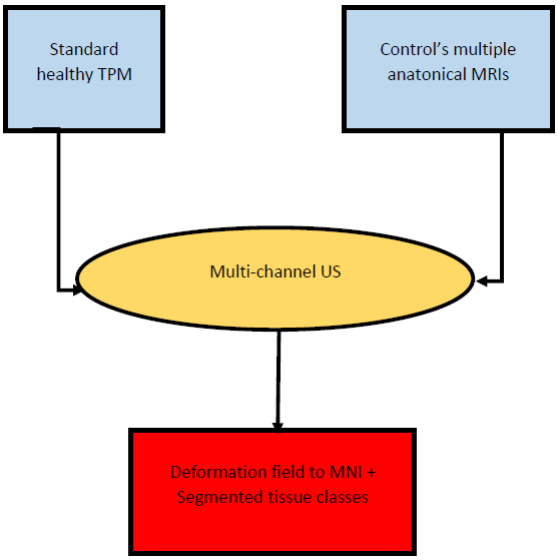

FIGURE 4.3: Unified segmentation (adapted from [22]).

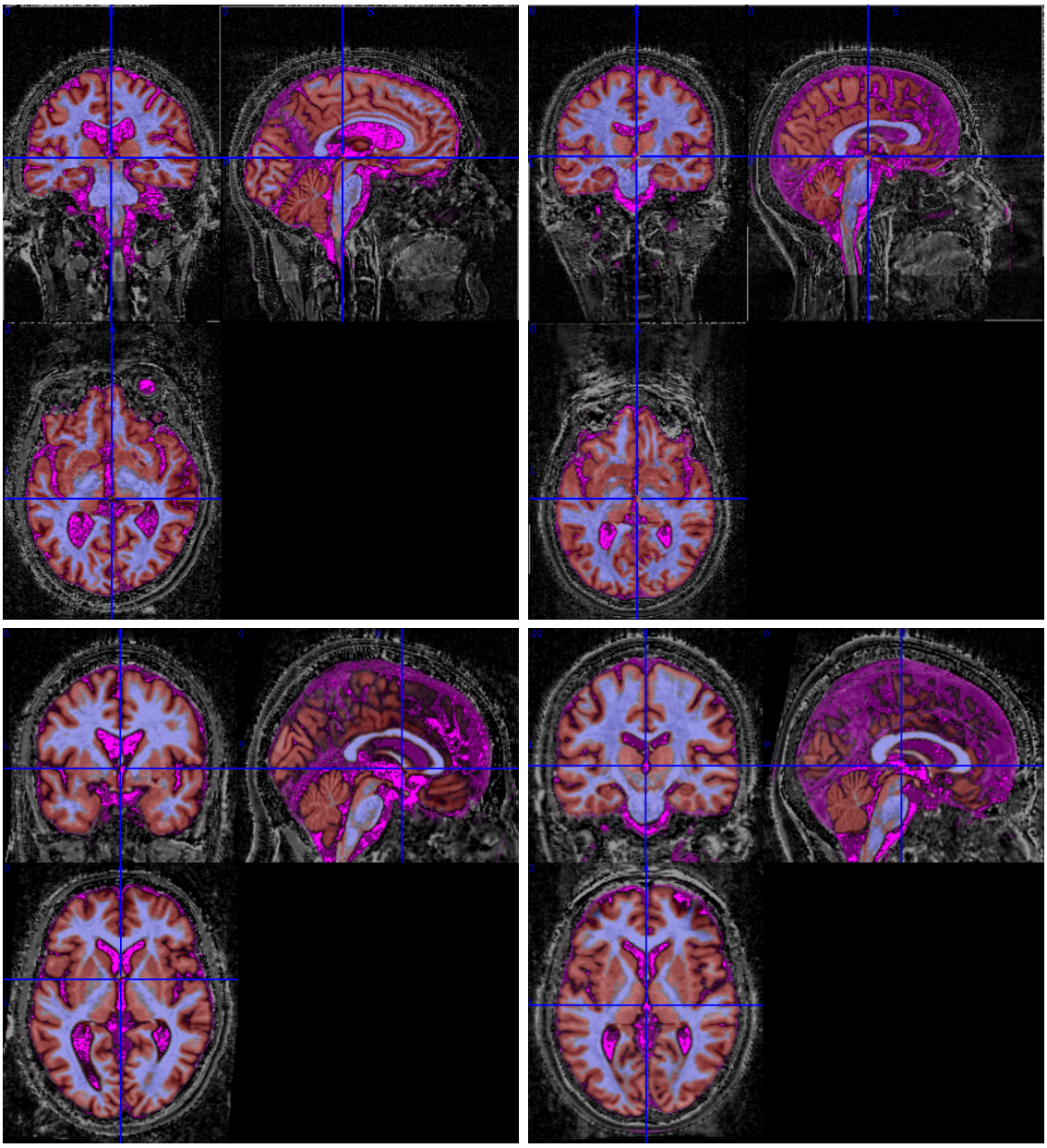

FIGURE 4.4: Superposition of the 3 main classes of tissues: GM (red), WM (light blue) and CSF (purple). Left: Control subject 001; Right: Control subject 23; Top: subject space; Bottom: MNI space.

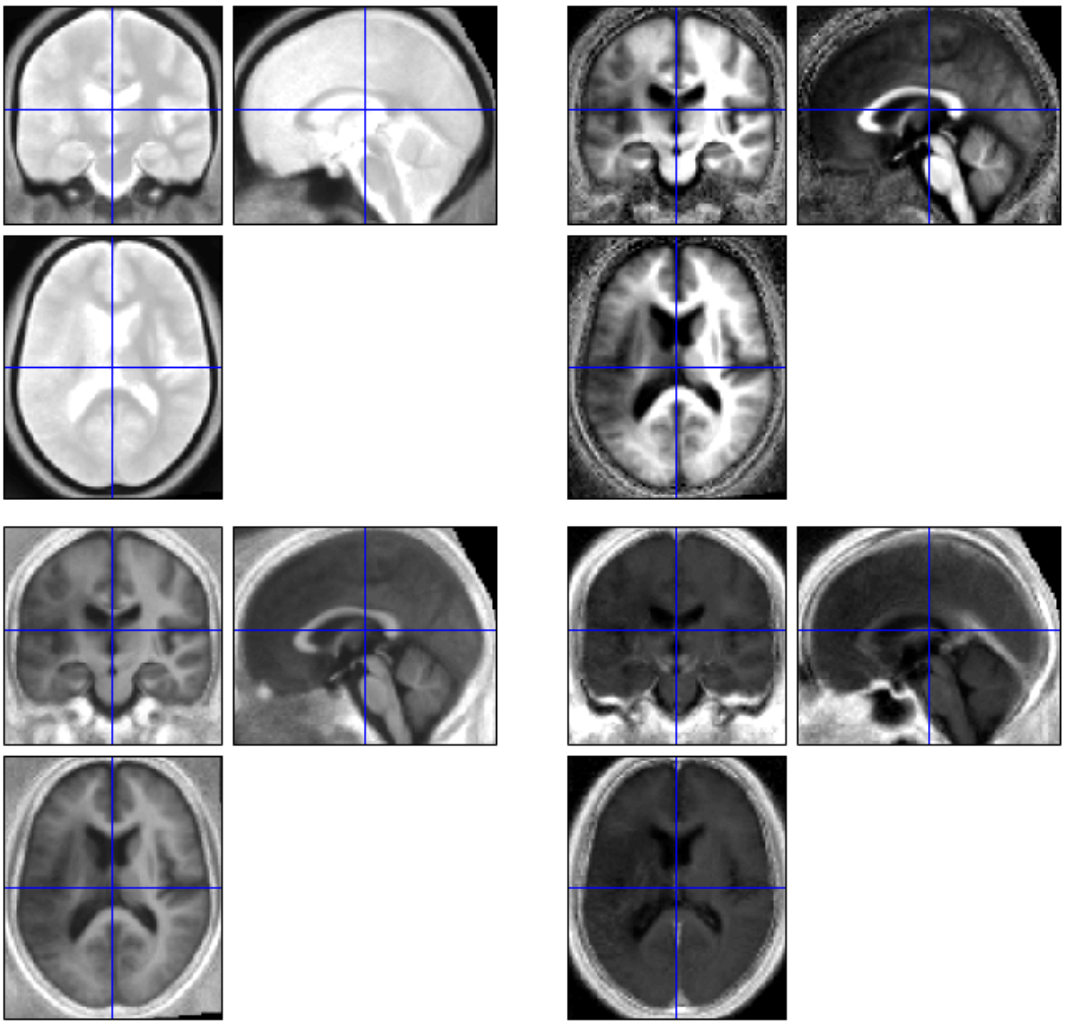

FIGURE 4.5: Mean of warped qMRI in the patients. From left to right and top to bottom: warped A qMRI, warped MT qMRI, warped R1 qMRI and warped R2s qMRI.

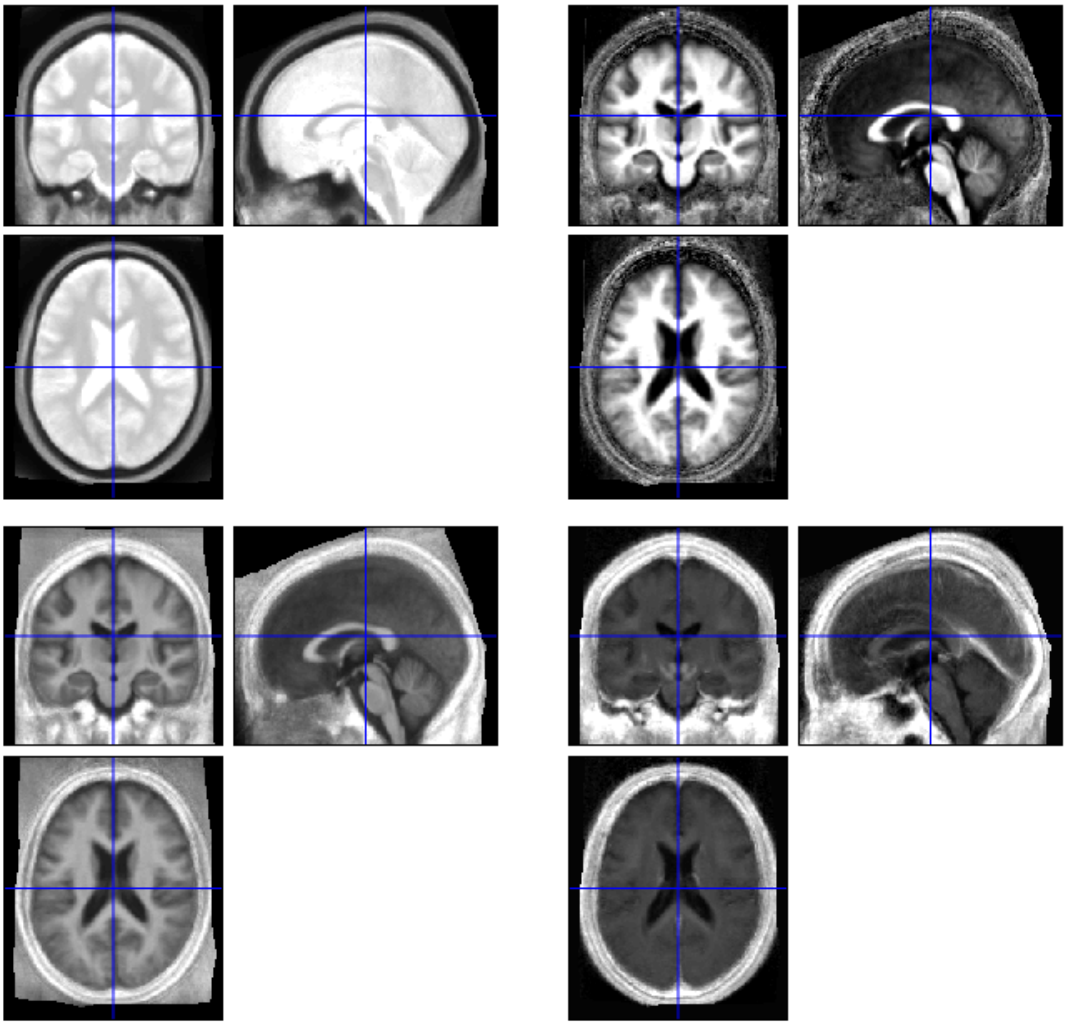

FIGURE 4.6: Mean of warped qMRI in the control subjects. From left to right and top to bottom: warped A qMRI, warped MT qMRI, warped R1 qMRI and warped R2s qMRI.

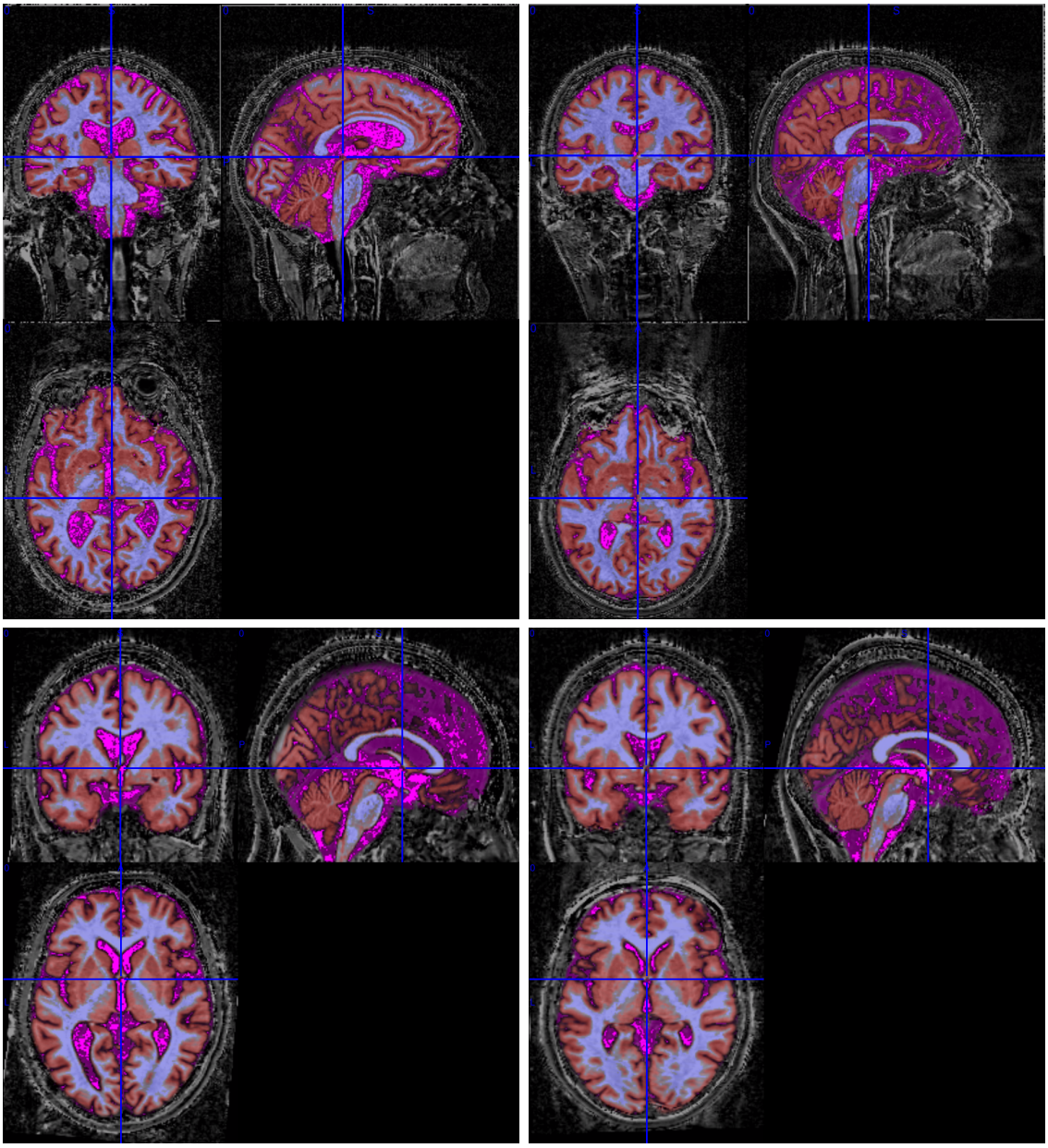

FIGURE 4.7: Superposition on control subjects using alternative pipeline of the 3 main classes of tissues: GM (red), WM (light blue) and CSF (purple). Left: Control subject 001; Right: Control subject 23; Top: subject space; Bottom: MNI space.

Chapter 5

Statistical Analysis

This chapter begins by explaining the set of parameters used for the statistical analyses. It then details the statistical analyses performed during this study and how they were carried out. These statistical analyses attempt to answer the two main questions of this study:

1. Are there any morphological or microstructural differences in the right hemisphere between patients and controls?
2. Are there microstructural differences between patients according to their performance?

A third, more methodologically oriented question was also addressed: Are there any differences between the results obtained on the control subjects with two different pipelines?

5.1 Parameters

Prof. J. Crinion provided a list of parameters for each subject that are likely to explain the results obtained by observing brain tissue. For the controls, the age and the gender are known (see A.1 to have information of these parameters for each control subject). For the patients, in addition to age, gender and post-stroke time, other information was provided (see A.2 for the values). This additional information is detailed in the subsections below.

5.1.1 Total lesional volume

Clinicians at the University College London had already computed the total volume of the lesions. The idea here is to calculate the lesion volume obtained after USwL processing in order to observe the difference between the volumes obtained using USwL and those obtained with the ALI method.

The USwL does not provide a binary lesion mask but a probability map representing the probability for each voxel to belong to the lesion class. In order to obtain a lesion mask and to be able to calculate its volume, the lesion probability maps were binarised.

This binarisation was carried out using the function `crc_binarise_segm` available in the `USwL toolbox`. This function takes as input the probability maps of GM, WM, CSF and lesion class in MNI space. It also needs a parameter imposing that the probability of the chosen class for the voxel must be greater than 0.2 and that the chosen class must be the most likely class. The function outputs the binary mask of each tissue for each subject. Therefore, the mask of the lesions in a specific patient is part of the output of the function `crc_binarise_segm`.

By running the function `crc_lesion_volumes` (also available in `USwL toolbox`) in with the lesion mask, the lesion volume is obtained. This function is called with the lesion mask of each patient to calculate the lesion volume for each patient. The lesion volumes obtained are shown for each patient in cm^3 in the TABLE A.2.

5.1.2 Boston naming test

As discussed in section 2.1.2, anomia is characterized by impairment of the ability to name objects. The Boston Naming Test (BNT) is performed on patients with anomia. This test measures the ability to name objects. It consists into showing to the subject images of objects (usually 60), with black and white lines, one after the other. For each image, the subject is given a 20 second interval to name it. In general, patients with anomia have greater difficulty in naming low frequency objects. [44]

For each image correctly named by the patient, 1 point is awarded. For each error, two types of cues can be given to the patient: a stimulus cue or a phonemic cue in order to facilitate the task. When the correct answer comes after a phonemic cue, it is not considered. Therefore, the total score reflects the number of correct responses obtained spontaneously or with the help of a stimulus cue. [44]

5.1.3 Comprehensive aphasia test

The comprehensive aphasia test (CAT) is relatively new, being published in 2005 [26]. This test gives a maximum of information on the language skills of the subjects in a reasonable time (90-120 min) [34].

In CAT, there are six specific points which are listed below:

- Naming objects (Nam-O)
- Naming actions (Nam-A)
- Comprehension of spoken words (Co-SW)
- Comprehension of written words (Co-WW)
- Comprehension of spoken sentences (Co-SS)
- Comprehension of written sentences (Co-WS)

The TABLE 5.1 provides information on the evaluation score. The cut-off is the threshold for being diagnosed as aphasic.

	Nam-O	**Nam-A**	**Co-SW**	**Co-WW**	**Co-SS**	**Co-WS**
Number items	24	5	15	15	16	16
Maximum score	48	10	30	30	32	32
Scoring with correct answer	2	2	2	2	2	2
Scoring with delayed response or self-correction	1	1	1	1	1	1
Scoring with incorrect answer	0	0	0	0	0	0
cut-off	43	8	25	27	27	23

TABLE 5.1: Parameters of comprehensive aphasia test.

5.1.4 Psycholinguistic assessment of language processing in aphasia

Psycholinguistic assessment of language processing in aphasia (PALPA) is a process for assessing patients undergoing treatment for aphasia. It was introduced in the 1980s. It is based on the assumption that the language system is composed of separate modules in the brain and that these can be impaired selectively by brain damage [33].

In the case of this study, three tasks were assessed. One task consisted of reciting monosyllabic words aloud (Mo-w). Another task consisted of repeating invented words, which do not exist (NW). The last one, named "word minimal pairs" (Min-P) is a subtest of the PALPA language battery - auditory discrimination of real word minimal words. For example, are the words man and van the same or are they different?

5.2 Controls vs Patients in right hemisphere

The aim of this study is to determine whether there is a change in the microstructures of the tissues in the hemisphere opposite to the injured one, i.e. in the healthy hemisphere. Is there plasticity in the right hemisphere to compensate for the lesions encountered in the left hemisphere? In order to answer this question, all the statistical analyses are carried out only in the part of the brain of interest to the study, i.e. in the right hemisphere.

5.2.1 Global statistical analysis

The global statistical analysis compares, patients against controls, for each tissue of interest the overall average of values over all the voxels belonging to the tissue in the right hemisphere.

The first step in extracting the voxel value of the tissues in the right hemisphere is to create a right hemisphere mask and a mask of each tissue which will be applied to each MPM map individually.

The mask of the right hemisphere is created from the ICV mask obtained by applying the USwL algorithm. This ICV mask corresponds to the inside of the skull (summation of GM, WM and CSF with the addition of smoothing). By taking this ICV mask in a normalized space and setting all the voxels of the left hemisphere to 0, the mask of the right hemisphere is obtained. The ICV mask and the right hemisphere mask are shown in the FIGURE 5.1.

For each subject, the probability maps of each tissue were found using the USwL method for patients and the US method for controls. As explained in 5.1.1, it is possible to extract the masks using the *crc_binarize_segm* function implemented in the USwL toolbox. Therefore, for each subject, the necessary masks for statistical analysis (i.e. GM and WM) are available.

By combining these tissue masks with the right hemisphere mask, we obtain the right hemisphere GM mask and the one of WM for each subject. FIGURE 5.2 shows the right hemispheric GM and WM mask in patient P35 and control C23.

Now, for each subject, the position of the voxels of each tissue class is known through the mask. Therefore, since images have the same dimensions and the same orientations, it is sufficient to search for the corresponding values in the 4 qMRIs and to extract the median value for each subject and tissue class. The values of the medians obtained are available in Appendix B.

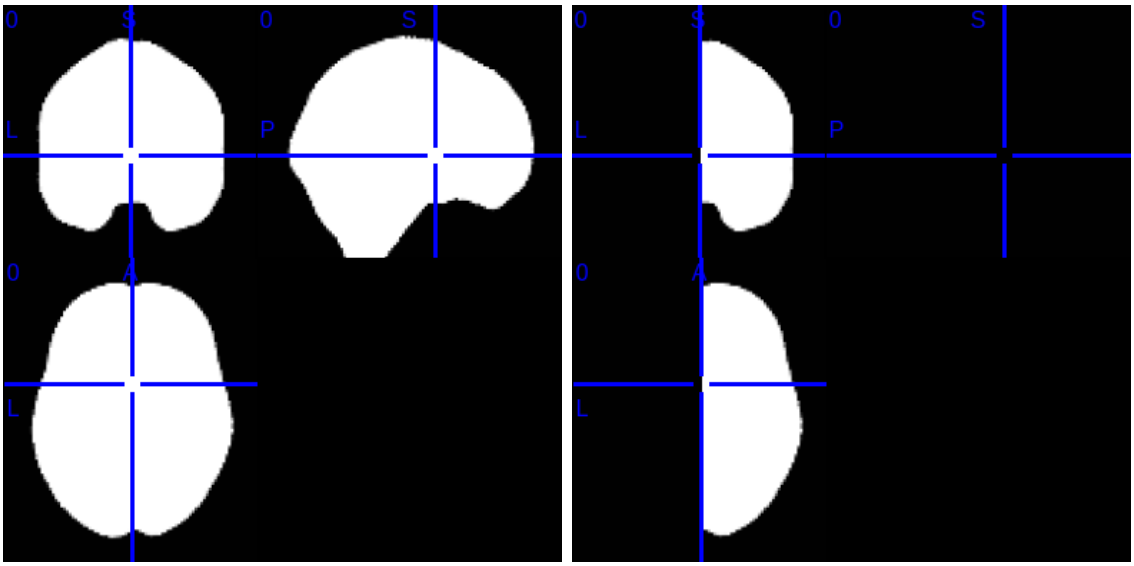

FIGURE 5.1: Entire and right hemisphere ICV.

Once the medians have been calculated, a two-sample t-test can be performed using the *ttest2* function already implemented in Matlab. This statistical inference tests the hypothesis that the two independent sample sets, the patient group and the control group, have a median distribution with similar means. The t-test is performed by assuming that the medians of the two groups follow a normal distribution and the variances are not equal. This test, called Welch's t-test computes the t-value as follows [47]:

$$t = \frac{\overline{X_1} - \overline{X_2}}{\sqrt{\frac{s_1^2}{n_1} + \frac{s_2^2}{n_2}}} \tag{5.1}$$

where,

- $\overline{X_1}$ and $\overline{X_2}$ are respectively the averages of group 1 and group 2
- s_1 and s_2 are respectively the unpool standard deviation of group 1 and group 2
- n_1 and n_2 are respectively the size of group 1 and group 2

The two-sample t-test allows to determine if the difference between the mean of the two groups is significantly different. The difference between the two groups is significant if it is very unlikely to be due to chance.

Performing a global analysis on the entire right hemisphere for each tissue class is not the most sensitive technique. Indeed, the right hemisphere is seen in its entirety, summarized by a single number for each tissue class. However, it is a sane check to observe if values make sense and if there are no subjects with outliers. The global analysis is a preliminary step to ensure the quality of the data.

5.2.2 Local statistical analysis - VBQ

Local statistical analysis is a voxel-wise analysis. In this type of analysis, a statistical value is assigned to each voxel. Therefore, the analysis is an imaging problem that is performed using SPM as opposed to the global analysis where a single value represented the entire grey or white matter tissue of the right hemisphere.

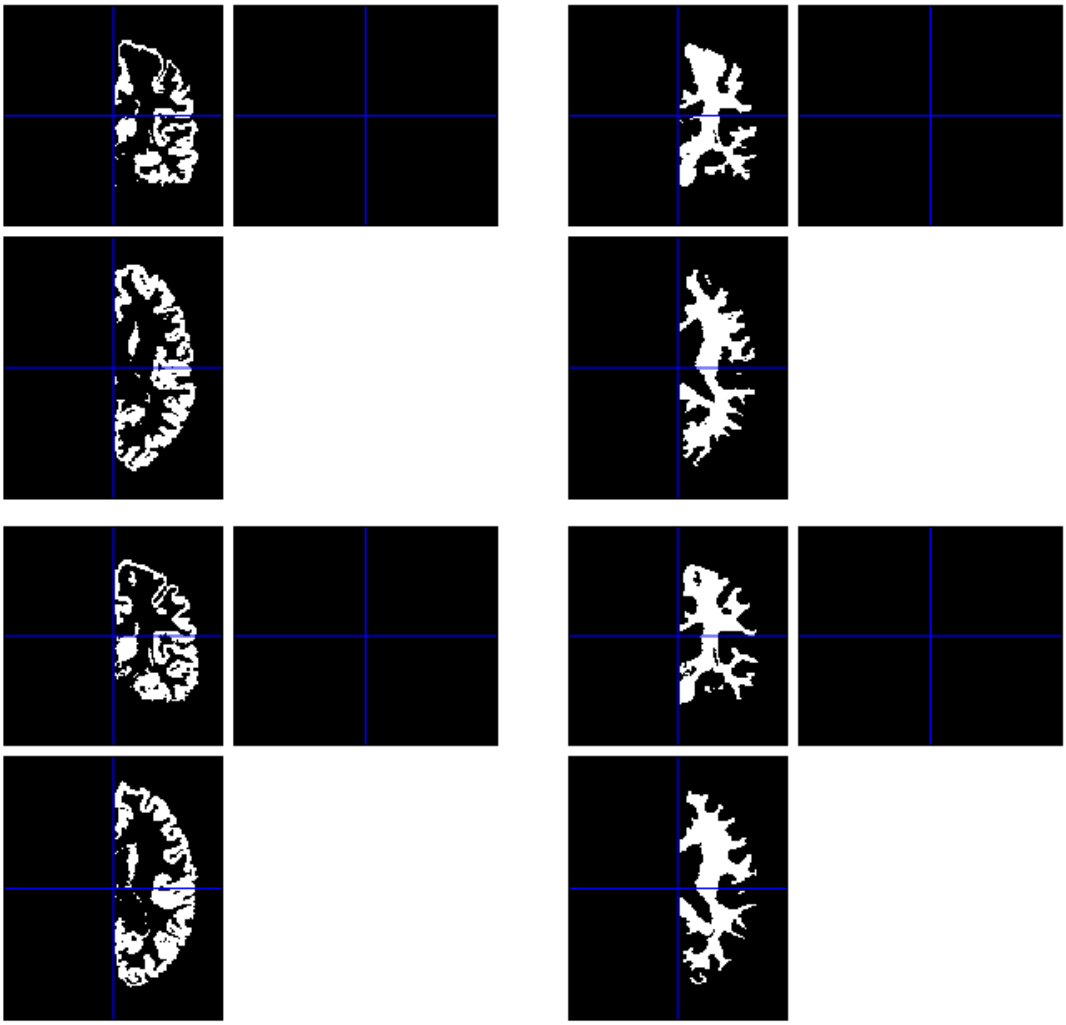

FIGURE 5.2: Right hemisphere mask of GM (left) and WM (right) in patient P35 (top) and control subject C23 (bottom).

General Linear Model

General linear model (GLM) is a way of performing a linear regression to find a relationship between the observed results for each voxel and parameters, called regressors, that explain the results obtained. The effects that explain the result are assumed to be linear and additive and the error in a GLM is assumed to follow a normal distribution [25]. The GLM mathematical model for k regressors is described in the Equation 5.2 [32].

$$\begin{aligned} \mathbf{Y} &= \hat{\mathbf{Y}} + \mathbf{e} \\ &= \beta_0 + \beta_1 \mathbf{X_1} + \beta_2 \mathbf{X_2} + ... + \beta_k \mathbf{X_k} + \mathbf{e} \end{aligned} \tag{5.2}$$

where,

- **Y** is the column matrix containing the observed value for each subject in the voxel. This is what is measured.
- $\hat{\mathbf{Y}}$ is the column matrix that contains the predictions of the values obtained by the GLM model.
- β_i is the weight assigned to the regressor i.
- $\mathbf{X_i}$ is the ith regressor.
- **e** is the error.

SPM allows the creation of a GLM via the SPECIFY 2ND-LEVEL button in its menu. A GLM is created for each tissue class and each relevant quantitative map. All GLMs are created independently of each other.

The A maps were not analysed with a GLM for two reasons. First the values in the A map for one patient, number 16, seemed incorrect. Furthermore, the quantitative map A is in fact a semi-quantitative map with uncorrected B_1^- bias. It refers to the proton density but does not directly represent the proton density. There are thus two arguments for not considering the A-maps. Firstly, proton density is not the most important parameter in this study and secondly, the deletion of a patient in a study where the number of subjects is already very limited is not recommended if one wants to have relevant results.

The design of the model was developed using the FACTORIAL DESIGN SPECIFICATION module. In order to establish this model, it is necessary to specify that two different groups (patients and controls) are considered, and that the variance in the two groups is probably different. The smoothed parameters maps obtained with the tissue-weighted smoothing for the tissue considered must be provided for each subject. These images define the **Y** of the Equation 5.2. Moreover, one has to add the covariates, i.e. the age and gender regressors which could explain the differences obtained between the subjects but whose effects are not interesting for the study.

When designing the GLM, it is also necessary to determine an explicit mask that represents the set of voxels to be considered in the analysis. In this study, the GLM is either applied to GM or to WM. Therefore, depending on the tissue to be analysed, the mask will be either that of the GM in the right hemisphere, or that of the WM in this same hemisphere.

In the design of the model, it is imposed that an implicit mask is calculated during the estimation of the model. This is explained in the next section named "Model Estimation".

After running the FACTORIAL DESIGN SPECIFICATION module specifying all the information to create the model, a *SPM.mat* file is created. This file contains all the information about the model such as the number of subjects, the different groups represented, their ages, their genders, the degree of freedom of the model... In other words, it contains the **Y** and **X** matrix of the model. The *SPM.mat* file is the input for estimating the model.

Model Estimation

The MODEL ESTIMATION in SPM takes care of the model estimation and is available in the STAT part of the SPM batch editor.

First, the algorithm calculates the implicit mask. This latter is based on the intensity of the images. By considering all the images and averaging the intensities of the voxels, the

algorithm obtains an average signal. If the value in a voxel is too low compared to this average signal, the voxel will not appear in the study even if it is in the explicit mask. The final mask that determines which voxels will be analysed is a combination of the explicit mask and the implicit mask.

The estimation of the model consists of estimating two quantities. On the one hand, the β values that best explain the results obtained and, on the other hand, the variance of the residuals.

Since the variance is not identical between the two groups, an ordinary least square procedure cannot be used to estimate the model parameters. These parameters are therefore estimated using a weighted least square approach. In this method, the variance is first estimated. The variance obtained determines the weighting applied to each voxel. The weight applied is inversely proportional to the noise variance. Thus, data with a large variance are weighted with a smaller weight compared to data with a small variance. The value of the weighting is equivalent to the inverse of the variance.

When the estimation is completed, the parametric maps of each β are created as well as the residual mean square.

Once the set of parameters has been estimated, the model can be analysed through statistical tests.

Statistical tests

When performing the statistical test, there are several ways to ask the question to obtain the desired results. Knowing that X_1 is the matrix designating the group 1 (patient) and X_2 that designating the group 2 (control). Therefore β_1 is related to the average signal of group 1 and β_2 to that of group 2. The three ways of asking the question to find out if there is a difference between the right hemisphere of the patients and that of the controls are as follows:

1. Is β_1 different from β_2?
2. Is β_1 larger than β_2?
3. Is β_1 smaller than β_2?

The last two questions require directionality. When directionality is not known, which is the case for this study, the first question is asked.

In SPM, it is possible to perform either a t-test or an F-test. The t-test implemented in SPM is uni-directional, while the F-test is bi-directional, i.e. looks for any difference. Since directionality is not known in this study, the latter will be used to determine whether there are differences in the right hemisphere between the two groups.

F-test This test is a classical statistical inference. $\beta_1 \neq \beta_2$ is the interesting hypothesis. The null hypothesis is therefore $\beta_1 = \beta_2$ and is assumed valid for the whole population. When dealing with real data, the difference is never exactly zero. The calculation of the F-value makes it possible to determine the probability that the observed deviation occurred by chance. A large F-value means a very low probability that it happened by chance. Therefore, when the F-value exceeds a certain threshold, the null hypothesis can be rejected, which means that the alternative hypothesis is accepted.

In SPM, an F-test can be performed via the RESULT button in the menu. Then, by imposing a contrast and a p-value, the software has all the necessary information to perform an F-test.

Testing $\beta_1 - \beta_2 = 0$ or $\beta_2 - \beta_1 = 0$ is equivalent. The contrast used here is 1 -1 but a -1 1 contrast would give the same results.

There are several ways of determining the threshold, by controlling the risk of false positives. This threshold, called p-value, false positive rate or significance level is the minimum probability to reject the null hypothesis. The first possibility to determine this p-value is to perform a single voxel inference and to determine the acceptable error for each voxel. The more voxels there are, the higher the chance of having a high number of false positives. When this method of determining the p-value is chosen, one works with an uncorrected p. In studies with a large number (typically more than 10000) of voxels, it is preferable to determine a family-wise error rate (FWER). In this case, a corrected p threshold is used. For example, a corrected p-value equal to 0.1 means that on 10 repetitions of experiments, only one will show some false positive voxel anywhere in the image, in the brain. [25]

When a corrected p of 0.05 is applied, there are two different definitions of whether or not there is a significant difference within a voxel: peak level and cluster level. For the peak-level inference, the voxel has a large enough F value that the voxel has a probability $p < 0.05$ of incorrectly rejecting to the null hypothesis. For the cluster-level inference, the statistical map is first thresholded at an uncorrected p-value threshold, typically $p < 0.001$, then the size of each cluster is examined. Then the null hypothesis is rejected if the cluster size has a probability of occurring under the null-hypothesis at $p < 0.05$ corrected for all clusters. The cluster level takes into account the search space. The larger the search volume, the more clusters it is likely to have. The more clusters there are, the more likely there are to be large clusters. [25]

Direction of the effect The problem with the results obtained with an F-test is that there is no information about the direction of the effect. The result shows the parts of the right hemisphere where there is a difference between the two groups but does not show which group has a larger β. One way to overcome this issue is to look afterwards at the direction of the effect by checking the sign of the difference between β_1 and β_2.

5.2.3 Local statistical analysis - VBM

In VBM, the objective is to compare tissue, for example GM, volume or density across subjects over the whole brain. The image used, for each subject are the segmented tissue class, warped into a reference space and smoothed, i.e. each voxel contains a value which is representative of the amount of tissue around that voxel. Therefore, since a VBM analysis is performed on patient data and on control data, a comparison of the GM volume between the two groups is possible.

General Linear Model and model estimation

The pipeline for performing a statistical analysis in a VBM analysis is similar to that for a VBQ analysis. The first step is also to develop a GLM. The GLM design is a two-sample t-test as two groups are compared. The first group is the patients and the second is the healthy subjects. In a VBM, whose aim is to detect GM volume change, the images introduced into the model are the smoothed modulated quantitative grey matter maps.

These images used here are the results of segmentation, normalization and smoothing on the R_1 map. Furthermore, the explicit mask is the right hemisphere mask. Since the aim here is to look at the difference in GM volume between the two groups, it is preferable to look at all the voxels rather than those belonging only to the GM mask built from patient and control data.

Then, the GLM is estimated using the MODEL ESTIMATION implemented in SPM as explained in 5.2.2.

Statistical tests

Patient < Control By performing a t-test with a contrast [-1 1] and a corrected p of 0.025, the voxels that show a significantly smaller amount of GM in patients than in controls according to their peak level are displayed. The second type of inference evaluated is based on clusters. Cluster-level inference, based on an uncorrected $p < 0.001$ voxel-wise cluster forming threshold, shows the cluster whose size (number of voxels) has a $p < 0.025$ of showing up by chance. Therefore, using an uncorrected p of 0.001 and imposing a minimum number of voxels in a cluster for there to be a probability greater than 0.025 of observing a difference in this cluster, all voxels belonging to a significant cluster with a $p_{FWE-corr} < 0.025$ are obtained.

Patient > Control Similarly by performing a t-test with a contrast [1 -1] and a corrected p of 0.025, voxels that have significantly more GM in patients than in controls are detected.

5.3 Differences within the patients in right hemisphere

The aim of comparing patients with each other is to relate brain microstructures to patient parameters. These parameters will therefore be modelled as regressors of interest in this study. Several tests were performed on the patients in order to obtain several kinds of parameters related to their performance. The different parameters available are explained in 5.1 and the values for each patient are given in the TABLE A.2.

The TABLE A.2 is missing one piece of data, the value of the parameter NW for patient P21. In addition, for patient P21, there is the value 0 assigned to the parameter Min-P. However, when we look at the values of the other patients for this parameter, the minimum value after 0 is 38. It is therefore assumed that the value 0 is a wrong value. The sample of patients is not large and deleting a patient seems in this case not to be the best solution.

Instead of deletion, an imputation of missing data is performed. The idea is to fill in the table by adding a value for the missing data and changing the supposedly wrong value. When information is missing, the data should be completed without providing additional information. A solution is to complete data by imputing the mean value from the other subjects. In this way, patient P21 was assigned a value of 33 for the NW parameter and a value of 97 for the Min-P parameter.

5.3.1 Principal Component Analysis (PCA)

The number of parameters to describe performance is relatively large. Indeed, 10 different parameters are assigned for each patient. Using 10 regressors of interest in the GLM model is too high as there are only 26 patients. So we have a maximum of 26 degrees of

freedom. The more regressors we use in the analysis, the more this degree of freedom decreases. A solution is to perform a principal component analysis in order to reduce the number of regressors while retaining a maximum of information. Indeed, PCA is a technique that suggests that the variables vary together and thus makes it possible to reduce the number of variables by choosing the best combinations of variables to keep a maximum of information [38].

The Matlab function *pca* has been used to perform a PCA on the 10 performance parameters. This function returns the coefficients of the principal components, the score for each patient and for each PCA and the percentage of the total variance explained by each principal component.

One decided to take a number of components that explain 90% of the variance. By taking the first 3 PCAs, more than 90% of the variance is explained. Indeed, PCA1 explains 57.5393% of the variance, PCA2 20.2008% and PCA3 14.0686%. Principal component coefficients for these first three principal components are displayed in TABLE 5.2. The first component is mainly correlated with the BNT, Nam-O and NW score. As anomic patients tend to have difficulty naming objects, it is not surprising that these three variables are positively correlated and that the first component is more strongly correlated with the BNT, Nam-O and NW variables.

	PCA1	**PCA2**	**PCA3**
BNT	0.5369	0.0154	-0.5213
Nam-O	0.4321	0.0578	-0.4564
Nam-A	0.0992	-0.0177	-0.1122
Co-SW	0.0683	0.0524	-0.0258
Co-WW	0.0312	0.0749	-0.0347
Co-SS	0.0526	-0.0686	-0.0017
Co-WS	0.0298	-0.0396	-0.1280
Mo-W	0.1975	-0.1455	0.1593
NW	0.5767	-0.5302	0.5408
Min-P	0.3664	0.8241	0.4139

TABLE 5.2: Principal component coefficients/loadings for the first three principal components.

5.3.2 General Linear Model and model estimation

Equation 5.2 explains the GLM principle. This model explained above, in section 5.2.2, is also used here to detect correlations within a single group of subjects. Since we are working with a single group, the design is that of a one-sample t-test where only the weighted average parameters maps of the patients are entered into the model.

When one looks at the group of patients, there are regressors that are not of interest. These are regressors that could explain some of the results but are not investigated in this study. However, even if they are not interesting for the study, they should be considered. Age, gender and time post stroke are regressors of no interest. In addition to these regressors of no interest, there are 3 regressors of interest represented by the first 3 PCAs. These regressors of interest represent patient performance.

Once the model is created, it is estimated using the MODEL ESTIMATION module.

5.3.3 Statistical tests

F-test The F-test detects whether inter-patient variability can be explained by the regressors of interest. An F-test is performed with a contrast that allows testing the effect of the 3 regressors of interest taken together. Thereby, the contrast used in the F-test is the following:

$$\begin{matrix} 0 & 0 & 0 & 0 & 1 & 0 & 0 \\ 0 & 0 & 0 & 0 & 0 & 1 & 0 \\ 0 & 0 & 0 & 0 & 0 & 0 & 1 \end{matrix}$$

In this contrast, each column is linked to a regressor. The first is the average of the patients. Then, in column order, there are the following regressors: age, gender, time post stroke, PCA1, PCA2 and PCA3. This contrast will thus highlight voxels whose inter-patient variability can be explained by a linear combination of the 3 PCAs, i.e. the performance parameters.

5.4 Pipeline effects on control data

Two different pipelines were used to spatially process the control data. A first pipeline uses the default parameters of the spatial processing pipeline of the hMRI toolbox (see 4.2) and a second tries to get as close as possible to the pipeline used to analyse patient data.

The comparison of these two pipelines would allow to know the influence of the pipeline used on the results obtained. As the input data to the two pipelines is identical, there is a correlation between the images obtained with the first pipeline and those obtained with the second pipeline. Therefore, a paired samples t-test is used to compare the results of the two pipelines and see if there is a significant difference between these latter.

5.4.1 VBQ

General Linear Model and model estimation

Six GLMs are designed: there is a GLM for the MT, R_1 and R_2^* quantitative maps and the two tissue classes (GM and WM). For each GLM, the model design is based on 17 pairs of data since there are 17 healthy subjects. The first image of each pair is the image obtained with the pipeline close to the one used in the patients and the second image is the one obtained with the full pipeline already implemented in the hMRI toolbox. In addition to these images, an explicit mask is introduced to inform on which voxel the model should be performed. Thus the explicit mask corresponds either to the voxels of the GM of the right hemisphere or to the voxels of the WM of the right hemisphere, depending on the tissue under consideration.

Once this model is created, it is estimated with the MODEL ESTIMATION module.

Statistical tests

F-test The F-test detects if there are differences between the two pipelines. The applied contrast is [1 -1]. The null hypothesis is therefore β_1-β_2=0 which means that the average of the two populations are equal. If F is large enough, this hypothesis is rejected in favour of the alternative hypothesis that the two means are different. The acceptable range of

F values for the null hypothesis depends on the p-value used. For this statistical test a threshold at $p < 0.05$ after FWE correction was applied.

5.4.2 VBM

Similarly, a paired t-test on the modulated quantitative GM maps indicates whether there is a difference in volume between the morphological results of the two pipelines.

General Linear Model and model estimation

One GLM where the input images are 17 pairs of images, one pair for each control subject. The first image of each pair is the modulated quantitative GM map obtained with the pipeline that is similar to the pipeline applied on the patient data while the second image of each pair is the modulated quantitative GM map obtained with the default pipeline implemented in hMRI toolbox. The explicit mask is that of the right hemisphere as this is the hemisphere on which the analysis takes place.

Statistical tests

F-test The use of a corrected p of 0.05 imposes a threshold to determine whether the difference is significant or not. Significance is looked at the peak level but also at the cluster level. Indeed, a voxel may not be significant but could belong to a significant cluster.

Chapter 6

Results

This chapter presents the results obtained following the analysis described in the previous chapter. First, the chapter refers to the differences observed between the two groups (patients and controls). Secondly, it explains the results found in the patient group in relationship to patient performance. Finally, the chapter is concluded by pointing out the differences observed between the two pipelines used on the control subjects.

6.1 Controls vs Patients in right hemisphere

6.1.1 Global statistical analysis

Global statistical analysis is a preliminary step to ensure the quality of the data. It allows to see if the observed values are well within the norm or if there are some outliers. TABLES 6.1 and 6.2 show the mean of the median voxel values for each patient and control in grey and white matter respectively. Furthermore, these tables contain the p-value of the two sample t-test between the means of the two groups. If we consider that the result of the parametric test is significant when the p-value is less than 0.05, we conclude that there is a significant difference between the patients and the control subjects in the GM of the quantitative map R_2^*.

Except for the GM signal in R_2^*, the values between patients and controls are very similar, so it is difficult to conclude anything. Maybe there is no difference, maybe the signal values are higher in one part of the brain and lower in the other, which cannot be seen in such a global analysis like this. There is a need for further analysis and local analysis (see sections 6.1.2 and 6.1.3). The global analysis, which is easy to perform, does not give much information except that some subjects have outlier medians.

Indeed, before computing these averages for all patients and all controls, it was necessary to compute the median values of GM and WM for each subject. These values are available in Appendix B. The values of the controls were similar to each other. Similarly, the median values for each patient were similar except in A map for patient 16 where the values are outliers (see TABLES B.1 and B.2).

	Mean		
	Patients	**Controls**	**p-value**
A	82.8369 ($\pm$6.1947)	81.2496 ($\pm$0.9574)	0.3025
MT	0.8329 ($\pm$0.0299)	0.8399 ($\pm$0.0359)	0.4895
R1	646.0553 ($\pm$24.3831)	655.4668 ($\pm$15.3711)	0.1646
R2s	0.0168 ($\pm$0.0006)	0.0173 ($\pm$0.0006)	0.0095

TABLE 6.1: Global statistical result for the GM.

	Mean		
	Patients	**Controls**	**p-value**
A	70.3867 (±5.2449)	69.2656 (±0.1764)	0.3855
MT	1.6182 (±0.0763)	1.5907 (±0.0517)	0.2001
R1	1000.2749 (±45.8651)	1000.9892 (±27.7566)	0.9544
R2s	0.0208 (±0.0007)	0.0209(±0.0007)	0.5717

TABLE 6.2: Global statistical result for the WM.

6.1.2 Local statistical analysis - VBQ

The F-test comparing the patient's right hemisphere with that of the control taking into account their age and gender, only detected significant results when an uncorrected $p = 0.001$ was used. Only one voxel in the entire local analysis is significant with a corrected $p = 0.05$. This voxel is located in the WM of the right hemisphere in the MT map (see FIGURE C.4) and the value of this voxel in patients is significantly smaller than in healthy subjects. The results of the F-test are illustrated with the help of some brain cross sections. FIGURES 6.1, 6.2 and 6.3 show the most interesting brain slices to illustrate the differences between the two groups in GM in MT, R_1 and R_2^* maps respectively. Similarly, FIGURES 6.4, 6.5 and 6.6 show the significant voxels in the white matter with an uncorrected p of 0.001 for MT, R_1 and R_2^* maps respectively. The illustration of the results in FIGURES 6.1 to 6.6 is not exhaustive. A complete list of significant voxels with uncorrected p-value of 0.001 can be found in the Appendix C in FIGURES C.1 to C.6.

Regarding the direction of difference of the statistical test, the signal is smaller in patients than in controls in the GM for MT map and R1 map but it is larger or smaller in the other quantitative maps according to brain regions.

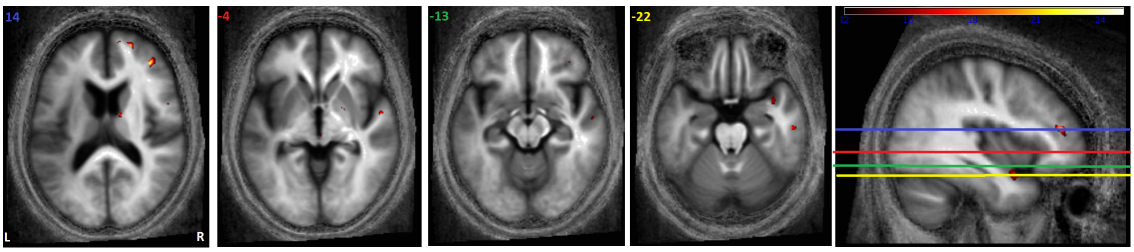

FIGURE 6.1: Statistical parameter maps of GM regions where there is a significant difference in MT map between patients and controls with an uncorrected p at 0.001. The results are superimposed on the mean MT map in MNI space of all subjects.

6.1.3 Local statistical analysis - VBM

Two t-tests were performed at the $p < 0.025$ FWE corrected level. There is no voxel whose value is significantly larger in patients than in healthy subjects.

However, in some region, there is a GM atrophy in patients. Some slices of statistical parameter map showing GM atrophy in patients are in FIGURE 6.7. GM atrophy is located in brain stem, right thalamus proper, right supplementary motor cortex and right lingual gyrus. For the VBM analysis between patients and control, the exhaustive list of significant voxel and their position in MNI space is in Appendix C, in FIGURE C.7 for peak level and in the FIGURE C.8 for cluster level.

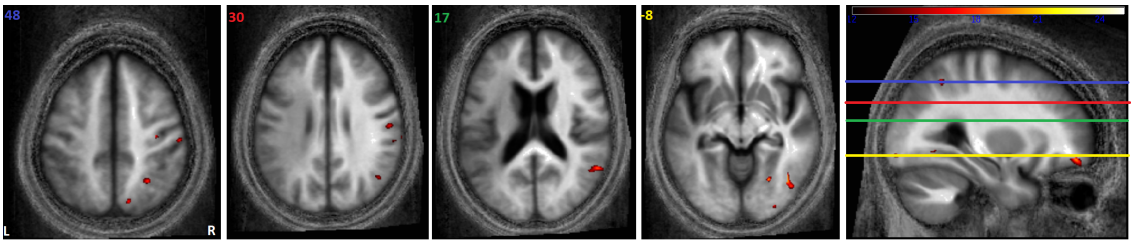

FIGURE 6.2: Statistical parameter maps of GM regions where there is a significant difference in R_1 map between patients and controls with an uncorrected p at 0.001. The results are superimposed on the mean MT map in MNI space of all subjects.

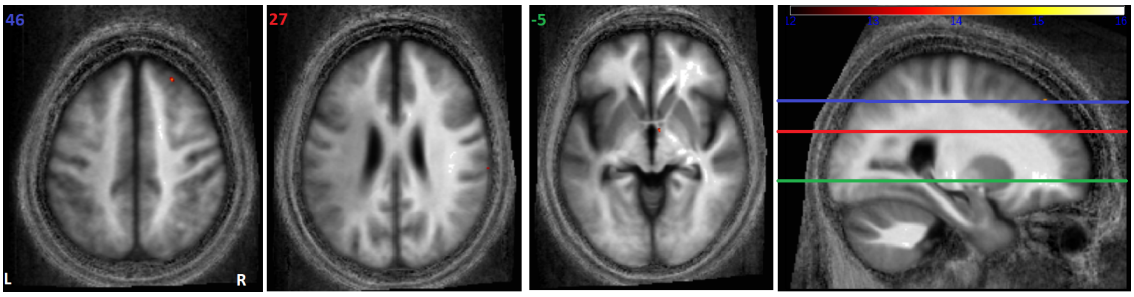

FIGURE 6.3: Statistical parameter maps of GM regions where there is a significant difference in R_2^* map between patients and controls with an uncorrected p at 0.001. The results are superimposed on the mean MT map in MNI space of all subjects.

6.2 Within patient analysis in the right hemisphere

After performing an F-test as explained in subsection 5.3.3, no voxel is significant when a corrected p of 0.05 is applied. Similarly for an uncorrected p of 0.001, there is no results in the WM of the MT map and R_1 map. Significant voxels with an uncorrected p of 0.001 are listed in FIGURES C.9, C.10, C.11 and C.12 respectively for the GM of the MT, R_1 and R_2^* maps and the WM of the R_2^* map. For a visual interpretation, FIGURES 6.8, 6.9, 6.10 and 6.11 each display 4 brain cross-sections for GM in MT map, R_1 map and R_2^* map and WM in R_2^* map respectively. In these figures, significant voxels with an uncorrected p equal to 0.001 are displayed in colour according to the colour scale of the F values.

6.3 Pipeline effects on control data

6.3.1 VBQ

The choice of pipeline influences the results. FIGURES 6.12 to 6.17 show the brain regions with a significant difference ($p < 0.05$ FWE corrected level) in peak and cluster level between the two pipelines in GM (FIGURES 6.12, 6.13 and 6.14) and WM (FIGURES 6.15, 6.16 and 6.17).

For more information, Appendix C enumerates all significant voxels. Indeed, FIGURES C.13, C.15, C.17 list voxels whose the corrected p is inferior at 0.05 in peak level in the GM in the MT, R_1 and R_2^* maps respectively. Similarly, FIGURES C.19, C.21 and C.23 enumerate voxels whose the corrected p is inferior at 0.05 in the WM in the MT, R_1

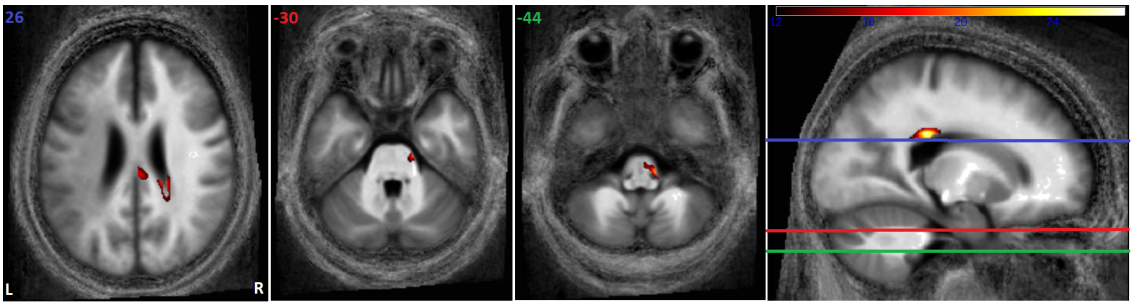

FIGURE 6.4: Statistical parameter maps of WM regions where there is a significant difference in MT map between patients and controls with an uncorrected p at 0.001. The results are superimposed on the mean MT map in MNI space of all subjects.

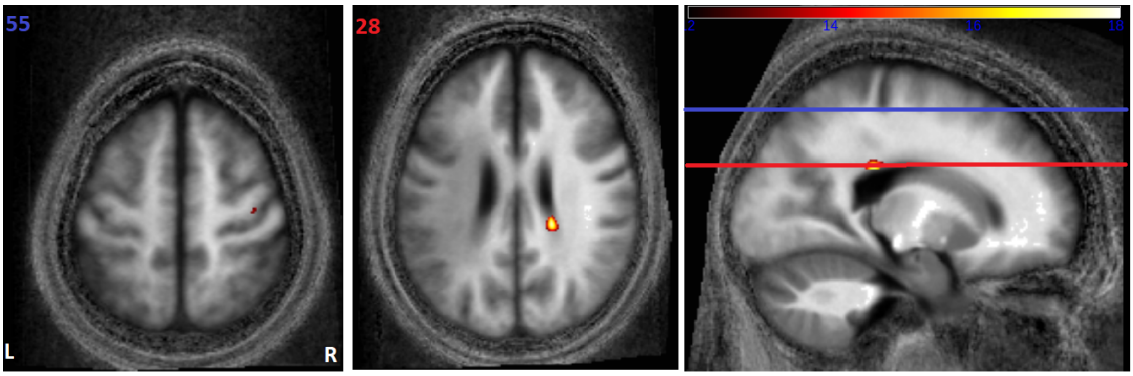

FIGURE 6.5: Statistical parameter maps of WM regions where there is a significant difference in R_1 map between patients and controls with an uncorrected p at 0.001. The results are superimposed on the mean MT map in MNI space of all subjects.

and R_2^* maps respectively. Furthermore, FIGURES C.14, C.16, C.18 list voxels whose the corrected p is inferior at 0.05 in cluster level in the GM in the MT, R_1 and R_2^* maps respectively and the same for FIGURES C.20, C.22 and C.24 but for WM.

6.3.2 VBM

There are morphological differences between the results of the two pipelines. These differences in grey matter volume are illustrated in FIGURE 6.18.

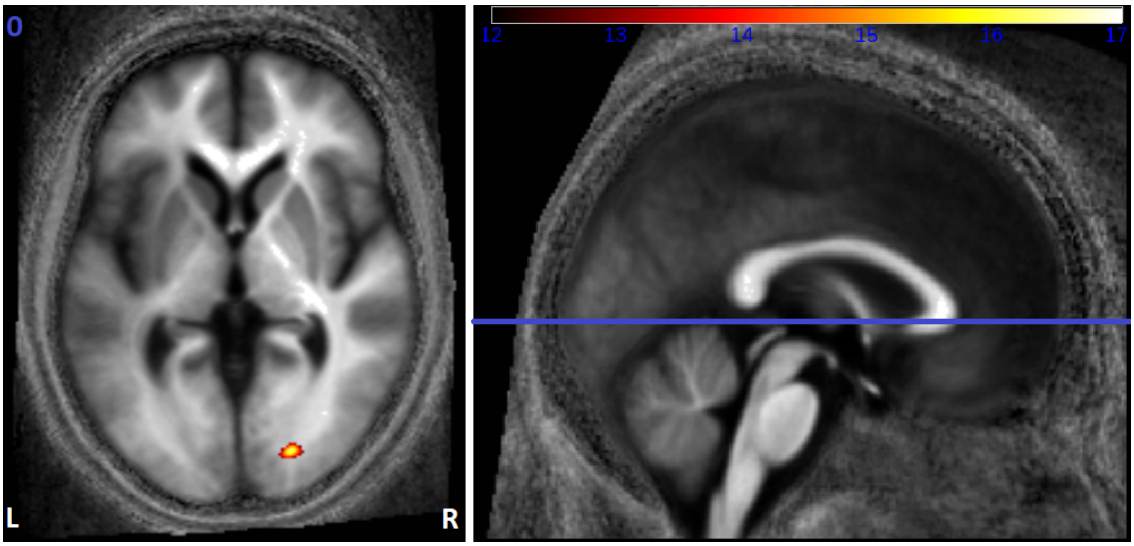

FIGURE 6.6: Statistical parameter maps of WM regions where there is a significant difference in R_2^* map between patients and controls with an uncorrected p at 0.001. The results are superimposed on the mean MT map in MNI space of all subjects.

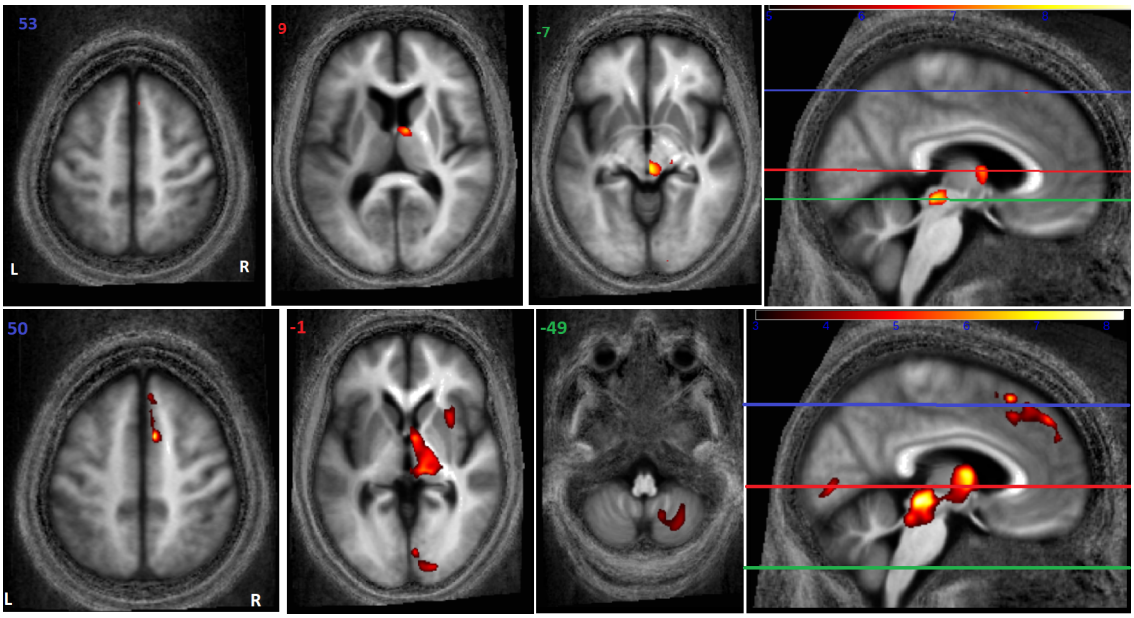

FIGURE 6.7: Statistical parameter maps showing GM atrophy in patients with p<0.025 FWE corrected level in peak level (top) and cluster level (bottom). Statistical parameter maps are superimposed on the mean MT map in MNI space of all subjects.

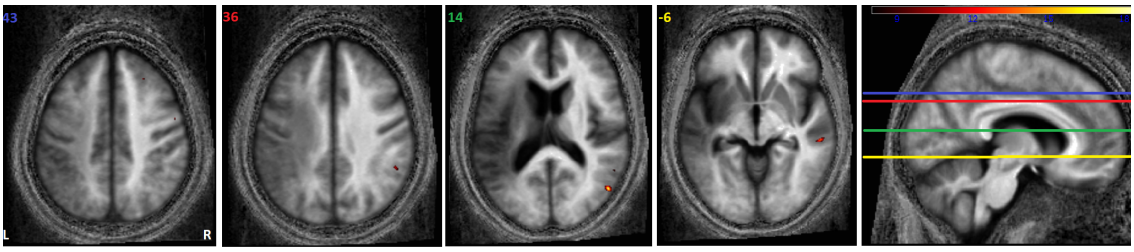

FIGURE 6.8: Statistical parameter maps of GM regions where there is a significant difference in MT map within the patient group with an uncorrected p at 0.001. The results are superimposed on the mean MT map in MNI space of all patients.

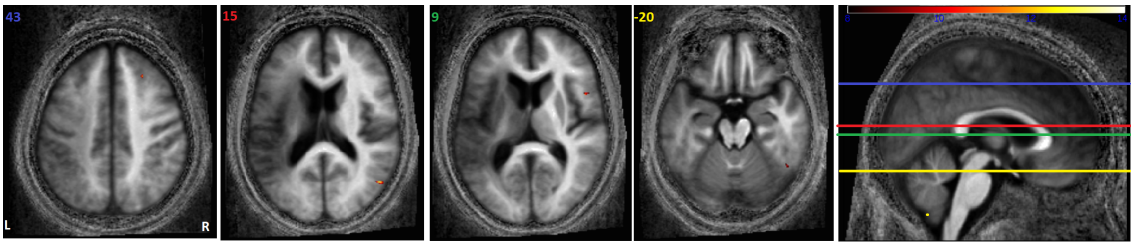

FIGURE 6.9: Statistical parameter maps of GM regions where there is a significant difference in R_1 map within the patient group with an uncorrected p at 0.001. The results are superimposed on the mean MT map in MNI space of all patients.

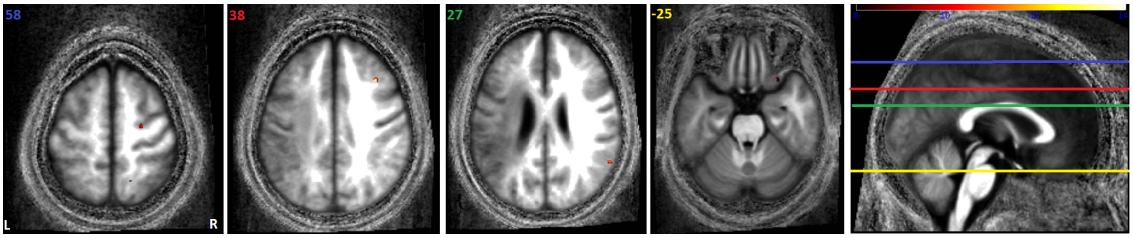

FIGURE 6.10: Statistical parameter maps of GM regions where there is a significant difference in R_2^* map within the patient group with an uncorrected p at 0.001. The results are superimposed on the mean MT map in MNI space of all patients.

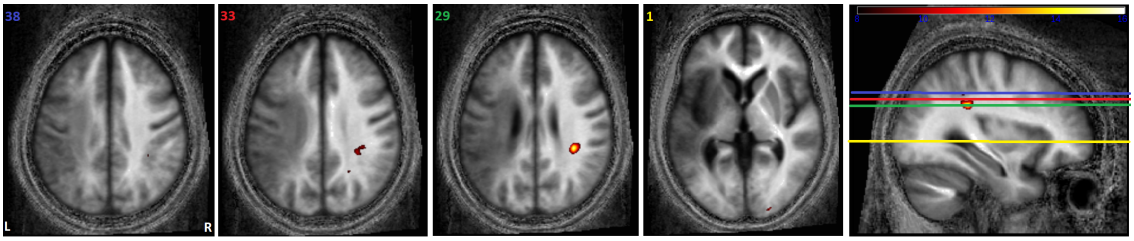

FIGURE 6.11: Statistical parameter maps of WM regions where there is a significant difference in R_2^* map within the patient group with an uncorrected p at 0.001. The results are superimposed on the mean MT map in MNI space of all patients.

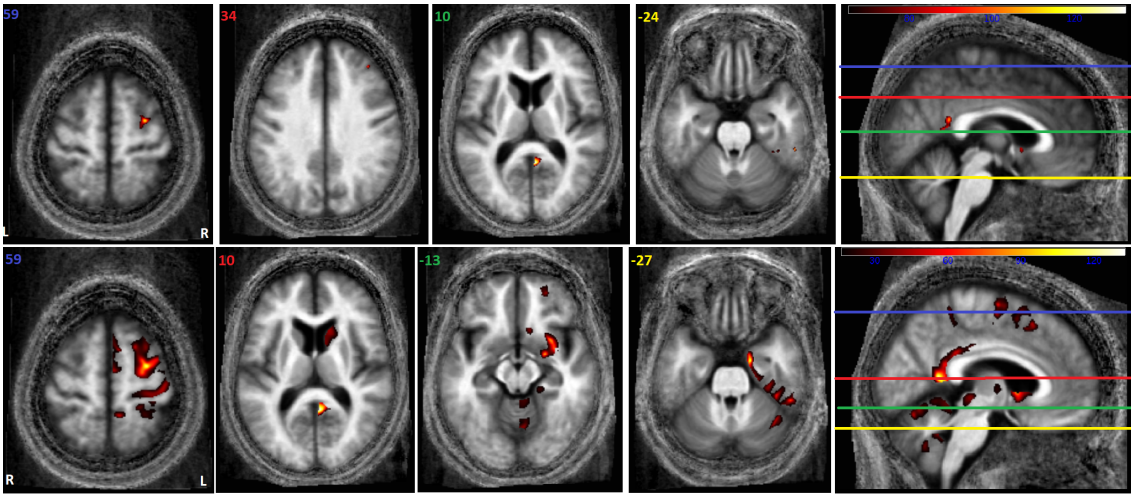

FIGURE 6.12: Statistical parameter maps of significant difference in peak level (top) and cluster level (bottom) with p corrected at 0.05 between two different pipelines for controls' right hemisphere in MT map grey matter. The results are superimposed on the mean MT map in MNI space of all controls.

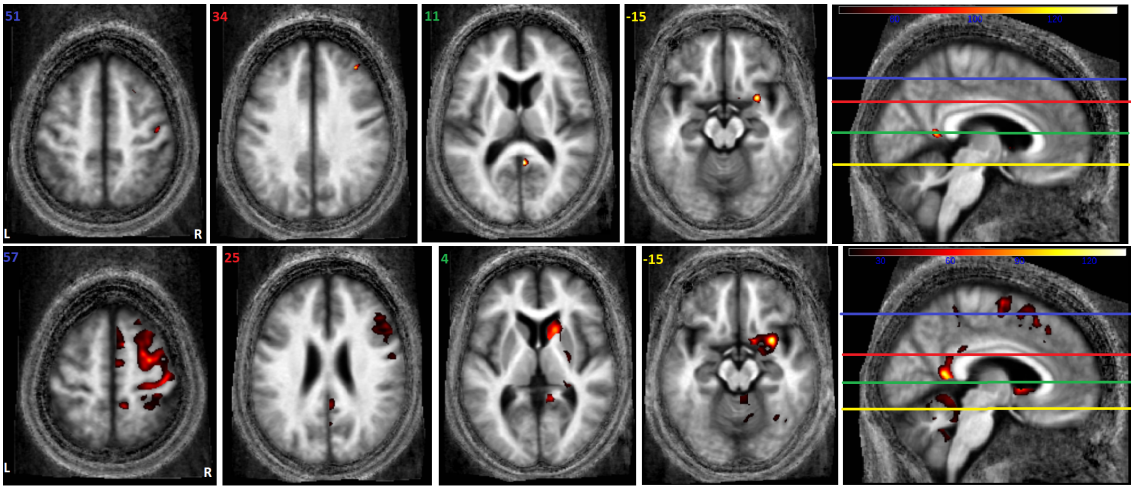

FIGURE 6.13: Statistical parameter maps of significant difference in peak level (top) and cluster level (bottom) with p corrected at 0.05 between two different pipelines for controls' right hemisphere in R_1 map grey matter. The results are superimposed on the mean MT map in MNI space of all controls.

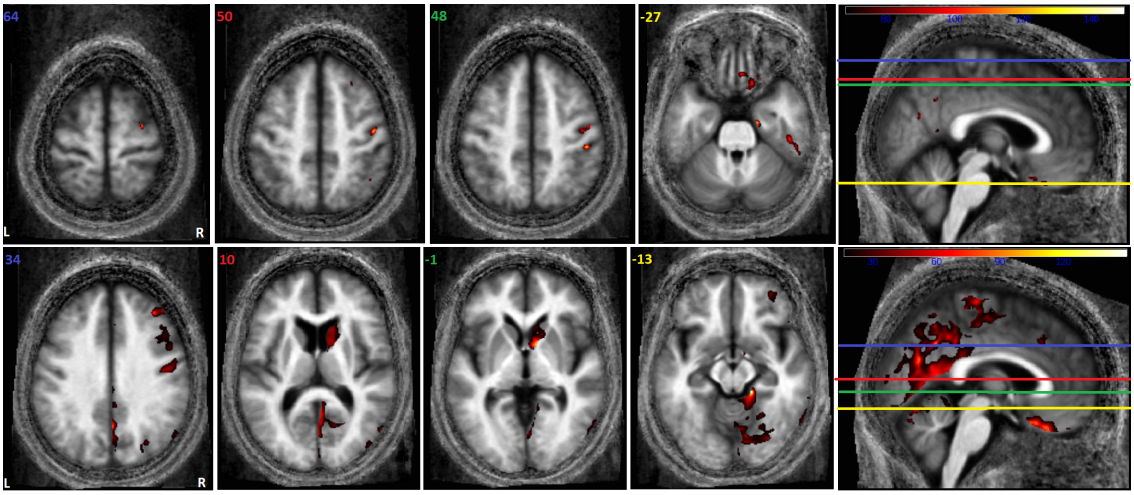

FIGURE 6.14: Statistical parameter maps of significant difference in peak level (top) and cluster level (bottom) with p corrected at 0.05 between two different pipelines for controls' right hemisphere in R_2^* map grey matter. The results are superimposed on the mean MT map in MNI space of all controls.

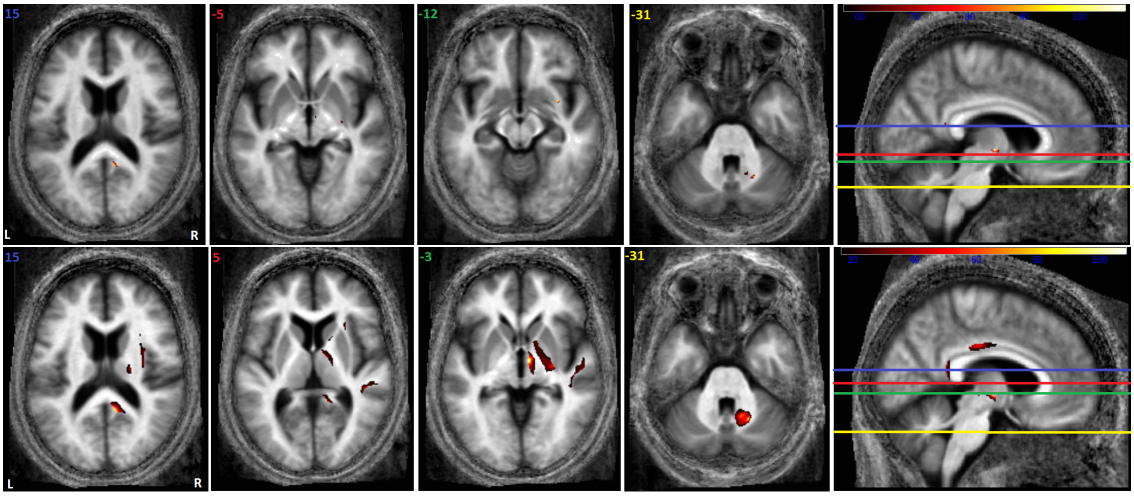

FIGURE 6.15: Statistical parameter maps of significant difference in peak level (top) and cluster level (bottom) with p corrected at 0.05 between two different pipelines for controls' right hemisphere in MT map white matter. The results are superimposed on the mean MT map in MNI space of all controls.

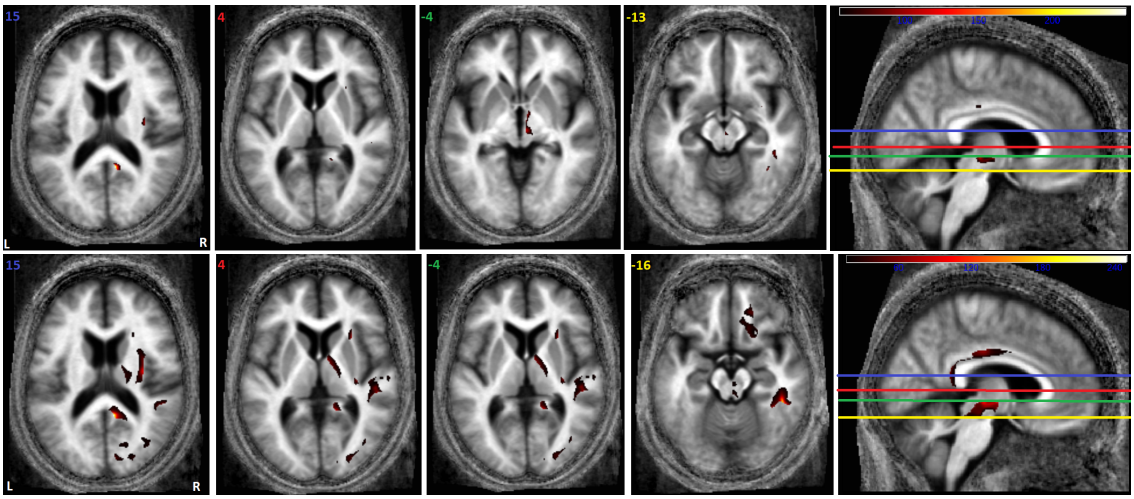

FIGURE 6.16: Statistical parameter maps of significant difference in peak level (top) and cluster level (bottom) with p corrected at 0.05 between two different pipelines for controls' right hemisphere in R_1 map white matter. The results are superimposed on the mean MT map in MNI space of all controls.

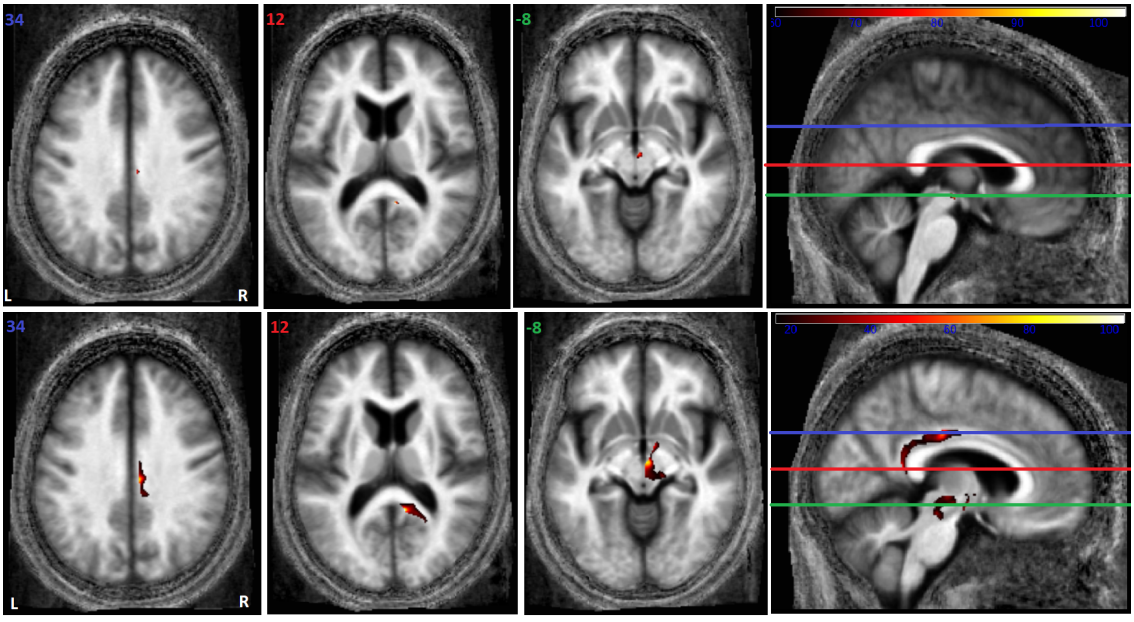

FIGURE 6.17: Statistical parameter maps of significant difference in peak level (top) and cluster level (bottom) with p corrected at 0.05 between two different pipelines for controls' right hemisphere in R_2^* map white matter. The results are superimposed on the mean MT map in MNI space of all controls.

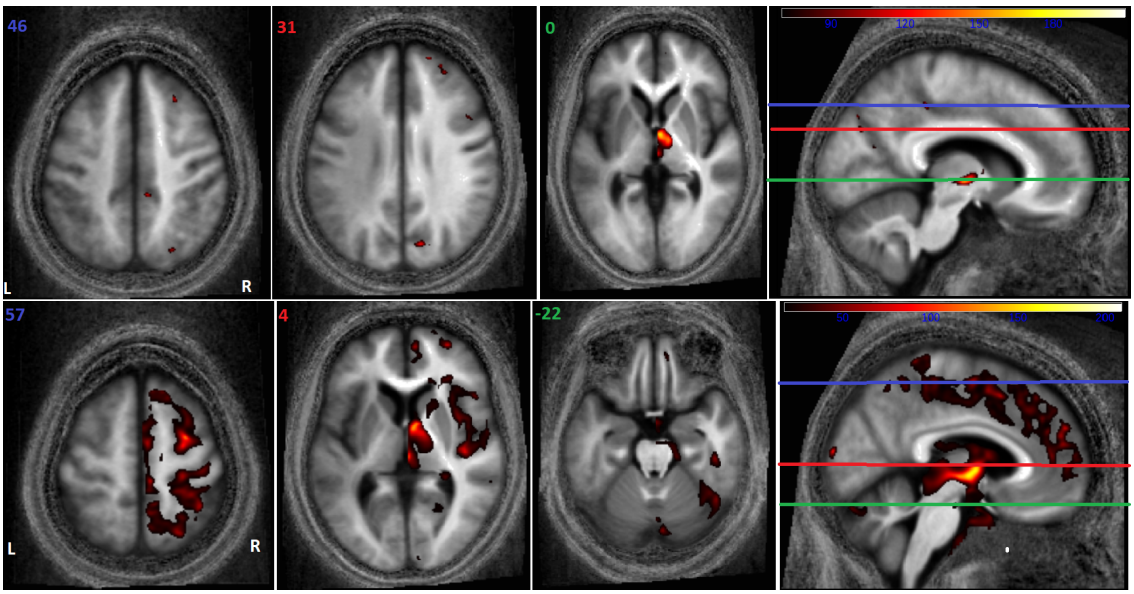

FIGURE 6.18: Statistical parameter maps showing significant differences in peak level (top) and cluster level (bottom) with a p corrected at 0.05 in GM volume between the two pipelines on the control data. Statistical parameter maps are superimposed on the mean MT map in MNI space of all controls.

Chapter 7

Discussion

Segmentation and normalization worked well, both on patients using the USwL approach and on control subjects using the US approach.

The lesion volume obtained after the USwL approach can vary greatly from the lesion mask volume obtained with the ALI method. For two patients, P30 and P33, the lesion volume is slightly larger (114.33 cm^3 vs. 112.62 cm^3 and 133.54 cm^3 vs. 130.10 cm^3) with the USwL approach while for all other patients the lesion is much larger with the ALI method. Visually, it can be seen that the mask obtained with ALI tends to overestimate the lesion volume. This overestimation can explain the observed difference in volume: the USwL method adapts the mask obtained with ALI by adjusting it as good as based on the multichannel data.

The VBM analysis between patients and controls revealed significant results, namely decreased local GM volume in patients compared to controls in the following regions: brain stem, right thalamus proper, right supplementary motor cortex and right lingual gyrus. Another significant result, after the whole right hemisphere correction, is the significant decrease in MT values for patients versus controls in one voxel in the right cerebral WM; this could reflect a variation in the amount of myelin between patients and control subjects. This was not an expected result. Indeed, one expected to see increased changes in the right hemisphere of the brain, in regions homologous to the damaged regions in the left hemisphere. Different significant results were expected, but one must put this into perspective and acknowledge that this study nevertheless allowed to distinguish morphological changes and, for one voxel, a change in the microstructure of the brain. A larger sample size would probably have allowed to obtain more significant results. Moreover, the five-month delay before observing the injured brain may not be sufficient to observe changes in the microstructure. It is possible that a longer period of time is needed for changes to appear.

Furthermore, the analysis within the patient group, to know the relationship between their performance and the observed results, did not yield any clear results. Indeed, the significant results observed are all obtained with an uncorrected threshold. This confirms the idea that using a larger sample size would be beneficial. For the within patient study, it was expected that the variation in speech production abilities would correlate with changes of signal in structurally intact right hemisphere brain regions, especially in Broca's area homologue.

The significant differences between the two pipelines used on the control subjects highlight the importance of the pipeline employed. Indeed, this study reveals that different pipelines lead to significantly different results. Therefore, it is important that the pipeline

applied to the healthy subjects' data is as close as possible to the one used on the patients' data.

Patient 14 was excluded from the study because no suitable a priori mask existed. Manual segmentation could be done to obtain a suitable mask and thus include patient 14 in the study.

Furthermore, in addition to a cross-sectional study, a longitudinal analysis could be beneficial from a neurological point of view. This would allow to observe the change in the microstructures of the brain during the recovery of language skills. One could not access the data to perform such an analysis. However, one knows that this data has been acquired for some patients, making a longitudinal study possible. This kind of study would be the next step of this work and would likely provide additional information.

Chapter 8

Conclusion

Working with quantitative MRIs is complex because of the need to manipulate complex images while retaining all the information they provide. In addition, stroke patients have damaged brains, which complicates the methodology for analysing the images. Indeed, most of the properties of a healthy brain are known (tissue probability maps, etc.) but in damaged brains, there are more unknowns, which complicates the data processing. Therefore, working on quantitative images of patients with aphasia following a stroke is very challenging.

MPM approach allows for the acquisition of quantitative data. The innovative ALI and USwL methods allow segmenting and normalizing injured brains. However, in this study it was found that the masks obtained with the USwL method seem more accurate because the output lesion masks seem closer to the actual lesion masks. Nevertheless, the USwL approach needing an a priori lesion mask, the mask obtained with the ALI method shall be used. The two methods are therefore complementary.

Although the segmentation, normalization and smoothing of the data seem to be executed correctly, the results are not as expected. Indeed, one expected to see more significant changes in the right hemisphere of the patients. In addition to an increase in patients in the part of the right hemisphere homologous to the injured one, it was also expected that there would be a variation in speech production abilities correlated with signal changes in structurally intact right hemisphere brain regions, especially in Broca's area homologue. These hypotheses were not confirmed in this study, but that does not mean that they are incorrect. More research would allow understanding the plasticity of the brain during revalidation treatment and thus to have more tools to improve these treatments and thus reduce the irreversible impacts on these patients (disability...).

One will conclude by highlighting the importance of the processing used to treat the data. Indeed, this master thesis shows that using slightly different processings can lead to results with significant differences. It is therefore of utmost importance to use the right processing tools to treat data.

Appendix A

Additional information on subjects

TABLE A.1 informs about the age (in years) and the gender of control subjects and TABLE A.2 gives patients' information and raw score in the linguistic assessment. In this table, TPS represents the time post-stroke in months, the age is in years and the lesion volume is in cm^3. The scores in bold belong to the aphasic range and N/A means not available.

ID	Age	Gender
C01	69	M
C02	69	M
C03	65	M
C04	69	F
C05	64	M
C06	71	F
C07	50	F
C10	72	M
C11	63	F
C13	65	M
C14	67	F
C16	69	F
C17	53	M
C18	55	M
C20	62	F
C21	56	F
C23	66	F

TABLE A.1: Control subject's information.

				Lesion volume			CAT						PALPA		
ID	**Age**	**Gender**	**TPS**	**London**	**Liège**	**BNT**	**Nam-O**	**Nam -A**	**Co-SW**	**Co-WW**	**Co-SS**	**Co-WS**	**Mo-w**	**NW**	**Min-P**
P01	63	M	69	213.75	128.89	47	47	9	30	**25**	**23**	27	37	34	116
P03	49	F	9	83.42	60.49	12	**21**	**4**	**22**	**20**	28	27	40	36	38
P04	69	M	176	145.38	109.09	31	**42**	**7**	28	**26**	29	25	46	60	98
P05	73	M	62	68.57	59.19	55	48	10	30	30	30	30	46	52	94
P10	49	F	283	233.22	202.98	36	**39**	**7**	30	30	**27**	**22**	46	54	114
P11	54	M	72	321.62	276.29	14	**21**	**4**	**22**	**24**	**25**	24	18	16	90
P12	41	M	59	233.45	168.81	28	**32**	**4**	26	29	**20**	**19**	46	46	92
P13	48	M	51	161.79	47.32	34	**37**	9	30	29	**24**	27	31	9	84
P15	66	M	55	104.61	73.78	52	**42**	**8**	30	28	**23**	**17**	46	39	108
P16	44	F	67	71.13	61.38	34	**39**	**8**	27	**27**	28	26	46	60	106
P17	54	M	29	99.91	82.95	35	**36**	**8**	29	**27**	**21**	**20**	46	47	112
P18	63	M	94	244.46	208.15	33	**39**	**5**	30	28	28	24	46	23	102
P19	62	F	75	78.86	51.84	43	46	**7**	30	29	**27**	24	35	18	82
P20	67	M	42	279.50	217.44	42	44	**7**	28	30	**27**	**19**	45	55	118
P21	40	F	16	265.00	192.74	30	**35**	**2**	**24**	28	**24**	**17**	42	N/A	0
P22	41	M	8	72.66	60.23	23	**32**	**2**	26	28	30	28	43	46	102
P23	63	M	262	146.69	122.91	51	46	10	30	**27**	**25**	**23**	45	53	115
P24	47	M	50	277.37	234.11	16	**23**	**0**	29	**25**	**14**	**14**	42	22	106
P25	66	M	38	282	144.66	1	**0**	**0**	27	**27**	**21**	**16**	34	18	86
P27	60	F	133	111.69	100.50	27	**31**	**3**	**22**	**27**	**20**	**12**	42	48	84
P28	41	M	18	79.14	67.42	42	46	**7**	27	30	**12**	**18**	39	25	90
P29	51	F	63	138.46	109.02	47	**42**	**8**	**19**	30	**20**	24	43	37	92
P30	21	F	33	112.62	114.33	18	**27**	**3**	28	29	**26**	**21**	37	17	92
P31	47	F	53	139.58	126.11	9	**27**	**0**	**18**	30	**25**	**23**	21	0	108
P33	43	F	5	130.10	133.54	21	**34**	**5**	30	30	**23**	24	42	11	107
P35	68	M	55	208.82	138.05	1	**0**	**0**	**23**	**26**	**17**	**20**	37	6	86

TABLE A.2: Patients' information and raw score in the linguistic assessment.

Appendix B

Global analysis: Raw values

	Median in warped A map	
Patients	**GM**	**WM**
P01	81.3605	69.6657
P03	79.4726	69.0503
P04	82.0647	69.5245
P05	80.6324	69.3861
P10	83.3746	69.7217
P11	80.9280	69.4506
P12	83.3487	69.5992
P13	82.0443	69.3371
P15	81.2830	69.9344
P16	112.4102	96.0706
P17	82.1387	69.1133
P18	84.8639	69.5457
P19	79.4264	69.0364
P20	82.0943	69.6776
P21	82.7172	69.3227
P22	82.0784	69.0294
P23	81.6261	69.3464
P24	83.9207	69.6146
P25	79.2958	69.5042
P27	79.3095	69.1910
P28	81.8715	69.3465
P29	80.1632	69.0914
P30	82.7529	69.1075
P31	81.0514	69.1260
P33	81.6916	68.8874
P35	81.8394	69.3732

TABLE B.1: Median warped A map voxels belonging to right hemisphere GM and WM for each patient.

	Median in warped A map	
Controls	**GM**	**WM**
C01	82.6337	69.3058
C02	80.6856	69.2494
C03	82.0200	69.5405
C04	79.6070	68.8969
C05	81.1371	69.2100
C06	80.2537	69.3168
C07	81.1756	69.2364
C10	81.6047	69.3112
C11	82.9221	69.2823
C13	79.4944	69.1563
C14	81.4437	69.1773
C16	82.0978	69.7375
C17	81.9818	69.2476
C18	81.5327	69.2537
C20	81.3044	69.1684
C21	80.4634	69.3059
C23	80.8855	69.1194

TABLE B.2: Median warped A map voxels belonging to right hemisphere GM and WM for each control.

	Median in warped MT map	
Patients	**GM**	**WM**
P01	0.7662	1.4472
P03	0.8627	1.6111
P04	0.8102	1.5661
P05	0.8081	1.5062
P10	0.8207	1.6279
P11	0.8257	1.5841
P12	0.8552	1.6965
P13	0.8489	1.6219
P15	0.8298	1.4993
P16	0.7954	1.5831
P17	0.8370	1.6661
P18	0.8509	1.7487
P19	0.8622	1.5821
P20	0.8060	1.5632
P21	0.8718	1.7216
P22	0.8250	1.6744
P23	0.8374	1.6163
P24	0.8201	1.7205
P25	0.8089	1.5290
P27	0.8478	1.6364
P28	0.8680	1.7222
P29	0.8814	1.6849
P30	0.7782	1.5973
P31	0.8147	1.5845
P33	0.8776	1.6860
P35	0.8456	1.5975

TABLE B.3: Median warped MT map voxels belonging to right hemisphere GM and WM for each patient.

	Median in warped MT map	
Controls	**GM**	**WM**
C01	0.8241	1.6275
C02	0.8139	1.5248
C03	0.7980	1.5389
C04	0.7509	1.5519
C05	0.8489	1.5997
C06	0.8399	1.4982
C07	0.8805	1.6426
C10	0.8103	1.5624
C11	0.8606	1.6670
C13	0.8326	1.5291
C14	0.8645	1.6575
C16	0.8050	1.5627
C17	0.8575	1.6186
C18	0.8653	1.6162
C20	0.8800	1.6156
C21	0.8615	1.5782
C23	0.8856	1.6514

TABLE B.4: Median warped MT map voxels belonging to right hemisphere GM and WM for each control.

	Median in warped R_1 map	
Patients	**GM**	**WM**
P01	594.6948	892.8184
P03	656.4594	995.7042
P04	658.9201	996.6180
P05	626.9937	942.5966
P10	608.7685	964.8032
P11	625.1616	951.3639
P12	637.0975	1011.4070
P13	646.9993	994.5627
P15	622.2228	915.2843
P16	643.7716	994.0233
P17	634.8670	999.1631
P18	644.1038	1060.9144
P19	642.0609	962.9507
P20	616.8568	973.8965
P21	680.3984	1075.8595
P22	649.2357	1035.0546
P23	658.7140	1006.6649
P24	643.8391	1038.5808
P25	652.0826	966.8718
P27	673.9301	1038.7577
P28	685.7045	1062.6967
P29	698.5145	1068.4587
P30	618.2897	1003.7772
P31	647.3028	1004.2674
P33	657.7977	1028.1002
P35	672.6499	1021.9510

TABLE B.5: Median warped R_1 map voxels belonging to right hemisphere GM and WM for each patient.

	Median in warped R_1 map	
Controls	**GM**	**WM**
C01	637.5596	1000.9592
C02	649.6628	980.4170
C03	643.4767	988.3649
C04	630.1639	959.8559
C05	647.4498	998.2108
C06	651.9718	966.5318
C07	662.8224	998.4008
C10	645.8503	990.4243
C11	674.0198	1047.1972
C13	661.2930	985.7985
C14	679.4511	1030.3577
C16	636.0275	977.7691
C17	676.8810	1048.3699
C18	672.0001	1027.3215
C20	665.5569	1026.0634
C21	643.1607	969.4879
C23	665.5879	1021.2870

TABLE B.6: Median warped R_1 map voxels belonging to right hemisphere GM and WM for each control.

	Median in warped R_2^* map	
Patients	**GM**	**WM**
P01	0.0167	0.0202
P03	0.0176	0.0209
P04	0.0179	0.0217
P05	0.0167	0.0201
P10	0.0160	0.0203
P11	0.0168	0.0203
P12	0.0158	0.0205
P13	0.0177	0.0215
P15	0.0158	0.0191
P16	0.0175	0.0207
P17	0.0166	0.0208
P18	0.0169	0.0224
P19	0.0174	0.0206
P20	0.0170	0.0213
P21	0.0165	0.0218
P22	0.0168	0.0211
P23	0.0165	0.0207
P24	0.0162	0.0209
P25	0.0169	0.0206
P27	0.0172	0.0207
P28	0.0164	0.0210
P29	0.0164	0.0202
P30	0.0155	0.0200
P31	0.0172	0.0205
P33	0.0167	0.0204
P35	0.0175	0.0217

TABLE B.7: Median warped R_2^* map voxels belonging to right hemisphere GM and WM for each patient.

	Median in warped R_2^* map	
Controls	**GM**	**WM**
C01	0.0168	0.0212
C02	0.0174	0.0208
C03	0.0172	0.0215
C04	0.0180	0.0203
C05	0.0172	0.0210
C06	0.0166	0.0196
C07	0.0170	0.0198
C10	0.0176	0.0220
C11	0.0177	0.0216
C13	0.0186	0.0212
C14	0.0180	0.0222
C16	0.0170	0.0209
C17	0.0167	0.0207
C18	0.0165	0.0205
C20	0.0173	0.0207
C21	0.0166	0.0198
C23	0.0179	0.0213

TABLE B.8: Median warped R_2^* map voxels belonging to right hemisphere GM and WM for each control.

Appendix C

Statistical Tables

C.1 Controls vs Patients in right hemisphere

C.1.1 Local statistical analysis - VBQ

Statistics: ***p-values adjusted for search volume***

set-level		cluster-level				peak-level					mm	mm	mm
p	c	$p_{FWE\text{-}corr}$	$q_{FDR\text{-}corr}$	k_E	p_{uncorr}	$p_{FWE\text{-}corr}$	$q_{FDR\text{-}corr}$	F	(Z_E)	p_{uncorr}			
0.006	22	0.751	0.926	150	0.115	0.323	0.309	24.77	4.20	0.000	21	55	15
		0.886	0.926	106	0.180	0.327	0.309	24.72	4.19	0.000	32	38	25
		0.542	0.926	214	0.065	0.441	0.314	23.27	4.09	0.000	38	40	15
		0.997	0.926	31	0.470	0.821	0.545	19.31	3.77	0.000	10	58	12
		0.994	0.926	38	0.421	0.844	0.545	19.05	3.74	0.000	56	-19	-21
		0.992	0.926	41	0.403	0.846	0.545	19.01	3.74	0.000	15	-94	10
		0.986	0.926	50	0.354	0.867	0.545	18.76	3.72	0.000	11	-3	12
		0.978	0.926	58	0.318	0.933	0.650	17.72	3.62	0.000	55	-4	-5
		0.986	0.926	50	0.354	0.955	0.672	17.24	3.58	0.000	7	50	26
		0.999	0.926	15	0.628	0.977	0.744	16.56	3.51	0.000	2	-24	-6
		0.834	0.926	124	0.149	0.989	0.806	15.99	3.46	0.000	38	5	-20
		0.999	0.926	15	0.628	0.996	0.831	15.31	3.39	0.000	37	39	-11
		0.999	0.926	19	0.580	0.997	0.831	15.11	3.36	0.000	2	2	-1
		1.000	0.926	14	0.641	0.998	0.831	14.91	3.34	0.000	57	-9	-14
		0.999	0.926	20	0.569	0.999	0.868	14.36	3.28	0.001	21	-1	-6
		1.000	0.926	2	0.886	1.000	0.935	13.74	3.22	0.001	16	59	13
		1.000	0.926	3	0.853	1.000	0.935	13.60	3.20	0.001	53	5	14
		1.000	0.926	2	0.886	1.000	0.941	13.28	3.16	0.001	57	-16	4
		1.000	0.926	4	0.825	1.000	0.941	13.27	3.16	0.001	18	47	32
		1.000	0.926	2	0.886	1.000	0.975	13.01	3.13	0.001	58	-31	-9
		1.000	0.926	1	0.926	1.000	0.985	12.84	3.11	0.001	35	5	-10
		1.000	0.926	1	0.926	1.000	0.988	12.70	3.10	0.001	20	0	-1

table shows 3 local maxima more than 8.0mm apart

Height threshold: F = 12.66, p = 0.001 (1.000)
Extent threshold: k = 0 voxels
Expected voxels per cluster, <k> = 62.864
Expected number of clusters, <c> = 12.03
FWEp: 32.879, FDRp: Inf, FWEc: Inf, FDRc: Inf

Degrees of freedom = [1.0, 39.0]
FWHM = 9.8 8.8 9.3 mm mm mm; 9.8 8.8 9.3 {voxels}
Volume: 512722 = 512722 voxels = 553.6 resels
Voxel size: 1.0 1.0 1.0 mm mm mm; (resel = 798.19 voxels)

FIGURE C.1: Significant difference in voxel level with p uncorrected at 0.001 between patient's and control's right hemisphere in MT map grey matter.

Statistics: ***p-values adjusted for search volume***

set-level		cluster-level				peak-level					mm mm mm
p	c	$p_{FWE\text{-}corr}$	$q_{FDR\text{-}corr}$	k_E	p_{uncorr}	$p_{FWE\text{-}corr}$	$q_{FDR\text{-}corr}$	F	(Z_E)	p_{uncorr}	
0.000	33	0.653	0.598	187	0.094	0.281	0.608	25.14	4.22	0.000	37 40 13
		0.209	0.598	392	0.021	0.424	0.608	23.20	4.08	0.000	44 -71 -6
						0.601	0.608	21.32	3.94	0.000	41 -63 -9
		0.895	0.598	105	0.200	0.485	0.608	22.52	4.03	0.000	38 -9 -28
		0.631	0.598	194	0.089	0.548	0.608	21.85	3.98	0.000	59 -14 -30
						0.999	0.736	14.28	3.28	0.001	55 -18 -22
		0.892	0.598	106	0.198	0.574	0.608	21.60	3.96	0.000	25 -65 -7
		0.622	0.598	197	0.086	0.633	0.608	21.00	3.91	0.000	45 -61 27
		0.634	0.598	193	0.089	0.786	0.608	19.46	3.78	0.000	28 50 -12
		0.859	0.598	119	0.174	0.790	0.608	19.42	3.78	0.000	13 -70 46
		0.994	0.761	35	0.461	0.864	0.608	18.55	3.70	0.000	65 -41 -21
		0.718	0.598	166	0.113	0.890	0.608	18.19	3.67	0.000	56 -54 17
		0.845	0.598	124	0.166	0.907	0.608	17.95	3.64	0.000	37 -17 52
		0.913	0.598	97	0.217	0.931	0.608	17.52	3.60	0.000	28 -54 48
		0.968	0.724	66	0.307	0.956	0.608	16.98	3.55	0.000	30 -88 -9
		0.991	0.756	42	0.417	0.959	0.608	16.92	3.55	0.000	67 -24 28
		0.993	0.756	39	0.435	0.960	0.608	16.88	3.54	0.000	47 -39 -16
		0.911	0.598	98	0.215	0.965	0.608	16.74	3.53	0.000	56 -17 31
		0.990	0.756	43	0.412	0.970	0.613	16.58	3.51	0.000	47 -49 41
		0.989	0.756	45	0.401	0.981	0.636	16.18	3.47	0.000	54 -21 48
		0.998	0.799	25	0.539	0.989	0.644	15.76	3.43	0.000	44 -29 58
		0.988	0.756	47	0.390	0.991	0.644	15.57	3.41	0.000	59 -30 31
		0.957	0.710	74	0.280	0.991	0.644	15.55	3.41	0.000	48 -60 4
		0.997	0.799	28	0.513	0.992	0.644	15.46	3.40	0.000	31 -83 6
		1.000	0.930	8	0.749	0.997	0.666	14.96	3.35	0.000	34 -31 51
		1.000	0.930	4	0.833	0.997	0.666	14.96	3.35	0.000	20 59 4
		0.998	0.799	23	0.557	0.998	0.696	14.72	3.32	0.000	36 8 40
		1.000	0.930	8	0.749	0.999	0.736	14.28	3.28	0.001	38 -75 10
		1.000	0.930	9	0.731	0.999	0.736	14.20	3.27	0.001	14 -93 10
		1.000	0.930	1	0.930	1.000	0.874	13.46	3.18	0.001	23 -58 24

table shows 3 local maxima more than 8.0mm apart

Height threshold: F = 12.66, p = 0.001 (1.000)
Extent threshold: k = 0 voxels
Expected voxels per cluster, <k> = 68.365
Expected number of clusters, <c> = 11.26
FWEp: 32.576, FDRp: Inf, FWEc: Inf, FDRc: Inf

Degrees of freedom = [1.0, 39.0]
FWHM = 10.0 9.0 9.6 mm mm mm; 10.0 9.0 9.6 {voxels}
Volume: 512580 = 512580 voxels = 507.2 resels
Voxel size: 1.0 1.0 1.0 mm mm mm; (resel = 868.03 voxels)
Page 1

Statistics: ***p-values adjusted for search volume***

set-level		cluster-level				peak-level					mm mm mm
p	c	$p_{FWE\text{-}corr}$	$q_{FDR\text{-}corr}$	k_E	p_{uncorr}	$p_{FWE\text{-}corr}$	$q_{FDR\text{-}corr}$	F	(Z_E)	p_{uncorr}	
		1.000	0.930	2	0.892	1.000	0.950	13.11	3.14	0.001	23 -96 -11
		1.000	0.930	1	0.930	1.000	0.950	12.97	3.13	0.001	40 17 9
		1.000	0.930	3	0.860	1.000	0.950	12.97	3.13	0.001	11 -75 -3
		1.000	0.930	1	0.930	1.000	0.981	12.77	3.10	0.001	41 -29 23
		1.000	0.930	1	0.930	1.000	0.981	12.72	3.10	0.001	36 50 -2

table shows 3 local maxima more than 8.0mm apart

Height threshold: F = 12.66, p = 0.001 (1.000)
Extent threshold: k = 0 voxels
Expected voxels per cluster, <k> = 68.365
Expected number of clusters, <c> = 11.26
FWEp: 32.576, FDRp: Inf, FWEc: Inf, FDRc: Inf

Degrees of freedom = [1.0, 39.0]
FWHM = 10.0 9.0 9.6 mm mm mm; 10.0 9.0 9.6 {voxels}
Volume: 512580 = 512580 voxels = 507.2 resels
Voxel size: 1.0 1.0 1.0 mm mm mm; (resel = 868.03 voxels)
Page 2/2

FIGURE C.2: Significant difference in voxel level with p uncorrected at 0.001 between patient's and control's right hemisphere in R_1 map grey matter.

C.1.2 Local statistical analysis - VBM

Statistics: ***p-values adjusted for search volume***

set-level		cluster-level				peak-level					mm mm mm
p	c	$p_{FWE\text{-}corr}$	$q_{FDR\text{-}corr}$	k_E	p_{uncorr}	$p_{FWE\text{-}corr}$	$q_{FDR\text{-}corr}$	F	(Z_E)	p_{uncorr}	
0.995	3	0.999	0.878	13	0.707	0.995	0.886	14.49	3.30	0.000	25 38 46
		0.999	0.878	9	0.762	0.997	0.886	14.28	3.28	0.001	6 -3 -5
		1.000	0.878	3	0.878	1.000	0.886	13.06	3.14	0.001	66 -25 27

table shows 3 local maxima more than 8.0mm apart

Height threshold: F = 12.66, p = 0.001 (1.000)
Extent threshold: k = 0 voxels
Expected voxels per cluster, <k> = 84.527
Expected number of clusters, <c> = 9.33
FWEp: 31.768, FDRp: Inf, FWEc: Inf, FDRc: Inf

Degrees of freedom = [1.0, 39.0]
FWHM = 10.6 9.7 10.4 mm mm mm; 10.6 9.7 10.4 {voxels}
Volume: 512722 = 512722 voxels = 411.7 resels
Voxel size: 1.0 1.0 1.0 mm mm mm; (resel = 1073.24 voxels)

FIGURE C.3: Significant difference in voxel level with p uncorrected at 0.001 between patient's and control's right hemisphere in R_2^* map grey matter.

C.2 Within patient analysis in the right hemisphere

No statistical results, obtained at p<0.001 uncorrected for MT and R_1 in white matter.

Statistics: ***p-values adjusted for search volume***

set-level		cluster-level				peak-level					mm mm mm
p	c	$p_{FWE\text{-}corr}$	$q_{FDR\text{-}corr}$	k_E	p_{uncorr}	$p_{FWE\text{-}corr}$	$q_{FDR\text{-}corr}$	F	(Z_E)	p_{uncorr}	
0.031	5	0.172	0.549	714	0.110	0.030	0.141	26.79	4.34	0.000	20 -32 29
						0.619	0.669	14.54	3.30	0.000	20 -42 26
		0.518	0.665	173	0.424	0.143	0.358	20.80	3.89	0.000	11 -33 -44
						0.549	0.669	15.18	3.37	0.000	4 -28 -44
		0.600	0.665	109	0.532	0.236	0.417	18.84	3.73	0.000	15 -22 -30
		0.573	0.665	129	0.494	0.404	0.601	16.61	3.52	0.000	3 -27 26
		0.813	0.973	1	0.973	0.815	0.979	12.73	3.10	0.001	20 -62 -3

table shows 3 local maxima more than 8.0mm apart

Height threshold: F = 12.66, p = 0.001 (0.821)
Extent threshold: k = 0 voxels
Expected voxels per cluster, <k> = 289.226
Expected number of clusters, <c> = 1.72
FWEp: 24.816, FDRp: Inf, FWEc: Inf, FDRc: Inf

Degrees of freedom = [1.0, 39.0]
FWHM = 15.4 15.5 15.4 mm mm mm; 15.4 15.5 15.4 {voxels}
Volume: 248375 = 248375 voxels = 57.9 resels
Voxel size: 1.0 1.0 1.0 mm mm mm; (resel = 3672.31 voxels)

FIGURE C.4: Significant difference in voxel level with p uncorrected at 0.001 between patient's and control's right hemisphere in MT map white matter.

Statistics: ***p-values adjusted for search volume***

set-level		cluster-level				peak-level					mm mm mm
p	c	$p_{FWE\text{-}corr}$	$q_{FDR\text{-}corr}$	k_E	p_{uncorr}	$p_{FWE\text{-}corr}$	$q_{FDR\text{-}corr}$	F	(Z_E)	p_{uncorr}	
0.352	2	0.453	0.876	203	0.487	0.239	0.441	17.63	3.61	0.000	20 -33 28
		0.663	0.876	16	0.876	0.625	0.791	13.41	3.18	0.001	38 -16 55

table shows 3 local maxima more than 8.0mm apart

Height threshold: F = 12.66, p = 0.001 (0.711)
Extent threshold: k = 0 voxels
Expected voxels per cluster, <k> = 441.839
Expected number of clusters, <c> = 1.24
FWEp: 23.531, FDRp: Inf, FWEc: Inf, FDRc: Inf

Degrees of freedom = [1.0, 39.0]
FWHM = 18.2 17.8 17.3 mm mm mm; 18.2 17.8 17.3 {voxels}
Volume: 248375 = 248375 voxels = 37.9 resels
Voxel size: 1.0 1.0 1.0 mm mm mm; (resel = 5610.05 voxels)

FIGURE C.5: Significant difference in voxel level with p uncorrected at 0.001 between patient's and control's right hemisphere in R_1 map white matter.

C.3 Pipeline effects on control data

C.3.1 VBQ

Statistics: ***p-values adjusted for search volume***

cluster-level				peak-level					mm mm mm
$p_{FWE\text{-}corr}$	$q_{FDR\text{-}corr}$	k_E	p_{uncorr}	$p_{FWE\text{-}corr}$	$q_{FDR\text{-}corr}$	F	(Z_E)	p_{uncorr}	
0.528	0.367	177	0.367	0.491	0.330	16.31	3.49	0.000	21 -85 0

table shows 3 local maxima more than 8.0mm apart

Height threshold: F = 12.66, p = 0.001 (0.871)
Extent threshold: k = 0 voxels
Expected voxels per cluster, <k> = 234.345
Expected number of clusters, <c> = 2.05
FWEp: 25.494, FDRp: Inf, FWEc: Inf, FDRc: Inf

Degrees of freedom = [1.0, 39.0]
FWHM = 15.5 13.9 13.8 mm mm mm; 15.5 13.9 13.8 {voxels}
Volume: 248375 = 248375 voxels = 71.4 resels
Voxel size: 1.0 1.0 1.0 mm mm mm; (resel = 2975.49 voxels)

FIGURE C.6: Significant difference in voxel level with p uncorrected at 0.001 between patient's and control's right hemisphere in R_2^* map white matter.

C.3.2 VBM

Statistics: ***p-values adjusted for search volume***

set-level		cluster-level				peak-level					mm mm mm
p	c	$p_{FWE\text{-}corr}$	$q_{FDR\text{-}corr}$	k_E	p_{uncorr}	$p_{FWE\text{-}corr}$	$q_{FDR\text{-}corr}$	T	(Z_E)	p_{uncorr}	
0.000	6	0.000	0.000	679	0.000	0.000	0.027	8.23	6.23	0.000	4 -29 -8
						0.008	0.436	6.41	5.27	0.000	17 -23 -5
		0.000	0.000	500	0.000	0.000	0.053	7.57	5.90	0.000	8 -2 9
						0.004	0.378	6.67	5.42	0.000	12 -7 14
		0.004	0.322	21	0.161	0.001	0.064	7.40	5.81	0.000	8 9 50
		0.011	0.544	6	0.453	0.006	0.419	6.55	5.35	0.000	5 23 53
		0.015	0.607	3	0.607	0.012	0.550	6.28	5.19	0.000	15 -93 -6
		0.010	0.544	8	0.383	0.015	0.663	6.17	5.13	0.000	2 -33 -18

table shows 3 local maxima more than 8.0mm apart

Height threshold: T = 5.99, p = 0.000 (0.025)
Extent threshold: k = 0 voxels
Expected voxels per cluster, <k> = 11.324
Expected number of clusters, <c> = 0.03
FWEp: 5.730, FDRp: 7.921, FWEc: 3, FDRc: 500

Degrees of freedom = [1.0, 39.0]
FWHM = 8.7 9.1 8.9 mm mm mm; 8.7 9.1 8.9 {voxels}
Volume: 1019560 = 1019560 voxels = 1400.4 resels
Voxel size: 1.0 1.0 1.0 mm mm mm; (resel = 697.36 voxels)

FIGURE C.7: List of voxels in which GM atrophy in patients occurs after a t-test with a p<0.025 FWE corrected level.

Statistics: ***p-values adjusted for search volume***

set-level		cluster-level				peak-level					mm mm mm
p	c	$p_{FWE\text{-}corr}$	$q_{FDR\text{-}corr}$	k_E	p_{uncorr}	$p_{FWE\text{-}corr}$	$q_{FDR\text{-}corr}$	T	(Z_E)	p_{uncorr}	
0.000	5	0.000	0.000	11841	0.000	0.000	0.001	8.23	6.23	0.000	4 -29 -8
						0.000	0.001	7.57	5.90	0.000	8 -2 9
						0.004	0.009	6.67	5.42	0.000	12 -7 14
		0.000	0.000	2521	0.000	0.001	0.002	7.40	5.81	0.000	8 9 50
						0.006	0.010	6.55	5.35	0.000	5 23 53
						0.069	0.048	5.61	4.77	0.000	6 46 41
		0.000	0.000	2204	0.000	0.012	0.013	6.28	5.19	0.000	15 -93 -6
						0.323	0.154	4.96	4.34	0.000	19 -92 -13
						0.450	0.179	4.79	4.22	0.000	5 -80 -1
		0.000	0.000	1909	0.000	0.403	0.179	4.85	4.26	0.000	24 -72 -45
						0.968	0.424	4.07	3.69	0.000	30 -65 -49
						0.985	0.473	3.98	3.63	0.000	15 -61 -48
		0.001	0.001	1683	0.000	0.413	0.179	4.84	4.26	0.000	29 14 3
						1.000	0.851	3.50	3.25	0.001	25 21 6
						1.000	0.860	3.49	3.24	0.001	36 -4 10

table shows 3 local maxima more than 8.0mm apart

Height threshold: T = 3.31, p = 0.001 (1.000)
Extent threshold: k = 1683 voxels, p = 0.000 (0.001)
Expected voxels per cluster, <k> = 68.395
Expected number of clusters, <c> = 0.00
FWEp: 5.730, FDRp: 5.606, FWEc: 1683, FDRc: 1683

Degrees of freedom = [1.0, 39.0]
FWHM = 8.7 9.1 8.9 mm mm mm; 8.7 9.1 8.9 {voxels}
Volume: 1019560 = 1019560 voxels = 1400.4 resels
Voxel size: 1.0 1.0 1.0 mm mm mm; (resel = 697.36 voxels)

FIGURE C.8: List of voxels belonging to a significant cluster with p<0.025 FWE corrected level in which GM atrophy in patients occurs after a t-test.

Statistics: ***p-values adjusted for search volume***

set-level		cluster-level				peak-level					mm mm mm
p	c	$p_{FWE\text{-}corr}$	$q_{FDR\text{-}corr}$	k_E	p_{uncorr}	$p_{FWE\text{-}corr}$	$q_{FDR\text{-}corr}$	F	(Z_E)	p_{uncorr}	
0.820	16	0.333	0.332	208	0.021	0.368	0.399	18.64	4.35	0.000	51 -68 15
		0.990	0.895	47	0.237	0.862	0.860	14.09	3.92	0.000	57 -30 -6
		1.000	0.895	18	0.468	0.977	0.942	12.31	3.70	0.000	45 26 26
		0.999	0.895	28	0.361	0.997	0.942	11.18	3.56	0.000	59 -2 -16
		0.994	0.895	42	0.263	0.999	0.942	10.79	3.50	0.000	51 -44 36
		1.000	0.895	11	0.579	1.000	0.942	10.42	3.45	0.000	50 36 -1
		1.000	0.895	6	0.694	1.000	0.942	10.02	3.39	0.000	57 33 8
		1.000	0.895	1	0.895	1.000	0.942	9.66	3.33	0.000	25 10 -29
		1.000	0.895	4	0.757	1.000	0.942	9.64	3.33	0.000	26 30 43
		1.000	0.895	7	0.668	1.000	0.942	9.43	3.29	0.000	53 -2 44
		1.000	0.895	3	0.795	1.000	0.987	8.53	3.14	0.001	58 2 -22
		1.000	0.895	3	0.795	1.000	0.987	8.46	3.12	0.001	56 -52 14
		1.000	0.895	2	0.839	1.000	0.987	8.46	3.12	0.001	60 13 18
		1.000	0.895	1	0.895	1.000	0.987	8.36	3.10	0.001	34 43 37
		1.000	0.895	1	0.895	1.000	0.987	8.35	3.10	0.001	47 -55 -19
		1.000	0.895	1	0.895	1.000	0.987	8.31	3.10	0.001	40 -32 52

table shows 3 local maxima more than 8.0mm apart

Height threshold: F = 8.28, p = 0.001 (1.000)
Extent threshold: k = 0 voxels
Expected voxels per cluster, <k> = 36.226
Expected number of clusters, <c> = 19.58
FWEp: 27.124, FDRp: Inf, FWEc: Inf, FDRc: Inf

Degrees of freedom = [3.0, 19.0]
FWHM = 10.0 8.8 9.1 mm mm mm; 10.0 8.8 9.1 {voxels}
Volume: 512580 = 512580 voxels = 547.4 resels
Voxel size: 1.0 1.0 1.0 mm mm mm; (resel = 804.34 voxels)

FIGURE C.9: Significant difference with p uncorrected at 0.001 between patients' right hemisphere in MT map grey matter.

Statistics: ***p-values adjusted for search volume***

set-level		cluster-level				peak-level					mm mm mm
p	c	$p_{FWE\text{-}corr}$	$q_{FDR\text{-}corr}$	k_E	p_{uncorr}	$p_{FWE\text{-}corr}$	$q_{FDR\text{-}corr}$	F	(Z_E)	p_{uncorr}	
0.947	8	0.974	0.880	63	0.278	0.852	0.904	13.02	3.79	0.000	51 -67 15
		1.000	0.880	16	0.599	0.968	0.904	11.48	3.60	0.000	26 29 43
		0.998	0.880	26	0.492	0.981	0.904	11.10	3.55	0.000	49 10 9
		1.000	0.880	14	0.626	0.999	0.904	9.73	3.34	0.000	48 -56 -20
		1.000	0.880	6	0.766	1.000	0.904	9.33	3.28	0.001	45 -13 -33
		1.000	0.880	3	0.845	1.000	0.965	8.76	3.18	0.001	12 9 67
		1.000	0.880	2	0.880	1.000	0.965	8.55	3.14	0.001	5 -83 -33
		1.000	0.880	2	0.880	1.000	0.965	8.36	3.11	0.001	54 -32 -5

table shows 3 local maxima more than 8.0mm apart

Height threshold: F = 8.28, p = 0.001 (1.000)
Extent threshold: k = 0 voxels
Expected voxels per cluster, <k> = 57.910
Expected number of clusters, <c> = 13.05
FWEp: 25.282, FDRp: Inf, FWEc: Inf, FDRc: Inf

Degrees of freedom = [3.0, 19.0]
FWHM = 11.7 10.2 10.8 mm mm mm; 11.7 10.2 10.8 {voxels}
Volume: 512580 = 512580 voxels = 342.4 resels
Voxel size: 1.0 1.0 1.0 mm mm mm; (resel = 1285.81 voxels)

FIGURE C.10: Significant difference with p uncorrected at 0.001 between patients' right hemisphere in R_1 map grey matter.

Statistics: ***p-values adjusted for search volume***

set-level		cluster-level				peak-level					mm mm mm
p	c	$p_{FWE\text{-}corr}$	$q_{FDR\text{-}corr}$	k_E	p_{uncorr}	$p_{FWE\text{-}corr}$	$q_{FDR\text{-}corr}$	F	(Z_E)	p_{uncorr}	
0.945	8	0.998	0.852	29	0.469	0.743	0.898	13.96	3.90	0.000	35 22 38
		0.994	0.852	40	0.391	0.935	0.898	12.05	3.67	0.000	57 -52 27
		0.997	0.852	32	0.445	0.979	0.898	11.15	3.55	0.000	50 0 -45
		0.998	0.852	28	0.477	0.995	0.914	10.36	3.44	0.000	24 -11 58
		0.999	0.852	22	0.532	0.999	0.914	9.85	3.36	0.000	28 18 -25
		1.000	0.923	1	0.923	1.000	0.945	8.75	3.18	0.001	45 -27 24
		1.000	0.923	2	0.880	1.000	0.945	8.67	3.16	0.001	16 -55 58
		1.000	0.923	1	0.923	1.000	0.945	8.41	3.11	0.001	46 -28 25

table shows 3 local maxima more than 8.0mm apart

Height threshold: F = 8.28, p = 0.001 (1.000)
Extent threshold: k = 0 voxels
Expected voxels per cluster, <k> = 58.413
Expected number of clusters, <c> = 12.95
FWEp: 25.250, FDRp: Inf, FWEc: Inf, FDRc: Inf

Degrees of freedom = [3.0, 19.0]
FWHM = 11.8 10.2 10.8 mm mm mm; 11.8 10.2 10.8 {voxels}
Volume: 512580 = 512580 voxels = 339.5 resels
Voxel size: 1.0 1.0 1.0 mm mm mm; (resel = 1296.96 voxels)

FIGURE C.11: Significant difference with p uncorrected at 0.001 between patients' right hemisphere in R_2^* map grey matter.

Statistics: ***p-values adjusted for search volume***

set-level		cluster-level				peak-level					mm mm mm
p	c	$p_{FWE\text{-}corr}$	$q_{FDR\text{-}corr}$	k_E	p_{uncorr}	$p_{FWE\text{-}corr}$	$q_{FDR\text{-}corr}$	F	(Z_E)	p_{uncorr}	
0.394	4	0.159	0.217	533	0.054	0.197	0.344	15.04	4.02	0.000	33 -36 29
						0.937	0.869	8.59	3.15	0.001	41 -31 25
		0.894	0.850	22	0.706	0.796	0.869	9.86	3.36	0.000	23 -95 1
		0.925	0.850	10	0.814	0.929	0.869	8.69	3.17	0.001	23 -54 33
		0.933	0.850	7	0.850	0.935	0.869	8.61	3.15	0.001	33 -40 38

table shows 3 local maxima more than 8.0mm apart

Height threshold: F = 8.28, p = 0.001 (0.959)
Extent threshold: k = 0 voxels
Expected voxels per cluster, <k> = 142.383
Expected number of clusters, <c> = 3.18
FWEp: 19.659, FDRp: Inf, FWEc: Inf, FDRc: Inf

Degrees of freedom = [3.0, 19.0]
FWHM = 15.9 14.1 14.1 mm mm mm; 15.9 14.1 14.1 {voxels}
Volume: 257487 = 257487 voxels = 69.7 resels
Voxel size: 1.0 1.0 1.0 mm mm mm; (resel = 3161.38 voxels)

FIGURE C.12: Significant difference with p uncorrected at 0.001 between patients' right hemisphere in R_2^* map white matter.

Statistics: ***p-values adjusted for search volume***

set-level		cluster-level				peak-level					mm mm mm
p	c	$p_{FWE\text{-}corr}$	$q_{FDR\text{-}corr}$	k_E	p_{uncorr}	$p_{FWE\text{-}corr}$	$q_{FDR\text{-}corr}$	F	(Z_E)	p_{uncorr}	
0.000	24	0.000	0.000	383	0.000	0.001	0.475	131.04	5.77	0.000	5 -51 10
						0.004	0.475	104.53	5.49	0.000	2 -47 20
						0.011	0.475	86.75	5.26	0.000	12 -46 5
		0.000	0.000	435	0.000	0.002	0.475	115.00	5.61	0.000	30 -4 59
						0.032	0.741	71.42	5.01	0.000	38 0 56
		0.000	0.011	58	0.003	0.003	0.475	113.08	5.59	0.000	43 -51 -34
		0.000	0.001	102	0.000	0.004	0.475	105.14	5.50	0.000	17 -8 -27
						0.005	0.475	102.44	5.46	0.000	21 -16 -30
		0.007	0.201	11	0.142	0.005	0.475	100.73	5.44	0.000	54 -37 -24
		0.000	0.000	126	0.000	0.007	0.475	94.14	5.36	0.000	32 2 -15
						0.014	0.475	83.92	5.22	0.000	29 9 -12
		0.003	0.109	21	0.050	0.008	0.475	93.79	5.35	0.000	37 36 34
		0.002	0.109	23	0.041	0.008	0.475	92.46	5.34	0.000	33 -45 -40
		0.000	0.011	56	0.003	0.008	0.475	91.90	5.33	0.000	4 8 -2
		0.000	0.001	94	0.000	0.009	0.475	90.91	5.32	0.000	43 -15 50
		0.004	0.164	16	0.082	0.013	0.475	84.56	5.23	0.000	24 -3 -13
		0.002	0.109	22	0.045	0.014	0.475	83.34	5.21	0.000	34 -40 -23
		0.027	0.611	2	0.535	0.014	0.475	83.05	5.20	0.000	9 9 57
		0.007	0.201	11	0.142	0.020	0.584	77.81	5.12	0.000	41 -51 -22
		0.022	0.557	3	0.441	0.021	0.584	77.10	5.11	0.000	10 -59 -39
		0.006	0.201	13	0.113	0.022	0.584	76.74	5.10	0.000	39 -39 -25
		0.006	0.201	12	0.127	0.023	0.584	76.35	5.10	0.000	23 8 54
		0.001	0.073	29	0.024	0.030	0.741	72.12	5.02	0.000	49 -26 48
		0.006	0.201	12	0.127	0.031	0.741	71.94	5.02	0.000	12 23 -1
		0.034	0.674	1	0.674	0.038	0.818	69.14	4.97	0.000	27 -41 -44
		0.022	0.557	3	0.441	0.038	0.818	69.09	4.97	0.000	25 18 52
		0.027	0.611	2	0.535	0.040	0.842	68.33	4.95	0.000	52 -42 -27
		0.034	0.674	1	0.674	0.041	0.848	67.88	4.95	0.000	39 -53 -21
		0.034	0.674	1	0.674	0.048	0.951	66.04	4.91	0.000	14 13 4

table shows 3 local maxima more than 8.0mm apart

Height threshold: F = 65.40, p = 0.000 (0.050)
Extent threshold: k = 0 voxels
Expected voxels per cluster, <k> = 5.376
Expected number of clusters, <c> = 0.05
FWEp: 65.397, FDRp: Inf, FWEc: 1, FDRc: 56

Degrees of freedom = [1.0, 16.0]
FWHM = 9.6 8.7 9.5 mm mm mm; 9.6 8.7 9.5 {voxels}
Volume: 512697 = 512697 voxels = 560.1 resels
Voxel size: 1.0 1.0 1.0 mm mm mm; (resel = 791.03 voxels)

FIGURE C.13: Significant difference in peak level with p corrected at 0.05 between two different pipelines for controls' right hemisphere in MT map grey matter.

Statistics: ***p-values adjusted for search volume***

set-level		cluster-level				peak-level					mm mm mm
p	c	$p_{FWE\text{-}corr}$	$q_{FDR\text{-}corr}$	k_E	p_{uncorr}	$p_{FWE\text{-}corr}$	$q_{FDR\text{-}corr}$	F	(Z_E)	p_{uncorr}	
0.000	14	0.000	0.000	2145	0.000	**0.001**	**0.011**	**131.04**	**5.77**	**0.000**	**5 -51 10**
						0.004	0.011	104.53	5.49	0.000	2 -47 20
						0.011	0.011	86.75	5.26	0.000	12 -46 5
		0.000	0.000	23854	0.000	**0.002**	**0.011**	**115.00**	**5.61**	**0.000**	**30 -4 59**
						0.009	0.011	90.91	5.32	0.000	43 -15 50
						0.023	0.013	76.35	5.10	0.000	23 8 54
		0.000	0.000	2160	0.000	**0.003**	**0.011**	**113.08**	**5.59**	**0.000**	**43 -51 -34**
						0.008	0.011	92.46	5.34	0.000	33 -45 -40
						0.146	0.049	52.24	4.61	0.000	40 -58 -28
		0.000	0.000	1394	0.000	**0.004**	**0.011**	**105.14**	**5.50**	**0.000**	**17 -8 -27**
						0.005	0.011	102.44	5.46	0.000	21 -16 -30
						0.352	0.087	42.10	4.33	0.000	19 -35 -10
		0.000	0.000	4045	0.000	**0.005**	**0.011**	**100.73**	**5.44**	**0.000**	**54 -37 -24**
						0.014	0.011	83.34	5.21	0.000	34 -40 -23
						0.020	0.013	77.81	5.12	0.000	41 -51 -22
		0.000	0.000	2475	0.000	**0.007**	**0.011**	**94.14**	**5.36**	**0.000**	**32 2 -15**
						0.013	0.011	84.56	5.23	0.000	24 -3 -13
						0.014	0.011	83.92	5.22	0.000	29 9 -12
		0.000	0.000	3445	0.000	**0.008**	**0.011**	**91.90**	**5.33**	**0.000**	**4 8 -2**
						0.031	0.017	71.94	5.02	0.000	12 23 -1
						0.048	0.021	66.04	4.91	0.000	14 13 4
		0.000	0.000	2512	0.000	**0.014**	**0.011**	**83.05**	**5.20**	**0.000**	**9 9 57**
						0.060	0.026	62.94	4.85	0.000	4 19 49
						0.087	0.033	58.33	4.75	0.000	7 -6 64
		0.001	0.000	1041	0.000	**0.021**	**0.013**	**77.10**	**5.11**	**0.000**	**10 -59 -39**
						0.038	0.018	69.14	4.97	0.000	27 -41 -44
						0.257	0.072	45.70	4.44	0.000	14 -43 -45
		0.033	0.013	513	0.002	**0.082**	**0.032**	**59.16**	**4.77**	**0.000**	**22 36 44**
		0.001	0.001	974	0.000	**0.181**	**0.058**	**49.73**	**4.55**	**0.000**	**9 -43 58**
						0.468	0.110	38.74	4.22	0.000	11 -32 49

table shows 3 local maxima more than 8.0mm apart

Height threshold: F = 16.12, p = 0.001 (1.000)
Extent threshold: k = 513 voxels, p = 0.002 (0.033)
Expected voxels per cluster, <k> = 44.619
Expected number of clusters, <c> = 0.03
FWEp: 65.397, FDRp: 52.236, FWEc: 513, FDRc: 339

Degrees of freedom = [1.0, 16.0]
FWHM = 9.6 8.7 9.5 mm mm mm; 9.6 8.7 9.5 {voxels}
Volume: 512697 = 512697 voxels = 560.1 resels
Voxel size: 1.0 1.0 1.0 mm mm mm; (resel = 791.03 voxels)
Page 1

Statistics: ***p-values adjusted for search volume***

set-level		cluster-level				peak-level					mm mm mm
p	c	$p_{FWE\text{-}corr}$	$q_{FDR\text{-}corr}$	k_E	p_{uncorr}	$p_{FWE\text{-}corr}$	$q_{FDR\text{-}corr}$	F	(Z_E)	p_{uncorr}	
		0.000	0.000	1629	0.000	**0.182**	**0.058**	**49.64**	**4.54**	**0.000**	**2 -51 -4**
						0.240	0.072	46.52	4.46	0.000	5 -70 -17
						0.788	0.195	31.37	3.95	0.000	2 -61 -8
		0.000	0.000	1144	0.000	**0.250**	**0.072**	**46.05**	**4.45**	**0.000**	**9 -8 1**
						0.546	0.125	36.81	4.15	0.000	6 -27 -5
		0.005	0.002	773	0.000	**0.267**	**0.073**	**45.26**	**4.42**	**0.000**	**24 48 -12**
						0.406	0.096	40.45	4.28	0.000	13 57 -24

table shows 3 local maxima more than 8.0mm apart

Height threshold: F = 16.12, p = 0.001 (1.000)
Extent threshold: k = 513 voxels, p = 0.002 (0.033)
Expected voxels per cluster, <k> = 44.619
Expected number of clusters, <c> = 0.03
FWEp: 65.397, FDRp: 52.236, FWEc: 513, FDRc: 339

Degrees of freedom = [1.0, 16.0]
FWHM = 9.6 8.7 9.5 mm mm mm; 9.6 8.7 9.5 {voxels}
Volume: 512697 = 512697 voxels = 560.1 resels
Voxel size: 1.0 1.0 1.0 mm mm mm; (resel = 791.03 voxels)
Page 2/2

FIGURE C.14: Significant difference in cluster level with p corrected at 0.05 between two different pipelines for controls' right hemisphere in MT map grey matter.

Statistics: ***p-values adjusted for search volume***

set-level		cluster-level				peak-level					mm mm mm
p	c	$p_{FWE\text{-}corr}$	$q_{FDR\text{-}corr}$	k_E	p_{uncorr}	$p_{FWE\text{-}corr}$	$q_{FDR\text{-}corr}$	F	(Z_E)	p_{uncorr}	
0.000	16	0.000	0.000	144	0.000	0.001	0.145	134.20	5.79	0.000	4 -50 11
		0.000	0.000	184	0.000	0.001	0.145	133.92	5.79	0.000	30 8 -16
		0.001	0.044	26	0.022	0.001	0.145	130.44	5.76	0.000	44 -48 -33
		0.000	0.004	58	0.001	0.002	0.204	116.66	5.62	0.000	37 36 34
		0.000	0.000	324	0.000	0.006	0.384	98.87	5.42	0.000	15 17 1
						0.007	0.384	98.14	5.41	0.000	10 7 0
		0.000	0.000	106	0.000	0.011	0.586	88.67	5.28	0.000	44 -15 51
		0.000	0.000	127	0.000	0.014	0.588	85.18	5.23	0.000	30 -4 59
		0.003	0.090	17	0.056	0.018	0.588	81.49	5.18	0.000	25 18 52
		0.021	0.462	3	0.404	0.018	0.588	81.37	5.18	0.000	33 -45 -41
		0.002	0.058	22	0.033	0.019	0.588	80.97	5.17	0.000	24 10 53
		0.000	0.011	43	0.005	0.020	0.589	79.85	5.15	0.000	47 -27 46
		0.033	0.647	1	0.647	0.029	0.723	74.26	5.06	0.000	27 -42 -44
		0.008	0.203	9	0.152	0.030	0.723	74.05	5.06	0.000	3 -47 20
		0.008	0.203	9	0.152	0.032	0.736	72.99	5.04	0.000	25 1 56
		0.025	0.534	2	0.501	0.038	0.835	70.39	4.99	0.000	13 7 -15
		0.021	0.462	3	0.404	0.040	0.835	69.83	4.98	0.000	50 3 37

table shows 3 local maxima more than 8.0mm apart

Height threshold: F = 66.81, p = 0.000 (0.050)
Extent threshold: k = 0 voxels
Expected voxels per cluster, <k> = 4.626
Expected number of clusters, <c> = 0.05
FWEp: 66.811, FDRp: Inf, FWEc: 1, FDRc: 26

Degrees of freedom = [1.0, 16.0]
FWHM = 9.3 8.3 9.0 mm mm mm; 9.3 8.3 9.0 {voxels}
Volume: 512697 = 512697 voxels = 630.3 resels
Voxel size: 1.0 1.0 1.0 mm mm mm; (resel = 702.94 voxels)

FIGURE C.15: Significant difference in peak level with p corrected at 0.05 between two different pipelines for controls' right hemisphere in R_1 map grey matter.

Statistics: ***p-values adjusted for search volume***

set-level		cluster-level				peak-level					mm mm mm		
p	c	$p_{FWE\text{-}corr}$	$q_{FDR\text{-}corr}$	k_E	p_{uncorr}	$p_{FWE\text{-}corr}$	$q_{FDR\text{-}corr}$	F	(Z_E)	p_{uncorr}			
0.000	14	0.000	0.000	1662	0.000	0.001	0.006	134.20	5.79	0.000	4	-50	11
						0.030	0.029	74.05	5.06	0.000	3	-47	20
						0.147	0.072	53.32	4.64	0.000	12	-45	4
		0.000	0.000	1809	0.000	0.001	0.006	133.92	5.79	0.000	30	8	-16
						0.038	0.034	70.39	4.99	0.000	13	7	-15
						0.793	0.246	32.09	3.98	0.000	19	-1	-15
		0.000	0.000	4574	0.000	0.001	0.006	130.44	5.76	0.000	44	-48	-33
						0.018	0.024	81.37	5.18	0.000	33	-45	-41
						0.101	0.059	57.79	4.74	0.000	35	-52	-37
		0.024	0.011	504	0.001	0.002	0.008	116.66	5.62	0.000	37	36	34
		0.000	0.000	3989	0.000	0.006	0.016	98.87	5.42	0.000	15	17	1
						0.007	0.016	98.14	5.41	0.000	10	7	0
						0.342	0.120	43.44	4.37	0.000	16	27	-3
		0.000	0.000	27973	0.000	0.011	0.024	88.67	5.28	0.000	44	-15	51
						0.014	0.024	85.18	5.23	0.000	30	-4	59
						0.018	0.024	81.49	5.18	0.000	25	18	52
		0.012	0.007	584	0.001	0.060	0.041	64.40	4.88	0.000	30	-14	-5
		0.000	0.000	1033	0.000	0.063	0.041	63.81	4.87	0.000	7	-6	64
		0.000	0.000	1850	0.000	0.067	0.042	63.01	4.85	0.000	43	-59	-20
						0.081	0.050	60.56	4.80	0.000	53	-49	-23
						0.530	0.173	38.11	4.20	0.000	52	-38	-21
		0.000	0.000	1487	0.000	0.125	0.065	55.27	4.68	0.000	9	9	57
						0.199	0.084	49.73	4.55	0.000	4	19	50
						0.350	0.121	43.17	4.36	0.000	4	29	43
		0.048	0.021	427	0.003	0.149	0.072	53.16	4.63	0.000	38	-40	-23
		0.018	0.010	541	0.001	0.194	0.083	50.05	4.55	0.000	25	34	39
						0.319	0.116	44.26	4.39	0.000	22	38	46
		0.002	0.001	850	0.000	0.218	0.089	48.67	4.52	0.000	10	-42	57
						0.734	0.222	33.45	4.03	0.000	11	-31	49
		0.021	0.011	519	0.001	0.814	0.253	31.58	3.95	0.000	33	-36	-2

table shows 3 local maxima more than 8.0mm apart

Height threshold: F = 16.12, p = 0.001 (1.000)
Extent threshold: k = 427 voxels, p = 0.003 (0.048)
Expected voxels per cluster, <k> = 39.650
Expected number of clusters, <c> = 0.05
FWEp: 66.811, FDRp: 63.013, FWEc: 427, FDRc: 323

Degrees of freedom = [1.0, 16.0]
FWHM = 9.3 8.3 9.0 mm mm mm; 9.3 8.3 9.0 {voxels}
Volume: 512697 = 512697 voxels = 630.3 resels
Voxel size: 1.0 1.0 1.0 mm mm mm; (resel = 702.94 voxels)
Page 1

Statistics: ***p-values adjusted for search volume***

set-level		cluster-level				peak-level					mm mm mm		
p	c	$p_{FWE\text{-}corr}$	$q_{FDR\text{-}corr}$	k_E	p_{uncorr}	$p_{FWE\text{-}corr}$	$q_{FDR\text{-}corr}$	F	(Z_E)	p_{uncorr}			
						0.911	0.301	28.84	3.84	0.000	26	-33	7
						1.000	0.677	20.02	3.36	0.000	26	-40	-1

table shows 3 local maxima more than 8.0mm apart

Height threshold: F = 16.12, p = 0.001 (1.000)
Extent threshold: k = 427 voxels, p = 0.003 (0.048)
Expected voxels per cluster, <k> = 39.650
Expected number of clusters, <c> = 0.05
FWEp: 66.811, FDRp: 63.013, FWEc: 427, FDRc: 323

Degrees of freedom = [1.0, 16.0]
FWHM = 9.3 8.3 9.0 mm mm mm; 9.3 8.3 9.0 {voxels}
Volume: 512697 = 512697 voxels = 630.3 resels
Voxel size: 1.0 1.0 1.0 mm mm mm; (resel = 702.94 voxels)
Page 2/2

FIGURE C.16: Significant difference in cluster level with p corrected at 0.05 between two different pipelines for controls' right hemisphere in R_1 map grey matter.

Statistics: ***p-values adjusted for search volume***

set-level		cluster-level				peak-level					mm mm mm
p	c	$p_{FWE\text{-}corr}$	$q_{FDR\text{-}corr}$	k_E	p_{uncorr}	$p_{FWE\text{-}corr}$	$q_{FDR\text{-}corr}$	F	(Z_E)	p_{uncorr}	
0.000	29	0.000	0.012	36	0.004	0.001	0.326	148.29	5.91	0.000	16 -36 -13
		0.000	0.006	45	0.002	0.001	0.326	141.44	5.86	0.000	11 -79 -19
		0.000	0.000	149	0.000	0.001	0.326	137.16	5.82	0.000	19 -14 -25
						0.003	0.335	114.81	5.60	0.000	28 -23 -31
		0.000	0.012	35	0.005	0.001	0.326	132.94	5.78	0.000	2 -55 36
		0.000	0.000	176	0.000	0.002	0.335	121.02	5.67	0.000	45 -14 50
		0.000	0.000	113	0.000	0.002	0.335	120.92	5.67	0.000	46 -28 48
						0.011	0.505	92.42	5.34	0.000	52 -25 43
		0.000	0.000	204	0.000	0.003	0.335	117.44	5.63	0.000	53 -39 -29
						0.007	0.420	99.50	5.43	0.000	47 -29 -27
		0.001	0.027	25	0.014	0.003	0.335	116.01	5.62	0.000	11 -1 68
		0.000	0.001	64	0.000	0.004	0.342	112.31	5.58	0.000	9 5 -1
		0.000	0.000	84	0.000	0.004	0.350	109.66	5.55	0.000	29 -6 64
		0.000	0.000	348	0.000	0.005	0.350	106.76	5.52	0.000	15 21 -28
						0.008	0.465	96.63	5.39	0.000	5 28 -27
						0.010	0.505	93.87	5.36	0.000	8 14 -26
		0.000	0.010	38	0.004	0.007	0.420	100.11	5.44	0.000	2 -67 25
		0.002	0.078	15	0.049	0.010	0.505	92.92	5.34	0.000	36 -31 -30
		0.000	0.006	46	0.002	0.012	0.534	90.54	5.31	0.000	30 28 -22
		0.001	0.049	19	0.029	0.014	0.579	87.19	5.26	0.000	20 26 -26
		0.001	0.025	27	0.011	0.015	0.579	86.73	5.26	0.000	27 24 51
		0.001	0.049	19	0.029	0.016	0.579	85.39	5.24	0.000	27 -10 59
		0.015	0.331	4	0.285	0.016	0.579	85.29	5.24	0.000	41 -53 50
		0.015	0.331	4	0.285	0.018	0.591	83.33	5.21	0.000	36 36 34
		0.006	0.168	9	0.116	0.020	0.623	82.01	5.19	0.000	2 -45 41
		0.001	0.026	26	0.013	0.023	0.642	80.06	5.16	0.000	41 -60 -21
		0.003	0.085	14	0.056	0.026	0.642	78.19	5.13	0.000	40 0 59
		0.010	0.255	6	0.193	0.026	0.642	77.81	5.12	0.000	5 -57 17
		0.015	0.331	4	0.285	0.036	0.828	73.39	5.05	0.000	6 -4 66
		0.007	0.189	8	0.137	0.037	0.842	72.83	5.04	0.000	3 -53 12

table shows 3 local maxima more than 8.0mm apart

Height threshold: F = 68.72, p = 0.000 (0.050)
Extent threshold: k = 0 voxels
Expected voxels per cluster, <k> = 3.788
Expected number of clusters, <c> = 0.05
FWEp: 68.718, FDRp: Inf, FWEc: 1, FDRc: 19

Degrees of freedom = [1.0, 16.0]
FWHM = 8.6 8.1 8.6 mm mm mm; 8.6 8.1 8.6 {voxels}
Volume: 512697 = 512697 voxels = 737.8 resels
Voxel size: 1.0 1.0 1.0 mm mm mm; (resel = 600.51 voxels)
Page 1

Statistics: ***p-values adjusted for search volume***

set-level		cluster-level				peak-level					mm mm mm
p	c	$p_{FWE\text{-}corr}$	$q_{FDR\text{-}corr}$	k_E	p_{uncorr}	$p_{FWE\text{-}corr}$	$q_{FDR\text{-}corr}$	F	(Z_E)	p_{uncorr}	
		0.023	0.488	2	0.454	0.039	0.852	72.18	5.02	0.000	16 12 2
		0.018	0.396	3	0.355	0.039	0.852	72.04	5.02	0.000	2 -69 13
		0.031	0.608	1	0.608	0.045	0.916	70.16	4.99	0.000	47 12 42
		0.031	0.608	1	0.608	0.049	0.978	69.02	4.97	0.000	46 13 43

table shows 3 local maxima more than 8.0mm apart

Height threshold: F = 68.72, p = 0.000 (0.050)
Extent threshold: k = 0 voxels
Expected voxels per cluster, <k> = 3.788
Expected number of clusters, <c> = 0.05
FWEp: 68.718, FDRp: Inf, FWEc: 1, FDRc: 19

Degrees of freedom = [1.0, 16.0]
FWHM = 8.6 8.1 8.6 mm mm mm; 8.6 8.1 8.6 {voxels}
Volume: 512697 = 512697 voxels = 737.8 resels
Voxel size: 1.0 1.0 1.0 mm mm mm; (resel = 600.51 voxels)
Page 2/2

FIGURE C.17: Significant difference in peak level with p corrected at 0.05 between two different pipelines for controls' right hemisphere in R_2^* map grey matter.

Statistics: ***p-values adjusted for search volume***

set-level		cluster-level				peak-level					mm mm mm
p	c	$p_{FWE\text{-}corr}$	$q_{FDR\text{-}corr}$	k_E	p_{uncorr}	$p_{FWE\text{-}corr}$	$q_{FDR\text{-}corr}$	F	(Z_E)	p_{uncorr}	
0.000	6	0.000	0.000	66253	0.000	0.001	0.011	148.29	5.91	0.000	16 -36 -13
						0.001	0.011	141.44	5.86	0.000	11 -79 -19
						0.001	0.011	137.16	5.82	0.000	19 -14 -25
		0.000	0.000	3672	0.000	0.004	0.011	112.31	5.58	0.000	9 5 -1
						0.039	0.028	72.18	5.02	0.000	16 12 2
						0.176	0.066	52.77	4.62	0.000	15 -4 21
		0.000	0.000	7243	0.000	0.005	0.011	106.76	5.52	0.000	15 21 -28
						0.008	0.015	96.63	5.39	0.000	5 28 -27
						0.010	0.016	93.87	5.36	0.000	8 14 -26
		0.028	0.031	429	0.001	0.018	0.019	83.33	5.21	0.000	36 36 34
		0.000	0.000	1849	0.000	0.103	0.048	59.24	4.77	0.000	30 -49 -60
						0.202	0.071	51.08	4.58	0.000	17 -58 -63
						0.985	0.376	25.88	3.70	0.000	5 -57 -60
		0.000	0.000	1210	0.000	0.944	0.297	28.57	3.82	0.000	54 -68 10
						0.958	0.314	27.87	3.79	0.000	49 -73 18
						0.993	0.406	24.86	3.64	0.000	46 -83 9

table shows 3 local maxima more than 8.0mm apart

Height threshold: F = 16.12, p = 0.001 (1.000)
Extent threshold: k = 429 voxels, p = 0.001 (0.028)
Expected voxels per cluster, <k> = 33.873
Expected number of clusters, <c> = 0.03
FWEp: 68.718, FDRp: 57.804, FWEc: 429, FDRc: 429

Degrees of freedom = [1.0, 16.0]
FWHM = 8.6 8.1 8.6 mm mm mm; 8.6 8.1 8.6 {voxels}
Volume: 512697 = 512697 voxels = 737.8 resels
Voxel size: 1.0 1.0 1.0 mm mm mm; (resel = 600.51 voxels)

FIGURE C.18: Significant difference in cluster level with p corrected at 0.05 between two different pipelines for controls' right hemisphere in R_2^* map grey matter.

Statistics: ***p-values adjusted for search volume***

set-level		cluster-level				peak-level					mm mm mm
p	c	$p_{FWE\text{-}corr}$	$q_{FDR\text{-}corr}$	k_E	p_{uncorr}	$p_{FWE\text{-}corr}$	$q_{FDR\text{-}corr}$	F	(Z_E)	p_{uncorr}	
0.000	5	0.000	0.010	51	0.006	0.002	0.188	107.80	5.53	0.000	7 -10 -3
		0.000	0.001	98	0.000	0.003	0.188	96.05	5.38	0.000	8 -49 15
		0.010	0.253	9	0.202	0.004	0.188	94.87	5.37	0.000	33 4 -12
		0.000	0.001	121	0.000	0.005	0.188	89.92	5.30	0.000	19 -58 -31
		0.017	0.339	5	0.339	0.030	0.644	63.78	4.87	0.000	28 -13 -5

table shows 3 local maxima more than 8.0mm apart

Height threshold: F = 57.35, p = 0.000 (0.050)
Extent threshold: k = 0 voxels
Expected voxels per cluster, <k> = 5.914
Expected number of clusters, <c> = 0.05
FWEp: 57.347, FDRp: Inf, FWEc: 5, FDRc: 51

Degrees of freedom = [1.0, 16.0]
FWHM = 8.8 9.1 9.0 mm mm mm; 8.8 9.1 9.0 {voxels}
Volume: 238547 = 238547 voxels = 285.8 resels
Voxel size: 1.0 1.0 1.0 mm mm mm; (resel = 714.25 voxels)

FIGURE C.19: Significant difference in peak level with p corrected at 0.05 between two different pipelines for controls' right hemisphere in MT map white matter.

Statistics: ***p-values adjusted for search volume***

set-level		cluster-level				peak-level					mm mm mm
p	c	$p_{FWE\text{-}corr}$	$q_{FDR\text{-}corr}$	k_E	p_{uncorr}	$p_{FWE\text{-}corr}$	$q_{FDR\text{-}corr}$	F	(Z_E)	p_{uncorr}	
0.000	7	0.000	0.000	1120	0.000	0.002	0.014	107.80	5.53	0.000	7 -10 -3
						0.191	0.144	42.64	4.35	0.000	22 -14 13
						0.996	0.816	18.63	3.27	0.001	9 -22 -4
		0.000	0.000	1619	0.000	0.003	0.014	96.05	5.38	0.000	8 -49 15
						0.105	0.086	48.93	4.52	0.000	6 -21 33
						0.563	0.312	31.14	3.94	0.000	15 -42 2
		0.000	0.000	2313	0.000	0.005	0.014	89.92	5.30	0.000	19 -58 -31
						0.051	0.066	57.14	4.73	0.000	30 -43 -39
						0.059	0.066	55.41	4.69	0.000	16 -52 -41
		0.000	0.000	1493	0.000	0.030	0.047	63.78	4.87	0.000	28 -13 -5
						0.340	0.201	36.68	4.15	0.000	21 -9 0
						0.626	0.332	29.85	3.88	0.000	15 1 -6
		0.004	0.004	649	0.000	0.100	0.086	49.54	4.54	0.000	37 40 -8
						0.239	0.152	40.30	4.27	0.000	22 46 -7
		0.006	0.006	588	0.001	0.192	0.144	42.58	4.34	0.000	31 14 12
						0.305	0.186	37.79	4.19	0.000	33 0 14
						0.397	0.231	35.04	4.09	0.000	33 -9 15
		0.001	0.001	813	0.000	0.229	0.150	40.73	4.29	0.000	45 -34 5
						0.446	0.255	33.78	4.04	0.000	50 -15 -5
						0.587	0.312	30.65	3.92	0.000	52 -29 4

table shows 3 local maxima more than 8.0mm apart

Height threshold: F = 16.12, p = 0.001 (1.000)
Extent threshold: k = 588 voxels, p = 0.001 (0.006)
Expected voxels per cluster, <k> = 40.288
Expected number of clusters, <c> = 0.01
FWEp: 57.347, FDRp: 63.778, FWEc: 588, FDRc: 588

Degrees of freedom = [1.0, 16.0]
FWHM = 8.8 9.1 9.0 mm mm mm; 8.8 9.1 9.0 {voxels}
Volume: 238547 = 238547 voxels = 285.8 resels
Voxel size: 1.0 1.0 1.0 mm mm mm; (resel = 714.25 voxels)

FIGURE C.20: Significant difference in cluster level with p corrected at 0.05 between two different pipelines for controls' right hemisphere in MT map white matter.

Statistics: ***p-values adjusted for search volume***

set-level		cluster-level				peak-level					mm mm mm
p	c	$p_{FWE\text{-}corr}$	$q_{FDR\text{-}corr}$	k_E	p_{uncorr}	$p_{FWE\text{-}corr}$	$q_{FDR\text{-}corr}$	F	(Z_E)	p_{uncorr}	
0.000	16	0.000	0.000	319	0.000	0.000	0.008	247.15	6.51	0.000	8 -49 15
						0.006	0.333	86.60	5.25	0.000	15 -46 5
		0.000	0.000	147	0.000	0.000	0.052	161.99	6.02	0.000	45 -39 -16
		0.000	0.000	416	0.000	0.002	0.333	105.15	5.50	0.000	6 -19 -4
						0.005	0.333	87.88	5.27	0.000	7 -6 -4
						0.009	0.385	79.58	5.15	0.000	2 -21 -12
		0.000	0.038	48	0.009	0.003	0.333	95.12	5.37	0.000	33 -11 15
		0.005	0.258	17	0.097	0.005	0.333	87.56	5.27	0.000	39 -52 -13
		0.016	0.623	6	0.312	0.008	0.385	82.10	5.19	0.000	32 3 -11
		0.003	0.169	24	0.053	0.016	0.555	71.03	5.00	0.000	46 -23 -22
		0.021	0.657	4	0.411	0.026	0.781	64.64	4.88	0.000	26 16 -11
		0.018	0.633	5	0.356	0.031	0.891	62.39	4.84	0.000	28 17 4
		0.012	0.556	8	0.243	0.035	0.918	61.06	4.81	0.000	6 -20 33
		0.029	0.702	2	0.571	0.039	0.928	59.65	4.78	0.000	33 -3 14
		0.029	0.702	2	0.571	0.040	0.928	59.58	4.78	0.000	36 -60 -11
		0.035	0.702	1	0.702	0.041	0.928	59.10	4.77	0.000	50 -30 4
		0.029	0.702	2	0.571	0.042	0.928	58.76	4.76	0.000	38 -43 -16
		0.035	0.702	1	0.702	0.045	0.928	58.01	4.74	0.000	29 16 8
		0.035	0.702	1	0.702	0.050	0.992	56.88	4.72	0.000	29 12 9

table shows 3 local maxima more than 8.0mm apart

Height threshold: F = 56.79, p = 0.000 (0.050)
Extent threshold: k = 0 voxels
Expected voxels per cluster, <k> = 6.332
Expected number of clusters, <c> = 0.05
FWEp: 56.791, FDRp: 247.151, FWEc: 1, FDRc: 48

Degrees of freedom = [1.0, 16.0]
FWHM = 9.2 9.3 8.8 mm mm mm; 9.2 9.3 8.8 {voxels}
Volume: 238547 = 238547 voxels = 270.8 resels
Voxel size: 1.0 1.0 1.0 mm mm mm; (resel = 753.58 voxels)

FIGURE C.21: Significant difference with p corrected at 0.05 between two different pipelines for controls' right hemisphere in R_1 map white matter.

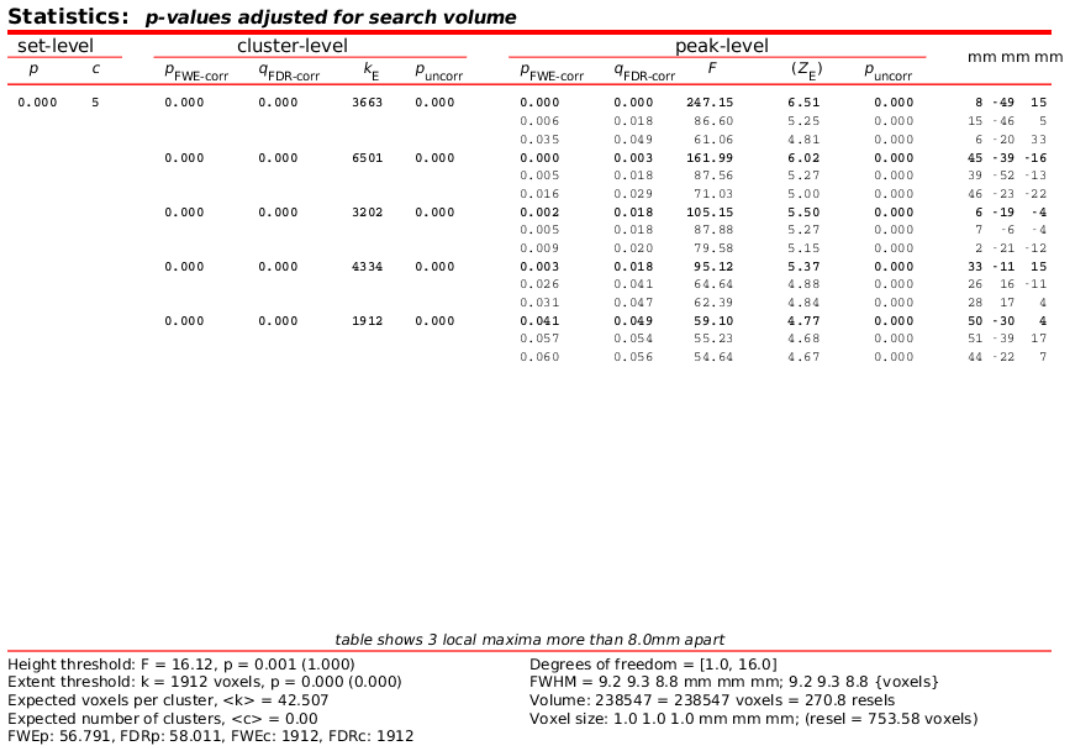

Statistics: ***p-values adjusted for search volume***

set-level		cluster-level				peak-level					mm mm mm
p	c	$p_{FWE\text{-}corr}$	$q_{FDR\text{-}corr}$	k_E	p_{uncorr}	$p_{FWE\text{-}corr}$	$q_{FDR\text{-}corr}$	F	(Z_E)	p_{uncorr}	
0.000	5	0.000	0.000	3663	0.000	0.000	0.000	247.15	6.51	0.000	8 -49 15
						0.006	0.018	86.60	5.25	0.000	15 -46 5
						0.035	0.049	61.06	4.81	0.000	6 -20 33
		0.000	0.000	6501	0.000	0.000	0.003	161.99	6.02	0.000	45 -39 -16
						0.005	0.018	87.56	5.27	0.000	39 -52 -13
						0.016	0.029	71.03	5.00	0.000	46 -23 -22
		0.000	0.000	3202	0.000	0.002	0.018	105.15	5.50	0.000	6 -19 -4
						0.005	0.018	87.88	5.27	0.000	7 -6 -4
						0.009	0.020	79.58	5.15	0.000	2 -21 -12
		0.000	0.000	4334	0.000	0.003	0.018	95.12	5.37	0.000	33 -11 15
						0.026	0.041	64.64	4.88	0.000	26 16 -11
						0.031	0.047	62.39	4.84	0.000	28 17 4
		0.000	0.000	1912	0.000	0.041	0.049	59.10	4.77	0.000	50 -30 4
						0.057	0.054	55.23	4.68	0.000	51 -39 17
						0.060	0.056	54.64	4.67	0.000	44 -22 7

table shows 3 local maxima more than 8.0mm apart

Height threshold: F = 16.12, p = 0.001 (1.000)
Extent threshold: k = 1912 voxels, p = 0.000 (0.000)
Expected voxels per cluster, <k> = 42.507
Expected number of clusters, <c> = 0.00
FWEp: 56.791, FDRp: 58.011, FWEc: 1912, FDRc: 1912

Degrees of freedom = [1.0, 16.0]
FWHM = 9.2 9.3 8.8 mm mm mm; 9.2 9.3 8.8 {voxels}
Volume: 238547 = 238547 voxels = 270.8 resels
Voxel size: 1.0 1.0 1.0 mm mm mm; (resel = 753.58 voxels)

FIGURE C.22: Significant difference in cluster level with p corrected at 0.05 between two different pipelines for controls' right hemisphere in R_1 map white matter.

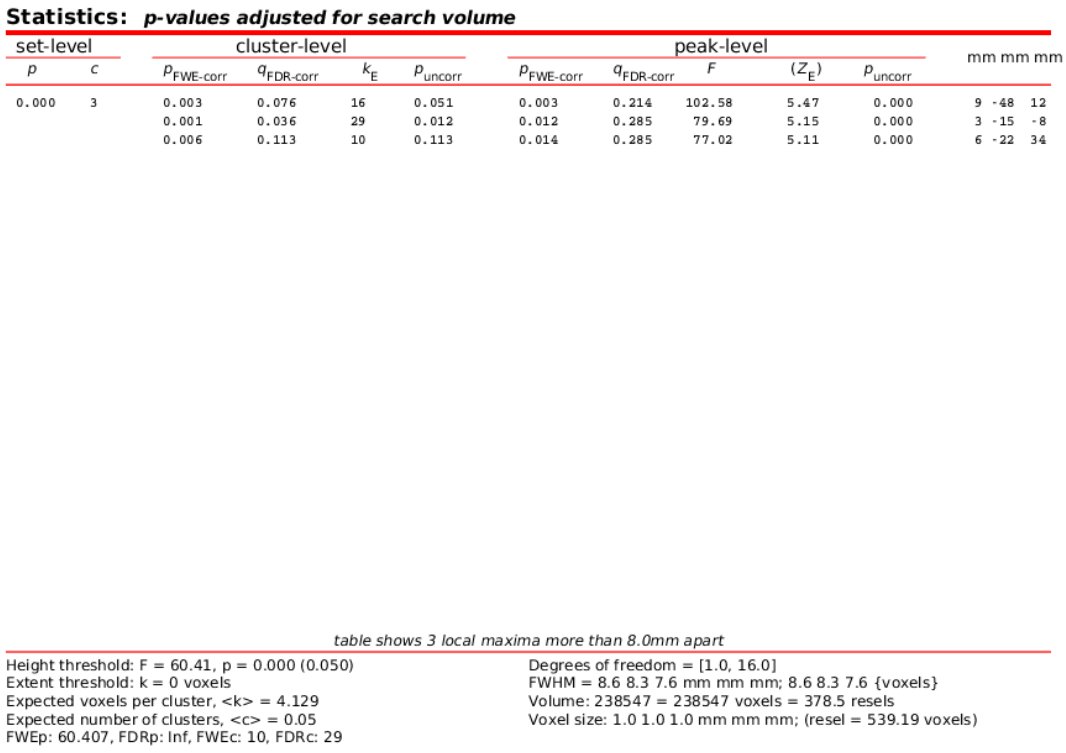

Statistics: ***p-values adjusted for search volume***

set-level		cluster-level				peak-level					mm mm mm
p	c	$p_{FWE\text{-}corr}$	$q_{FDR\text{-}corr}$	k_E	p_{uncorr}	$p_{FWE\text{-}corr}$	$q_{FDR\text{-}corr}$	F	(Z_E)	p_{uncorr}	
0.000	3	0.003	0.076	16	0.051	0.003	0.214	102.58	5.47	0.000	9 -48 12
		0.001	0.036	29	0.012	0.012	0.285	79.69	5.15	0.000	3 -15 -8
		0.006	0.113	10	0.113	0.014	0.285	77.02	5.11	0.000	6 -22 34

table shows 3 local maxima more than 8.0mm apart

Height threshold: F = 60.41, p = 0.000 (0.050)
Extent threshold: k = 0 voxels
Expected voxels per cluster, <k> = 4.129
Expected number of clusters, <c> = 0.05
FWEp: 60.407, FDRp: Inf, FWEc: 10, FDRc: 29

Degrees of freedom = [1.0, 16.0]
FWHM = 8.6 8.3 7.6 mm mm mm; 8.6 8.3 7.6 {voxels}
Volume: 238547 = 238547 voxels = 378.5 resels
Voxel size: 1.0 1.0 1.0 mm mm mm; (resel = 539.19 voxels)

FIGURE C.23: Significant difference in peak level with p corrected at 0.05 between two different pipelines for controls' right hemisphere in R_2^* map white matter.

Statistics: ***p-values adjusted for search volume***

set-level		cluster-level				peak-level					mm mm mm
p	c	$p_{FWE\text{-}corr}$	$q_{FDR\text{-}corr}$	k_E	p_{uncorr}	$p_{FWE\text{-}corr}$	$q_{FDR\text{-}corr}$	F	(Z_E)	p_{uncorr}	
0.000	2	0.000	0.000	1312	0.000	0.003	0.032	102.58	5.47	0.000	9 -48 12
						0.014	0.043	77.02	5.11	0.000	6 -22 34
						0.145	0.194	48.08	4.50	0.000	18 -50 9
		0.000	0.000	1107	0.000	0.012	0.043	79.69	5.15	0.000	3 -15 -8
						0.057	0.114	58.91	4.76	0.000	5 -22 -17
						0.097	0.172	52.54	4.62	0.000	8 -5 -9

table shows 3 local maxima more than 8.0mm apart

Height threshold: F = 16.12, p = 0.001 (1.000)
Extent threshold: k = 1107 voxels, p = 0.000 (0.000)
Expected voxels per cluster, <k> = 30.414
Expected number of clusters, <c> = 0.00
FWEp: 60.407, FDRp: 77.020, FWEc: 1107, FDRc: 1107

Degrees of freedom = [1.0, 16.0]
FWHM = 8.6 8.3 7.6 mm mm mm; 8.6 8.3 7.6 {voxels}
Volume: 238547 = 238547 voxels = 378.5 resels
Voxel size: 1.0 1.0 1.0 mm mm mm; (resel = 539.19 voxels)

FIGURE C.24: Significant difference in cluster level with p corrected at 0.05 between two different pipelines for controls' right hemisphere in R_2^* map white matter.

Statistics: ***p-values adjusted for search volume***

set-level		cluster-level				peak-level					mm mm mm
p	c	$p_{FWE\text{-}corr}$	$q_{FDR\text{-}corr}$	k_E	p_{uncorr}	$p_{FWE\text{-}corr}$	$q_{FDR\text{-}corr}$	F	(Z_E)	p_{uncorr}	
0.000	33	0.000	0.000	418	0.000	0.000	0.128	207.23	6.31	0.000	46 -30 -27
		0.000	0.000	1354	0.000	0.000	0.162	177.34	6.13	0.000	2 -6 -4
						0.001	0.196	152.45	5.95	0.000	9 -11 -1
		0.000	0.000	231	0.000	0.001	0.196	157.79	5.99	0.000	22 -23 -28
		0.000	0.000	493	0.000	0.001	0.287	135.12	5.80	0.000	22 -74 37
						0.004	0.287	115.93	5.62	0.000	13 -74 31
						0.009	0.359	98.37	5.41	0.000	25 -70 47
		0.000	0.001	123	0.000	0.002	0.287	132.51	5.78	0.000	35 26 -8
		0.000	0.003	84	0.001	0.003	0.287	120.85	5.67	0.000	53 11 28
						0.022	0.637	82.83	5.20	0.000	45 13 31
		0.000	0.000	137	0.000	0.003	0.287	118.49	5.64	0.000	29 -1 57
		0.001	0.026	44	0.010	0.003	0.287	118.20	5.64	0.000	18 -48 65
		0.000	0.018	51	0.006	0.005	0.324	108.35	5.53	0.000	9 -34 46
		0.000	0.001	124	0.000	0.006	0.324	105.16	5.50	0.000	19 52 32
						0.007	0.324	102.57	5.47	0.000	30 43 32
		0.007	0.240	12	0.146	0.006	0.324	104.18	5.49	0.000	6 -94 13
		0.000	0.018	52	0.006	0.007	0.324	103.30	5.47	0.000	27 28 46
		0.007	0.227	13	0.131	0.009	0.359	98.73	5.42	0.000	17 22 59
		0.000	0.003	84	0.001	0.010	0.359	96.12	5.39	0.000	38 -42 50
		0.000	0.003	88	0.001	0.010	0.359	95.85	5.38	0.000	13 -56 -38
		0.005	0.194	17	0.088	0.013	0.446	91.45	5.32	0.000	14 -22 -38
		0.007	0.227	13	0.131	0.015	0.455	89.15	5.29	0.000	10 -77 39
		0.002	0.111	24	0.047	0.024	0.637	81.85	5.18	0.000	24 -34 65
		0.017	0.523	5	0.341	0.024	0.637	81.49	5.18	0.000	8 54 1
		0.024	0.549	3	0.465	0.024	0.637	81.42	5.18	0.000	27 42 37
		0.006	0.227	14	0.118	0.024	0.637	81.27	5.18	0.000	41 -19 5
		0.024	0.549	3	0.465	0.026	0.648	80.47	5.16	0.000	19 47 38
		0.020	0.523	4	0.396	0.026	0.648	80.29	5.16	0.000	3 12 49
		0.007	0.227	13	0.131	0.030	0.732	78.11	5.12	0.000	29 -36 60
		0.020	0.523	4	0.396	0.035	0.808	76.03	5.09	0.000	28 58 9

table shows 3 local maxima more than 8.0mm apart

Height threshold: F = 70.70, p = 0.000 (0.050)
Extent threshold: k = 0 voxels
Expected voxels per cluster, <k> = 5.963
Expected number of clusters, <c> = 0.05
FWEp: 70.703, FDRp: Inf, FWEc: 1, FDRc: 44

Degrees of freedom = [1.0, 16.0]
FWHM = 9.8 9.9 10.2 mm mm mm; 9.8 9.9 10.2 {voxels}
Volume: 1019560 = 1019560 voxels = 989.9 resels
Voxel size: 1.0 1.0 1.0 mm mm mm; (resel = 986.61 voxels)
Page 1

Statistics: ***p-values adjusted for search volume***

set-level		cluster-level				peak-level					mm mm mm
p	c	$p_{FWE\text{-}corr}$	$q_{FDR\text{-}corr}$	k_E	p_{uncorr}	$p_{FWE\text{-}corr}$	$q_{FDR\text{-}corr}$	F	(Z_E)	p_{uncorr}	
		0.024	0.549	3	0.465	0.035	0.808	75.99	5.09	0.000	17 61 17
		0.020	0.523	4	0.396	0.037	0.846	75.00	5.07	0.000	10 -66 20
		0.020	0.523	4	0.396	0.040	0.886	74.04	5.06	0.000	34 -38 -26
		0.035	0.692	1	0.692	0.042	0.887	73.14	5.04	0.000	20 -57 62
		0.028	0.594	2	0.558	0.042	0.887	73.13	5.04	0.000	24 5 53
		0.028	0.594	2	0.558	0.043	0.887	72.96	5.04	0.000	50 9 34
		0.028	0.594	2	0.558	0.045	0.910	72.27	5.03	0.000	32 26 48
		0.035	0.692	1	0.692	0.047	0.939	71.58	5.01	0.000	11 -74 41

table shows 3 local maxima more than 8.0mm apart

Height threshold: F = 70.70, p = 0.000 (0.050)
Extent threshold: k = 0 voxels
Expected voxels per cluster, <k> = 5.963
Expected number of clusters, <c> = 0.05
FWEp: 70.703, FDRp: Inf, FWEc: 1, FDRc: 44

Degrees of freedom = [1.0, 16.0]
FWHM = 9.8 9.9 10.2 mm mm mm; 9.8 9.9 10.2 {voxels}
Volume: 1019560 = 1019560 voxels = 989.9 resels
Voxel size: 1.0 1.0 1.0 mm mm mm; (resel = 986.61 voxels)
Page 2/2

FIGURE C.25: List of significant voxels in which there is a significant difference ($p < 0.05$ FWE corrected level) in GM volume between the two control pipelines.

Statistics: ***p-values adjusted for search volume***

set-level		cluster-level				peak-level					mm	mm	mm
p	c	$p_{FWE\text{-}corr}$	$q_{FDR\text{-}corr}$	k_E	p_{uncorr}	$p_{FWE\text{-}corr}$	$q_{FDR\text{-}corr}$	T	(Z_E)	p_{uncorr}			
0.000	5	0.000	0.000	11841	0.000	**0.000**	**0.001**	**8.23**	**6.23**	**0.000**	**4**	**-29**	**-8**
						0.000	0.001	7.57	5.90	0.000	8	-2	9
						0.004	0.009	6.67	5.42	0.000	12	-7	14
		0.000	0.000	2521	0.000	**0.001**	**0.002**	**7.40**	**5.81**	**0.000**	**8**	**9**	**50**
						0.006	0.010	6.55	5.35	0.000	5	23	53
						0.069	0.048	5.61	4.77	0.000	6	46	41
		0.000	0.000	2204	0.000	**0.012**	**0.013**	**6.28**	**5.19**	**0.000**	**15**	**-93**	**-6**
						0.323	0.154	4.96	4.34	0.000	19	-92	-13
						0.450	0.179	4.79	4.22	0.000	5	-80	-1
		0.000	0.000	1909	0.000	**0.403**	**0.179**	**4.85**	**4.26**	**0.000**	**24**	**-72**	**-45**
						0.968	0.424	4.07	3.69	0.000	30	-65	-49
						0.985	0.473	3.98	3.63	0.000	15	-61	-48
		0.001	0.001	1683	0.000	**0.413**	**0.179**	**4.84**	**4.26**	**0.000**	**29**	**14**	**3**
						1.000	0.851	3.50	3.25	0.001	25	21	6
						1.000	0.860	3.49	3.24	0.001	36	-4	10

table shows 3 local maxima more than 8.0mm apart

Height threshold: T = 3.31, p = 0.001 (1.000)
Extent threshold: k = 1683 voxels, p = 0.000 (0.001)
Expected voxels per cluster, <k> = 68.395
Expected number of clusters, <c> = 0.00
FWEp: 5.730, FDRp: 5.606, FWEc: 1683, FDRc: 1683

Degrees of freedom = [1.0, 39.0]
FWHM = 8.7 9.1 8.9 mm mm mm; 8.7 9.1 8.9 {voxels}
Volume: 1019560 = 1019560 voxels = 1400.4 resels
Voxel size: 1.0 1.0 1.0 mm mm mm; (resel = 697.36 voxels)

FIGURE C.26: List of voxels belonging to a significant cluster ($p < 0.05$ FWE corrected level) in which a significant difference in GM volume between the two control pipelines occurs.

Bibliography

[1] In: *The free dictionary by Farlex* (). [Online; accessed 27 February 2021]. URL: https://medical-dictionary.thefreedictionary.com/stroke.

[2] "Accident vasculaire cérébral (AVC)". In: *Inserm* (). [Online; accessed 22 May 2021]. URL: https://www.inserm.fr/information-en-sante/dossiers-information/accident-vasculaire-cerebral-avc#.

[3] A. Mechelli et al. "Voxel-Based Morphometry of the Human Brain: Methods and Applications". In: *Current Medical Imaging Reviews* 1 (June 2005).

[4] B. Draganski et al. "Regional specificity of MRI contrast parameter changes in normal ageing revealed by voxel-based quantification (VBQ)". In: *NeuroImage* 55.4 (2011), pp. 1423–1434. ISSN: 1053-8119. URL: https://www.sciencedirect.com/science/article/pii/S1053811911000887.

[5] Bersano et al. "Heritable and non-heritable uncommon causes of stroke". In: *Journal of Neurology* (2020). URL: https://link.springer.com/article/10.1007/s00415-020-09836-x.

[6] D.Nardo et al. "Less is more: neural mechanisms underlying anomia treatment in chronic aphasic patients". In: *Brain* 140 (July 2017), pp. 3039–3054.

[7] Emilie Lommers et al. "Multiparameter MRI quantification of microstructural tissue alterations in multiple sclerosis". In: *NeuroImage: Clinical* 23 (2019), p. 101879. ISSN: 2213-1582. URL: https://www.sciencedirect.com/science/article/pii/S2213158219302293.

[8] G. Reuter et al. "Multiparameter quantitative histological MRI values in high-grade gliomas: a potential biomarker of tumor progression". In: *Neuro-Oncology Practice* 7.6 (2020), pp. 646–655. URL: http://hdl.handle.net/2268/255168.

[9] H. Mehrabian et al. "Glioblastoma (GBM) effects on quantitative MRI of contralateral normal appearing white matter". In: *Journal of Neuro-Oncology* 139 (2018), pp. 97–106. URL: https://link.springer.com/article/10.1007/s11060-018-2846-0.

[10] K.Tabelow et al. "hMRI-A toolbox for quantitative MRI in neuroscience and clinical research". In: *NeuroImage* 194 (Jan. 2019), pp. 191–210.

[11] M.F. Callaghan et al. "Widespread age-related differences in the human brain microstructure revealed by quantitative MRI". In: *Neurobiology of Ageing* 35 (2014). URL: https://www.sciencedirect.com/science/article/pii/S0197458014002000?via%5C%3Dihub.

[12] M.L. Seghier et al. "Lesion identification using unified segmentation-normalisation models and fuzzy clustering". In: *NeuroImage* 41 (2008), pp. 1253–1266.

[13] Martin J O'Donnell et al. "Risk factors for ischaemic and intracerebral haemorrhagic stroke in 22 countries (the INTERSTROKE study): a case-control study". In: *Fast track* 376.9735 (June 2010), pp. 112–123. URL: https://www.thelancet.com/journals/lancet/article/PIIS0140-6736(10)60834-3/fulltext.

[14] N. Weiskopf et al. "Quantitative multi-parameter mapping of R1, PD*, MT, and R2* at 3T: a multi-center validation". In: *Front. Neurosci.* 7.95 (June 2013). URL: https://www.frontiersin.org/articles/10.3389/fnins.2013.00095/full.

[15] O. Aguilar et al. "Anatomical changes in the brain macrostructure and microstructure of the right hemisphere in chronic aphasic stroke patients". In: *Science of Aphasia XVI, Poster Session I* (Sept. 2015), pp. 17–20. URL: https://sstp.nl/article/view/19314/16790.

[16] P. E.Turkeltaub et al. "The right hemisphere is not unitary in its role in aphasia recovery". In: *Cortex* 48 (Oct. 2012), pp. 1179–1186. URL: http://europepmc.org/backend/ptpmcrender.fcgi?accid=PMC3221765&blobtype=pdf.

[17] W. Johnson et al. "Stroke: a global response is needed". In: *Bulletin of the World Health Organization* (2016). URL: https://www.who.int/bulletin/volumes/94/9/16-181636.pdf.

[18] Weiskopf et al. "Estimating the apparent transverse relaxation time (R2*) from images with different contrasts (ESTATICS) reduces motion artifacts". In: *Front.Neurosci* 8.278 (Sept. 2014). URL: https://www.ncbi.nlm.nih.gov/pmc/articles/PMC4159978/.

[19] Dr Usman Bashir et al. Andrew Murphy. *T2 relaxation time*. [Online; accessed 28 April 2021]. URL: https://radiopaedia.org/articles/t2-relaxation.

[20] John Ashburner and Karl J. Friston. "Unified segmentation". In: *NeuroImage* 26.3 (2005), pp. 839–851. ISSN: 1053-8119. URL: https://www.sciencedirect.com/science/article/pii/S1053811905001102.

[21] R. W. Boer. "Magnetization transfer contrast Part 1 : MR physics". In:

[22] C. Pernet C. Phillips E. Lommers. *Unifying lesion masking and tissue probability maps for improved segmenta1on and normalization*. [Online; accessed 29 April 2021]. July 2017. URL: https://orbi.uliege.be/handle/2268/213972.

[23] Johan Carlin. "The MNI brain and the Talairach atlas". In: *University of Cambridge* (Jan. 2017). [Online; accessed 4 May 2021]. URL: https://imaging.mrc-cbu.cam.ac.uk/imaging/MniTalairach.

[24] Phillips Christophe. *GBIO0008-2 - Medical imaging*. Faculty of Applied Sciences (ULiège), 2020.

[25] Phillips Christophe. *STAT0722-1 - Introduction à la statistique médicale*. Faculty of Applied Sciences (ULiège), 2020.

[26] "Comprehensive aphasia test". In: *Wikipedia, the free encyclopedia* (). [Online; accessed 18 May 2021]. URL: https://en.wikipedia.org/wiki/Comprehensive_aphasia_test.

[27] Dr Jeremy Jones et al. Dr Patrick J Rock. *T1 relaxation time*. [Online; accessed 28 April 2021]. URL: https://radiopaedia.org/articles/t1-relaxation-time.

[28] A.Leroy-Willig E.de Kerviler. "Interprétation du signal et du contraste en IRM". In: (). URL: http://www.sfrnet.org/data/upload/files/a7e7222e420ac736c1256b6c0044cb07/irm_sign.pdf.

[29] Balteau Evelyne. *PHYS0128-1 - Bases de l'imagerie par résonance magnétique nucléaire*. Faculty of Applied Sciences (ULiège), 2020.

[30] Kevin Fenton. *Why acting FAST when it comes to a stroke is so important*. [Online; accessed 18 March 2021]. URL: https://publichealthmatters.blog.gov.uk/2015/10/29/why-acting-fast-when-it-comes-to-a-stroke-is-so-important/.

[31] Jenna Fletcher. "What is the difference between CT scans and MRI scans?" In: *Medical News Today* (2019). [Online; accessed 20 July 2021]. URL: https://www.medicalnewstoday.com/articles/326839.

[32] Carey Greg. *Quantitative Methods in Neuroscience*. University of Colorado, 2013. URL: http://psych.colorado.edu/~carey/qmin/qmin.php.

[33] R. Lesser a J. Kay and M. Coltheart. "Psycholinguistic assessments oflanguage processing in aphasia(PALPA): An introduction". In: *Aphasiology* 10.2 (2014), pp. 159–180. URL: http://dx.doi.org/10.1080/02687039608248403.

[34] G.Porter K. Swinburn and D. Howard. "Comprehensive Aphasia Test: Scoring Book". In: Psychology Press, 2004.

[35] Shahmir Kamalian and Michael H. Lev. "Stroke imaging". In: *Radiologic Clinic of North America* 57 (2019), pp. 717–732.

[36] Hosung Kim Kaori L. Ito and Sook-Lei Liew. "A comparison of automated lesion segmentation approaches for chronic stroke T1-weighted MRI data". In: *Hum Brain Mapp.* 40 (2019), pp. 4669–4685. URL: https://onlinelibrary.wiley.com/doi/pdf/10.1002/hbm.24729.

[37] "Lateral-view-of-the-brain". In: *Trusted Neurodiagnostics Academy* (). [Online; accessed 4 May 2021]. URL: https://trustedacademy.com/topic/hemispheres-and-lobes/lateral-view-of-the-brain/.

[38] *Lesson 11: Principal Components Analysis (PCA)*. [Online; accessed 10 June 2021]. URL: https://online.stat.psu.edu/stat505/lesson/11.

[39] Sonya Mehta et al. "Evaluation of voxel-based morphometry for focal lesion detection in individuals". In: *NeuroImage* 20.3 (2003), pp. 1438–1454. URL: https://www.sciencedirect.com/science/article/pii/S105381190300377X.

[40] *MRI More Sensitive Than CT in Diagnosing Most Common Form of Acute Stroke, Finds NIH Study*. [Online; accessed 3 March 2021]. Jan. 2007. URL: https://www.nih.gov/news-events/news-releases/mri-more-sensitive-ct-diagnosing-most-common-form-acute-stroke-finds-nih-study.

[41] Sebastian Ocklenburg and Onur Güntürkün. "Chapter 9 - Structural Hemispheric Asymmetries". In: *The Lateralized Brain*. Ed. by Sebastian Ocklenburg and Onur Güntürkün. San Diego: Academic Press, 2018, pp. 239–262. URL: https://www.sciencedirect.com/science/article/pii/B9780128034521000096.

[42] Ph.D. Stéphane Bastianetto. *L'aphasie, qu'est-ce que c'est ?* [Online; accessed 28 February 2021]. Mar. 2017. URL: https://www.passeportsante.net/fr/Maux/Problemes/Fiche.aspx?doc=aphasie.

[43] C. Phillips. *Tissue-weighted smoothing evaluation*. [Online; accessed 3 May 2021]. Mar. 2020. URL: https://github.com/CyclotronResearchCentre/TissueW_Smoothing_demo/blob/master/TechnicalNote.md.

[44] Carole Roth. "Boston Naming Test". In: *Encyclopedia of Clinical Neuropsychology*. Ed. by Jeffrey S. Kreutzer, John DeLuca, and Bruce Caplan. Springer New York, 2011, pp. 430–433. URL: https://doi.org/10.1007/978-0-387-79948-3_869.

[45] S. Appelhoff et al. *Brain Imaging Data Structure, Appendix XI: Quantitative MRI*. [Online; accessed 2 March 2021]. URL: https://bids-specification.readthedocs.io/en/bep-009/99-appendices/11-qmri.html#appendix-xi-quantitative-mri.

[46] "Simple illustration of the Jacobian determinant as a geometric scaling factor". In: *Matlab* (). [Online; accessed 22 May 2021]. URL: https://www.mathworks.com/matlabcentral/mlc-downloads/downloads/submissions/26884/versions/1/previews/html/modulation_tutorial.html.

[47] "Student's t-test". In: *Wikipedia, the free encyclopedia* (). [Online; accessed 28 June 2021]. URL: https://en.wikipedia.org/wiki/Student%5C%27s_t-test#Equal_or_unequal_sample_sizes,_unequal_variances_(sX1_%5C%3E_2sX2_or_sX2_%5C%3E_2sX1).

[48] R. Teasell and N. Hussein. *Clinical Consequencesof Stroke*. [Online; accessed 16 March 2021]. URL: http://www.ebrsr.com/sites/default/files/v18-SREBR-CH2-NET.pdf.

[49] *The internet stroke center*. [Online; accessed 17 March 2021]. URL: http://www.strokecenter.org/patients/stroke-diagnosis/how-a-stroke-is-diagnosed/.

[50] The University of Queensland - Brain Institute, Australia. *How to measure brain activity in people*. [Online; accessed 16 March 2021]. URL: https://qbi.uq.edu.au/brain/brain-functions/how-measure-brain-activity-people.

[51] Nora Silvana Viglieccа and Javier Alfredo Voos. "Remembering a name: Neuropsychological validity studies and a computer proposal for detection of anomia". In: *Dement Neuropsychol.* 13.4 (Oct. 2019), pp. 450–462. URL: http://www.scielo.br/pdf/dn/v13n4/1980-5764-dn-13-04-0450.pdf.

[52] William C. Shiel Jr., MD, FACP, FACR. *Stroke Causes, Symptoms, and Recovery*. [Online; accessed 27 February 2021]. Jan. 2016. URL: https://www.medicinenet.com/stroke_pictures_slideshow/article.htm.